DIRECT EVALUATION OF AKT KINASE ACTIVITY WITH SINGLE CELL RESOLUTION: INNOVATIONS IN THE DEVELOPMENT OF PEPTIDE REPORTERS FOR USE WITH CAPILLARY ELECTROPHORESIS

Emilie R. Mainz

A dissertation submitted to the faculty at the University of North Carolina at Chapel Hill in partial fulfillment of the requirements for the degree of Doctor of Philosophy in the Department of Chemistry.

Chapel Hill
2016

Approved by:

Nancy L. Allbritton

James W. Jorgenson

David S. Lawrence

Teresa K. Tarrant

Matthew R. Lockett

ABSTRACT

Emilie R. Mainz : Direct Evaluation of Akt Kinase Activity with Single Cell Resolution:
Innovations in the Development of Peptide Reporters for Use with Capillary Electrophoresis
(Under the direction of Nancy L. Allbritton)

Direct quantification of kinase activity at the single cell level has long been a goal from both a drug development and diagnostic standpoint. This is true for measurements of the protein kinase Akt, which is known to drive aberrant cell growth and metabolism in diseases including rheumatoid arthritis and pancreatic cancer. A more complete mechanistic profile of abnormal Akt activity in these diseases could drive the development of targeted inhibitors or companion diagnostics, but is hindered by the small and heterogeneous samples that can often be obtained from patients. Established tools including genetically encoded sensors and high throughput mass cytometry are incompatible with these primary samples.

Herein, a novel chemical cytometry approach is presented which utilizes peptide-based reporters to deliver direct measurements of Akt activity in single cells from cell lines as well as clinical samples. Methodological and chemical innovations resulted in the development of rapid and low cost assay development strategies, use of non-native amino acids as methods to impart additional stability on peptide probes, analysis of individual cells from rheumatoid arthritis subjects, and significant improvement in the overall throughput of analysis.

Dedicated to my brother, Drew.

You have always made the impossible look easy.

ACKNOWLEDGEMENTS

This dissertation would not have been possible without the many people who provided their support. First, I must thank my talented and well-organized advisor, Dr. Nancy Allbritton. Thank you for setting high scientific expectations while also allowing me to pursue my own projects and career interests. The knowledge I have gained as your student will prove invaluable. Dr. Chris Sims, thank you for sharing your rheumatology expertise and for providing me valuable opportunities to learn outside the lab. I also benefitted from fruitful collaborations with Dr. David Lawrence and Dr. Teresa Tarrant: thank you both for providing creative solutions and pointing out knowledge gaps. Dr. Qunzhao Wang, this work would have been impossible without your talent for peptide synthesis, and I am grateful for all of your help over the last 5 years.

Allbritton lab-mates, past and present, have made my time in graduate school such a positive experience. You gave my science the necessary support and critique to render it successful, and (perhaps more importantly) provided daily inspiration and creativity. I owe the most to Dr. Asad Ahmad. We rarely overlapped in research but managed to build TOPS from the ground up. I will always be proud of what we accomplished. Thank you for teaching me to aim high and for convincing me I could do much more than pipet – I needed it. I have to thank Pete Attayek for being a talented engineer and an even better friend. To Dr. Angie Proctor: you are a testament to the concept that organization will set you free. I hope I picked up a few good habits from you. Of course, the Allbritton lab is not the same without the

philosophizers, Doctors Ryan Phillips, Abby Turner, and Pavak Shah. You made all our heads hurt in the best way possible. Greg Woss, Dr. Jazz Dickinson, and Dr. Michelle Kovarik, thank you for always providing creative solutions to CE problems and for being well versed in the art of conversation. Dr. Nick Dobes, thank you for being a great collaborator and friend. I also need to thank my undergraduate, Tuong Nguyen, for his dedicated work in the lab. I wish you all the best as you move forward.

Looking back on my time at UNC, I realize I would not have made it this far without those who encouraged me to pursue research in the first place. Professor Sue Lunte: you were the most critical piece to my college education, and I will forever be grateful to a professor who dedicated so much time to mentor an undergraduate like myself. Last, and most importantly, are my parents. If I had to boil down 27 years of life lessons from you, it would come down to this: work hard, but stay curious. Thank you for providing your constant support and for expecting the best from me. Turns out the world does too.

TABLE OF CONTENTS

LIST OF TABLES

LIST OF FIGURES

LIST OF ABBREVIATIONS AND SYMBOLS

5FAM	5-carboxyfluorescein
°C	degrees Celsius
µg	Microgram
µL	Microliter
µM	Micromolar
6FAM	6-carboxyfluorescein
Acrylodan	6-acrylolyl-dimethylaminonapthalene
Ala	Alanine
Amol	Attomoles
Arg	Arginine
ATP	adenosine triphosphate
BSA	bovine serum albumin
$CaCl_2$	calcium chloride
CBD	cyclobutane dimer
CE	capillary electrophoresis
CE-LIF	capillary electrophoresis with laser induced fluorescence detection
CLA	cell line authentication
Cm	Centimeter
CML	chronic myelogenous leukemia
CO_2	carbon dioxide
CPP	cell-penetrating peptide

CSC	cancer stem cells
C-terminus	carboxy terminus
CTL	cytotoxic T-cells
CyTOF	cytometry by time-of-flight
CZE	free zone electrophoresis
DIC	Diisopropylcarbodiimide
DIPEA	N,N-Diisopropylethylamine
DMEM	Dulbecco's Modified Eagle Medium
DMF	Dimethylformamide
DMNB	2-4,5-dimethoxy-2-nitrobenzyl
dP	rate of phosphorylated product formation
DPBS	Dulbecco's Phosphate Buffered Saline
dS	rate of consumption of substrate
ECB	extracellular buffer
EDTA	ethylene diamine tetraacetic acid
EGFR	epidermal growth factor receptor
ESI	electrospray ionization
FBS	fetal bovine serum
FLS	fibroblast-like synoviocytes
Fmoc	9-fluoroenylmethoxycarbonyl
FRET	Förster resonance energy transfer
GPCR	G protein coupled receptor
H	Hour

HCTU	2-(6-chloro-1*H*-benzotriazole-1-yl)-1,1,3,3-tetramethylaminium hexafluorophosphate
HOBt	N-Hydroxybenzotrizaole
HPLC-MS	high performance liquid chromatography - mass spectrometry
HRP	horseradish peroxidase
ICP-MS	inductively coupled plasma-mass spectrometry
IHC	Immunohistochemistry
IMAP	Immobilized Metal Ion Affinity
KTR	kinase translocation reporter
LC	liquid chromatography
LDH	lactate dehydrogenase
LIF	laser induced fluoresence
MALDI-MS	matrix assisted laser desorption ionization time-of-flight mass spectrometry
MEKC	micellar electrokinetic capillary chromatography
Mg	Milligram
$MgCl_2$	magnesium chloride
MHC	major histocompatibility complex
Min	Minute
mL	Milliliter
mM	Millimolar
MMP	matrix metalloproteases
MOPS	3-(N-morpholino)propanesulfonic acid
Ms	Millisecond

MSNT	1-(mesitylene-2-sulfonyl)-3-nitro-1,2,4-trizaole
mW	Milliwatt
NaOH	Sodium hydroxide
Nd:YAG	neodymium-doped yttrium aluminum garnet
NDA	naphthalene-2,3-dicarboxyaldehyde
nL	Nanoliter
Nle	Norleucine
nM	Nanomolar
NMP	N-Methyl-2-prrolidone
NS	native substrate
N-terminus	amino terminus
OD	outer diameter
PBS	phosphate buffered saline
PDAC	Pancreatic ductal adenocarcinoma
PDK1	phosphoinositide dependent kinase -1
PDMS	poly(dimethyl) siloxane
PH	pleckstrin homology domain
Phe	Phenylalanine
PHLPP1/2	PH-domain leucine-rich repeat protein kinase 1or 2
PI3-K	phosphoinositide 3-kinase
PIP_2	phosphatidylinositol (4,5)-bisphosphate
PIP_3	phosphatidylinositol (3,4,5)-triphosphate
PKA	cAMP-dependent kinase

PKB	Protein Kinase B
PKG	cGMP-dependent kinase
PMT	photomultiplier tube
PO_3^{2-}	Phosphoryl
PP2A	protein phosphatase 2a
Pro	Proline
Protein Kinase B;	
PKB	Akt
PTEN	phosphatase and tensin homolog
PTM	post translational modification
PTP	protein tyrosine phosphatases
RA	rheumatoid arthritis
RFU	relative fluorescence units
RTK	receptor tyrosine kinase
S	Seconds
scWestern	single cell western blot
SDS	sodium dodecyl sulfate
Ser	Serine
Ser473	Serine residue in position 473
SPA	scintillation proximity assay
SPPS	solid phase peptide synthesis
T	Threonine
t1/2	half-life in a lysate

t50%P	time to 50% phosphorylation
TFA	trifluoroacetic acid
Thr	Threonine
TIS	Triisopropylsilane
TNFα	tumor necrosis factor alpha
TORC2	target of rapamycin complex 2
zmol	Zeptomole

Chapter 1: The Akt Pathway: Disease Implications and Assay Strategies

1.1 Protein Kinases and The Akt Pathway

1.1.1 Protein Kinases: Key Regulators of Cellular Functions

Physiology is greatly influenced by a diverse group of intracellular enzymes which

catalyze the chemical reactions required for typical cellular functions. Of these reactions,

post-translational modifications (PTMs) are an important device by which the functional

diversity of proteins is expanded while maintaining tight regulatory control.[1,2] For example,

ubiquitin is often conjugated to proteins fated for degradation by the ubiquitin-proteasome

pathway.[3] This PTM-based selection of specific proteins ensures that the proteolytic process

is highly discerning, which is critical for preventing excessive breakdown of cellular

contents. Such PTMs modulate the activity of most eukaryotic proteins, and include

phosphorylation, proteolysis, acetylation, dephosphorylation, glycosylation and methylation.[1]

Among the best studied are protein kinases, which catalyze phosphorylation; the addition of a

phosphoryl group (PO_3^{2-}) from a high energy adenosine triphosphate (ATP) molecule to a

serine, threonine, or tyrosine residue on a protein substrate.[4] The electrostatic properties of

the substrate are modified by the dual negative charges imparted by phosphorylation, which

in turn alters the structure, function, or localization of the protein substrate.[5] Protein kinases

play critical roles in cell growth, metabolism, and survival; activating these pathways through

rapid exchange of phosphoryl groups allows normal cells to swiftly react to stimuli and

afterwards return to basal enzyme activity.[6] Therefore, diseases which rely heavily on

atypical cell growth or metabolism can often be traced to one or more dysregulated kinase

pathways. Aberrations of protein kinases in cancer are likely the most well-known example.[7]

1.1.2 A Brief History of Protein Kinases and Inhibitors

Prior to 1950, phosphorylated proteins were known to exist but were considered

biologically inert.[8] The characterization of phosphorylase kinase by Fisher and Krebs in 1955

founded the field of protein kinases and later earned them a Nobel Prize.[6,9] By the late 1980s,

major roles of protein kinases in disease had been established through the discovery of

receptor tyrosine kinases (RTKs) and others as oncogenes.[10,11] Advancements in medicinal

chemistry then yielded the discovery of the natural product staurosporine, a potent kinase

inhibitor which also proved spectacularly nonspecific, and thus highly toxic.[12-14]

In 2001, the first blockbuster protein kinase inhibitor, imatinib, was developed. Often

hailed as the paragon of targeted cancer therapy, imatinib inhibits the constitutively active

driving force in chronic myelogenous leukemia (CML): the BCR/ABL fusion protein.[7] A

landmark study by O'Brien and colleagues demonstrated therapeutic effect in 87% of

patients versus 34% with standard treatment, effectively converting CML from fatal disease

to manageable condition.[7,15] The efficacy of imatinib also popularized oncogene addiction,

the concept that some cancers are reliant on a single prevailing mutation, as a route to

targeted anti-cancer therapeutics. Bolstered by the fact that 19 kinase inhibitors gained FDA

approval from 2011 through June 2015,[16] pharmaceutical development pipelines are stocked

with kinase inhibitors to treat a multitude of disorders, not limited to arthritis,[17] solid

tumors,[18] and pulmonary fibrosis.[19-21] Combination therapies with monoclonal antibodies or

other small molecule inhibitors are also being explored for synergistic effects.[22] Though

challenges in specificity and drug resistance remain, the impact of kinase inhibitors on modern medicine is undeniable.

1.1.3 Akt Kinase

The kinase Akt (Akt, also known as Protein Kinase B (PKB)) is a serine/threonine protein kinase recognized as a critical effector of survival-related cellular functions, including growth, proliferation, metabolism, and angiogenesis.[23-26] Akt is a member of the AGC protein kinase family, which originally contained cAMP-dependent kinase (PKA), cGMP-dependent kinase (PKG), and protein kinase C (PKC), so grouped due to their conserved catalytic domains and similar regulatory features.[27] The three isoforms of Akt ($1/\alpha$, $2/\beta$, and $3/\gamma$) are products of distinct genes but perform similar functions and possess 80% sequence homology.[28] Akt possesses an N-terminal pleckstrin homology (PH) domain that allows for recruitment to the membrane, a central kinase catalytic domain, and a short C-terminal regulatory domain that governs the interaction between signaling molecules.[26]

Since Akt elicits a broad spectrum of cell growth and survival behaviors, its activation is a tightly regulated process involving recruitment to the membrane and dual phosphorylation.[29] When upstream pathways including RTKs, cytokine receptors, integrins, or specific G-protein coupled receptors (GPCRs) are stimulated, phosphoinositide 3-kinase (PI3K) activation is triggered.[30] PI3K phosphorylates phosphatidylinositol (4,5)-bisphosphate (PIP_2) to generate phosphatidylinositol (3,4,5)-triphosphate (PIP_3),which acts as a ligand to the PH domain of Akt, anchoring it to the plasma membrane (Figure 1.1) . Partial activation of Akt is achieved by the phosphorylation of threonine 308 in the kinase domain by phosphoinositide dependent kinase -1 (PDK-1). This level of Akt activity is sufficient to

catalyze some downstream protein synthesis activities.[31] The enzyme or enzymes responsible for full activation of Akt by phosphorylation at serine 473 was the subject of much debate. Several studies in the 2000s confirmed that target of rapamycin complex 2 (TORC2), DNA-activated protein kinase (DNA-PK) and potentially rapamycin-insensitive TORC1 have this capability.[32-35] Once fully activated by dual phosphorylation, Akt diffuses away from the membrane to the cytosol or nucleus to phosphorylate downstream targets. When returning to basal signaling, Akt activity is reduced indirectly by the actions of phosphatase and tensin homolog (PTEN), which dephosphorylates PIP_3 to PIP_2 and acting to sever the PH domain interactions mooring Akt to the membrane.[36] Activity can also be halted by direct dephosphorylation at Thr308 or Ser473 by protein phosphatase 2A (PP2A) and PH-domain leucine-rich repeat protein kinase 1or 2 (PHLPP1/2), respectively. Though regulated tightly, aberrations at any of these signaling nodes can manifest in disease. Of the 538 kinases currently identified, those involved in the PI3K/Akt/mTOR pathway are often cited as the most frequently dysregulated in cancer and other diseases. [37] This dissertation will focus primarily on the distinct roles of Akt in pancreatic ductal adenocarcinoma (PDAC) and rheumatoid arthritis (RA).

1.2 Roles of Akt in Select Diseases

1.2.1 Pancreatic Ductal Adenocarcinoma

PDAC is the fourth leading cause of cancer-related death and is almost universally fatal, with five year survival rates of 7%.[38] PDAC is characterized by early and rapid metastasis with resistance to conventional and targeted therapeutic agents.[39] The role of deviant Akt signaling in PDAC is well established, either alone or as a result of upstream oncogenic KRAS activity.[29,40-44] It is reported that up to 70% of these tumors have a critical

dependency on hyperactive Akt for tumorigenesis[45], since Akt contributes to cancer

hallmarks such as unregulated cell growth and survival.[29,46] These results are consistent with

the correlation between elevated Akt activity and higher mortality rate in PDAC.[47,48]

Aberrant Akt signaling in PDAC usually arises by one of three mechanisms. The rarest is

direct mutation of the PH domain of Akt at position 49 (G to A), allowing it to associate with

the membrane without the need for PI3K activation, resulting in a constitutively active

kinase.[49,50] Akt gene amplification, mRNA and protein overexpression has also been

reported.[51] Most frequently, deletion of the PTEN gene results in the loss of the primary

negative feedback mechanism for Akt, increasing the overall activity.[52] Recent work

demonstrates that inhibition of PI3K with small molecules such as wortmannin and

LY294002 sensitizes PDAC to pro-apoptotic stimuli and cytotoxic agents, making this

signaling arm attractive for the development of targeted therapies.[37,53,54] Mounting evidence

also suggests that rare populations of rapidly growing and aggressively invasive cells are

often responsible for tumor metastasis or recurrence, but can be targeted through Akt

inhibition.[55-57] Single cell analyses would be essential to the identification of these rare cell

groups that would favorably respond to Akt inhibition even when the bulk of the tumor does

not show overactivation of this pathway, thereby guiding appropriate prescription of anti-Akt

therapies.

1.2.2 Rheumatoid Arthritis

Rheumatoid arthritis (RA) is the most common autoimmune disorder, and affects

more than 1.3 million Americans.[58] Despite innovations in engineered biologic therapies, the

management of RA remains challenging and its success varies across patients. This

variability in clinical management highlights the fact that RA is not a distinct disease entity,

but rather a complex syndrome with varied manifestations.[59] The exact etiology of RA remains uncertain, but is known to involve synovial hyperplasia leading to cartilage destruction and irreversible joint damage.[60] A mounting body of evidence suggests that Rheumatoid Arthritis Fibroblast-like Synoviocytes (FLS) contribute largely to this process by the infiltration and destruction of cartilage.[61-63] Early RA is typically only observed in a limited number of joints before spreading throughout the body; this progression has been linked to the transmigration of activated FLS.[64,65] It is postulated that selective destruction or growth inhibition of these cells which irreparably damage joints would be an excellent therapy, but thus far the signal transduction pathway aberrances leading to this invasive phenotype are largely unknown.

While in the past it may have been assumed *a priori* that the signaling pathways involved in RA maintain too much plasticity to address with targeted kinase inhibitor therapies, recent successes with inhibitors such as tofacitinib and baricitinib, both of which inhibit the Jak/Stat pathway, have added to growing evidence that numerous protein kinases are dysregulated in RA, and many autoimmune disorders in general.[17,66,67] Akt is a common downstream element of the majority of promiscuous chemokine signaling pathways that may be targeted for the next generation of anti-inflammatory drugs. Patients with RA have been found to possess Akt expression and activity abnormalities.[68,69] Akt is implicated in an anti-apoptotic role, allowing survival of cells responsible for synovial inflammation and eventual cartilage erosion.[70] These abnormalities are seen primarily in rheumatoid arthritis FLS and not in neighboring macrophages or other cell types, suggesting that overactive Akt in these cells may incite aggressive anti-apoptotic and invasive behavior, progressing the disease.

In addition to therapies consisting of Akt inhibitors, there is significant interest in utilizing Akt activity as a biomarker of patients who may be responsive to therapies targeting tumor necrosis factor alpha (TNFα). Biologic anti-TNFα therapies dominate RA treatment, but more than a third of patients are unresponsive.[71,72] Little is known regarding the mechanism of Akt activation by TNFα,[73] but results indicate that Akt acts as a survival signal in RA FLS after being stimulated by TNFα. [68,74] Thus, patients with elevated Akt activity may respond to therapies which remove the TNFα stimulus. However, the presence of contaminating cell types other than FLS that do not possess elevated Akt activity, but are often analyzed as such in bulk cell analysis, make this aberrant signaling difficult to interrogate. Chapter 2 will detail the first assay capable of directly measuring Akt activity in single cells from FLS from patients with RA.

1.3 Challenges in The Measurement of Akt Activity in Clinical Samples

In order to fully grasp Akt involvement in disease and potential as a therapeutic target, enzyme activity measurements will need to be performed with single cell resolution. Traditionally, thousands or millions of cells are required to prepare bulk lysates for ensemble measurements of Akt activity. This practice returns an ensemble average of the entire population, and obscures valuable information that can contribute to better understanding of the molecular mechanisms of disease. Information is lost due to the astounding heterogeneity among populations of cells, even those which are genetically identical and residue in the same tissue or tumor.[75] The following section will discuss the role of heterogeneity in protein kinase signaling and the benefits of single cell analysis for measuring Akt activity in clinical samples.

1.3.1 Heterogeneity in Kinase Signaling

In stark contrast to long-held opinions of homogeneity, recent biological and technical developments have shown that isogenic populations of cells frequently possess variable morphology, epigenetic state, proliferation rates, and protein expression.[76-78] These differences can be driven by selection pressure,[79] pre-programmed mechanisms such as differentiation,[80] or have stochastic causes.[81-83] For protein kinase signaling, differences often arise due to assorted splicings of a single RNA transcript,[84] leaky negative feedback systems,[85] and the evolution of cells that develop different functional properties, such as those observed in PDAC and RA.[74,77] All of these can contribute to a broad spectrum of kinase activity within a population of cells, which requires single cell analysis for accurate characterization. For example, utilizing techniques which can resolve kinase activity in single cells would easily disseminate a bimodal signaling distribution, while a bulk method would return a mean value that poorly reflects both groups.[75,86] Similarly, a rare population (<1%) of cells from a population would likely go undetected with bulk methods.

Interestingly, heterogeneity in Akt signaling is as much of a hallmark in healthy cells as those afflicted with disease.[87] Since the Akt pathway is so frequently dysregulated in disease, it is hypothesized that heterogeneous activation of this pathway benefits healthy cells by preventing overactivation of the pathway in the whole population, which could lead to unfettered growth or even senescence. There is also evidence to suggest that regulatory mechanisms in healthy cells such as rapid dephosphorylation by PTEN are crucial to keeping Akt at bay. However, when these growth signals cannot be regulated and Akt remains active, disease (and heterogeneity) abounds. Analysis of many solid tumors and FLS have demonstrated that Akt aberrances allowing for oncogenic or aggressive growth behaviors

often only represent a sub-fraction of the entire population.[87,88] It will be important to generate methodologies which can tease apart differences in the catalytic activity of Akt in healthy and diseased tissues. Since it has been shown that overexpressed Akt may not indeed be active, quantification of substrates and well as products of the kinase will be essential.[89]

1.3.2 Analysis of Small or Complex Clinical Samples

Basic research and the development of kinase inhibitors are reliant on immortalized cell lines, which are simple to culture, cost-effective, and produce rapid results. However, after several passages, cell characteristics can change and may become quite different to those found in the initial tissue. Increased growth rate, altered morphology, and modifications of cell surface marker expression have all been reported.[90,91] This is all the more troubling when attempting to model complex and heterogeneous diseases such as PDAC and RA, which are not well-represented by a single isogenic cell type. For this reason, primary human tissues should be utilized when possible. The challenges with such clinical samples from both diseases of interest of this dissertation will be discussed.

PDAC demonstrates marked genetic and phenotypic intratumoral heterogeneity that is thought to underlie the differential responses to standard chemotherapy. Research regarding Akt's role in treatment resistance identifies the kinase as an arbiter of cancer stem cell (CSC) fate, allowing rare CSC cells to evade systemic cytotoxic therapies and recapitulate the tumor.[55,57] Interestingly, rare subpopulations such as CSCs have been shown to be more sensitive than non-stem cells to Akt inhibition.[56] These cells are linked to clinical observations where chemotherapy greatly shrinks the tumor but fails to eradicate it, indicating a rare resistant cell phenotype. However, rare subpopulations are difficult to

detect in the heterogeneous intratumoral environment characteristic to PDAC and may go entirely undetected by bulk sample analyses. The impact of Akt role in CSCs is further hampered by the inability of diagnostic tests to directly measure enzyme activity.

Rheumatoid Arthritis is a highly complex disease with many cell types playing major roles in inflammation. The study of FLS biology is difficult due to the heterogeneous cellular nature of the RA-affected synovium, which contains at least five mixed cell types. Additionally, the individual heterogeneity between FLS phenotypes, as well as the unique enzymology and biological processes within each individual patient, make quantification of Akt activity difficult in bulk cell analyses. Furthermore, new techniques including fine needle biopsies[92] and ultrasound-guided sampling of synovial fluid[93] are generally less invasive than a full synovectomy but produce very small numbers of cells, which are difficult to analyze with traditional techniques requiring thousands to millions of cells. The development of new technologies capable of probing FLS functional phenotypes and addressing individual FLS heterogeneity would greatly enhance the ability to characterize and ultimately develop new therapeutics which targets these cells.

1.4 Assays for Measuring Akt Activity *in Vitro,* in Lysates or Single Cells

Numerous methods have been utilized to detect either the presence of protein kinases or their associated activities. In this dissertation, a method for determination of kinase activity is defined as one capable of quantifying the rate of phosphorylated product formation (dP) or consumption of the substrate (dS), typically as a function of time ($dP/dt = -dS/dt$).[94] In the following sections, customary methods as well as currently evolving single cell methods to detect Akt activity will be described.

1.4.1 *In Vitro* Assay Platforms

1.4.1.1 Radioactive Assay Platforms

Traditional radiometric assays exploit the fact that kinases require ATP as a phosphate source. By utilizing [γ-^{32}P]-labeled ATP during the reaction, the transfer of radioactive ^{32}P onto a protein substrate results in a radiolabeled protein or peptide substrate. After capturing the labeled substrate on a filter and washing to remove excess ^{32}P-ATP, the amount of product formed is quantified by ß-scintillation counting.[95] Morrow *et al.* utilized this method to compare the activity of Akt in response to upstream PI3K mutations *in vitro* and in lysates from a panel of colorectal cancer cell lines.[96] However, the filter capture steps in this method have important practical drawbacks. Typically, phosphoric acid is utilized to impart a positive charge on the labeled substrate for adequate binding to the negatively charged phosphocellulose filter membranes, severely limiting the utility of negatively charged substrates, such as those employed in some Akt inhibitor screens.[97,98]

The solution to the aforementioned issue is the homogenous scintillation proximity assay (SPA), which utilizes biotinylated peptide substrates.[99] The ^{32}P-tagged biotinylated peptide product is captured by SPA beads coated with streptavidin, bringing the scintillant in close proximity with the high energy radiolabel.[100] SPA assays have shown to be comparable in accuracy to modern high throughput mass spectrometry-based assays of Akt activity.[101] Although SPA improves the throughput and accuracy of radiometric protein kinase assays, radioactive assay platforms in general have decreased in popularity because these assays generate prohibitively large amounts of waste that are both hazardous and expensive to dispose of for the end user.

1.4.1.2 Fluorescence–Based Technologies

In many ways, *in vitro* fluorescence assays have become a favored alternative to *in vitro* radiometric assays to detect protein kinase activity. This is particularly true for high-throughput applications. There are a wide variety of assays which are beyond the scope of this dissertation, but several key techniques will be summarized. A dominant fraction of these assays utilize homogeneous formats which do not require sample processing in terms of centrifugation, washing, or separation steps. They populate an impressive suite of applications, including fluorescence anisotropy, lifetime variation, quenching, Förster resonance energy transfer (FRET) and time correlation methods.

1.4.1.2.1 Fluorescence Anisotropy

Fluorescence anisotropy kinase assays rely on the differing rotational properties of large (>100,000 Da) and small (<10,000 Da) molecules to detect phosphorylated and native substrates.[102] When molecules in solution are excited by plane polarized light, the degree to which the detected emission is polarized reflects the Brownian motion (i.e. rotations) the chromophore underwent between absorption and reemission. [103] Small molecules will tumble quickly and the resulting fluorescence is depolarized, or random, with respect to the polarization plane of the illuminating light. Conversely, small molecules which bind larger ones will experience a slower rotation or remain mostly stationary, and the detected emission will retain a comparable degree of polarization. Since the added phosphoryl group represents a very small mass change (80 Da),[104] phosphorylation alone is not sufficient to differentiate native and phosphorylated substrates.

Seethala was the first to describe an assay that utilized phospho-specific antibodies to selectively bind phosphorylated peptide substrates, imparting a mass sufficient for anisotropy

measurements.[105] This technique remains popular with RTK detection, primarily because anti-phosphotyrosine antibodies are relatively insensitive to the amino acids surrounding the tyrosine, enabling use with a broad range of substrates.[106] However, anti-phosphothreonine/serine antibodies are considerably more sensitive to the surrounding context, and in some cases necessitating the development of a unique antibody for each substrate of interest.[107] Numerous antibody-free solutions have been developed, including the use of cationic polyamino acids[108] and mixtures of zinc sulfate and bovine serum albumin[109] to selectively add mass to negatively charged phosphopeptides. The Immobilized Metal Ion Affinity (IMAP, Molecular Devices, CA) assay utilizes cationic trivalent nanoparticles to complex with phosphopeptides generated during a kinase assay, and has met with success for detection of Akt activity in *in vitro* settings.[100,110] The homogenous nature of these assays makes them favorable for automation in pharmaceutical lead development. Unfortunately, a classic downside of these assays is their susceptibility to interferences from complex samples or the substrates themselves, which can absorb light in the excitation or emission wavelengths of the assays, confounding anisotropy measurements. Turek-Etienne *et al*. overcame these limitations by developing red-shifted Cy3 and Cy5 labeled probes for Akt activity measurements in microbial extracts.[111] Overall, fluorescence anisotropy measurements remain some of the simplest and most popular methods for high throughput screens of potential kinase inhibitors. However, the limited sensitivity and dynamic range of these assays precludes their use with highly complex samples or single cells.[107]

1.4.1.2.2 Fluorescence Intensity Assays

The emission characteristics of many fluorophores are directly influenced by their environment, including pH, solvent polarity, and nearby biological analytes. A classic

example is dansyl chloride, which has very low fluorescence in water until its reaction with primary amines.[112] A similar strategy can be utilized to detect phosphorylation of peptides or proteins, where either an increase or decrease in fluorescence intensity signifies kinase activity. McIlroy *et al.* labeled a 25 amino acid PKC peptide with 6-acrylolyl-dimethylaminonapthalene (acrylodan), which experiences a 20% loss in fluorescence upon phosphorylation. [113] By pairing the probe with an electrophoresis step, probe-derivatized phosphopeptide was separated from the unphosphorylated version, enabling ratiometric quantification of PKC activity *in vitro* and in crude brain lysates. In a quenching assay developed using similar trivalent cation chemistry to that applied in the IMAP assay,[114] a phosphorylated peptide substrate is capable of quenching the fluorescence from a polymer deposited onto microspheres. Thus, a decrease in fluorescence correlates with kinase activity. These such methods are useful tools for the measurement of protein kinase activity in high throughput *in vitro* inhibitor screens and some lysates, but require large volumes (µL) which are not compatible with single cell analysis.

1.4.1.2.3 Förster Resonance Energy Transfer Assays

FRET is a distance-dependent phenomenon in which a donor chromophore can non-radiatively transfer energy to an acceptor molecule. Since FRET efficiency is principally dependent on the molecular propinquity of the donor and acceptor fluorophores (1-10 nm), it is often employed in biological studies that induce changes in conformation or proximity; these include protein kinase assays.

FRET's utility for *in vitro* kinase activity screens has been borne out in several commercial products. In the Z'-LYTE Kinase Assay (ThermoFisher Scientific, CA) a peptide

substrate with a centrally located protease clip site is adorned at each terminus with one member of a FRET fluorophore pair. Once the kinase reaction is complete, a proprietary cocktail containing a protease is added. If phosphorylated, the peptide substrate is immune to protease activity and remains intact. Conversely, any unmodified substrate will undergo cleavage at the central clip site, bringing the FRET pair into close proximity and increasing fluorescence. Thus, fluorescence intensifies when the kinase is inhibited. This assay is amenable to automation, and has been utilized by Pellechia and others to rapidly screen targeted Akt inhibitors, which verified the results of *in silico* methods to predict inhibitors based on known docking mechanisms.[116] Though this assay is useful for detecting the efficacy of kinase inhibitors *in vitro*, its use with unmodified lysates should be approached with skepticism and requires careful triage. The presence of interfering intracellular proteases or peptidases may cleave the substrate even with the presence of a phosphoryl group, leading to a false positive (false inhibition) rate of up to 15%.[117] Lysate studies are further complicated by the fact that substrates may not be optimized for specificity and thus phosphorylation may be due to several contributors.

In an ambitious study to identify Akt inhibitors from a library of more than 63,000 compounds, researchers at the UK Centre for Cancer Therapeutics utilized the AlphaScreen™ Technology (Perkin Elmer, Norwalk, CT); an antibody-based FRET assay.[118] This format utilizes a biotin-labeled Akt substrate, which is phosphorylated by Akt either from a recombinant source or from immunoprecipitated cell lysates. The addition of streptavidin-linked donor beads generates half of the FRET pair, which is completed when a phospho-specific antibody bound to protein-A labeled acceptor beads associates with the phosphorylated substrate. Therefore, fluorescence is only generated in the presence of

phosphorylated peptide, indicating the catalytic activity of Akt. With this method, the investigators identified that just 0.1% of the library compounds acted as significant Akt inhibitors. The primary limitation of this assay was the sensitivity of the donor beads to ambient light, which caused significant fluctuations in end-point fluorescence. False-positives, generated through simple aggregation of the inhibitor and resulting in apparent enzyme inhibition, were found to be mitigated by testing apparent library hits in the presence of Triton X100, which reduces the aggregates.

Overall, FRET-based *in vitro* fluorescence assays are useful to measure the potency of putative enzyme inhibitors, but require the kinase of interest of to exhibit high amounts of activity, which is not the case with several clinically important kinases.[119] Another classic downside with these assays is the substrates or FRET pairs are often themselves fluorescent, resulting in high background.[120] Furthermore, protein kinase inhibitor screens are often comprised of highly conjugated organic molecules which absorb light at wavelengths similar to those used for fluorescence emission. At typical compound screening concentrations of greater than 1 µM, interference artifacts can become significant.

1.4.1.3 Mobility Shift Assays

Among the methods utilized to detect kinase activity *in vitro,* mobility shift assays comprise an outlier in a large group of homogenous assay formats. Rather than detect radioactive phosphorus or generate a fluorescent signal upon the gain or loss of kinase activity, these assays exploit the dissimilar net charge that phosphorylated proteins possess relative to native substrates.[121] Caliper Technology (Caliper Life Sciences, Hopkinton, MA) is based on a microfluidic format which separates the product and substrate in an electric

field. This allows simultaneous detection of both, which can be monitored in real time.[122] However, when kinase activity in lysates is of interest, it is difficult to differentiate substrate phosphorylation from peptidase cleavage, since both may generate similar differences in electrophoretic mobility. Furthermore, these assays require large amounts of substrate (μM) and are low throughput.

1.4.2 Assay Platforms for Single Cell Analysis

In vitro studies or those utilizing lysates are a cost effective and simple model for investigating Akt activity, but they do not fully recapitulate the native cellular environment. Lysis disrupts local and encapsulated microenvironments present in cells, liberates proteases and phosphatases that are typically under tight regulation, and dilutes cell contents.[123] Prior work has shown that cleavage location and degradation rate can differ between lysates and single cells[31] and lysate experiments yield ensemble measurements that provide a population average, but do not allow discovery or interrogation of subpopulations. Therefore, in this work single cell analysis will be performed in addition to lysate experiments.

1.4.2.1 Immunohistochemistry

Developed in the 1930's, immunohistochemistry (IHC) has a long history in disease diagnostics and basic research.[124] IHC methods involve fixing and permeabilizing tissues before treating with antibodies directed against phosphorylated Akt (Ser473; considered active). Labeled tissues are examined by a highly trained pathologist, and the presence of Akt in tissue slices is visualized. This provides tissue localization information, but IHC is not quantitative and has garnered criticism for the subjectivity of result interpretation, since each pathologist has unique training.[125] Most importantly, cells are fixed and permeabilized before

17

analysis, which terminates intracellular signaling by crosslinking intracellular proteins. This is troublesome when considering the timescales of chemical fixation, which may be significantly longer (seconds to minutes)[126] when compared to the speed of kinase reactions occurring on the millisecond timescale.[127] Therefore, there is a significant window of time available for cells to activate cell survival responses such as Akt during the fixation process, which may produce measurements artifacts or obscure accurate measurements of kinase activity.

1.4.2.2 Western Blotting

The Western blot is the gold standard for identifying Akt in complex lysates from cells. Proteins in a sample are separated by molecular weight with gel electrophoresis before transferring the proteins to a solid support and labeling the kinase with a primary and secondary antibody.[128] In many cases, phosphorylated Akt (Ser473) is also labeled with a phospho-specific antibody to assess the fraction of Akt that is active. Several thousand cells are required for such analyses, which also require significant amounts of costly antibodies.

Recently, protein requirements have been miniaturized with the development of the single cell western blot (scWestern).[129,130] The primary differences between the bulk and single cell method lie within the polyacrylamide gel utilized for protein separation. Rather than depositing microliters of sample into a slab gel several millimeters thick, scWesterns rely on a thin (30 µm) layer of polyacrylamide pockmarked with an array of microwells. Individual cells are loaded into wells, lysed, and single cell protein lysates are separated. Instead of the traditional transfer of proteins to a phosphocellulose support for detection, the thin gel is photopolymerized to immobilize proteins before probing with primary and

secondary antibodies. While promising, several limitations of the technology include crosstalk between microwells due to lysate diffusion out of microwells, physical overlap of proteins of interest within the short separation length of the miniaturized blot, and poor resolving power due to the short separation lanes.

1.4.2.3 Genetically Encoded Fluorescent Sensors

Major innovations in molecular biology, in particular green fluorescent protein (GFP), have driven the development of genetically encoded intracellular fluorescent biosensors which can probe disease-relevant signaling pathways at the single cell level. Many of these sensors rely on the same principles as the fluorescent *in vitro* sensors described above. For example, Sasaki demonstrated that by flanking an Akt substrate and linker with two variations of GFP, phosphorylation by the kinase brought the GFP pair within the Förster radius, generating a fluorescent signal correlating with Akt activity.[131] A similar reporter of Akt activity utilized a FOXO1 substrate which was expressed in a construct with the Cerulean/cpVenus fluorescent protein couple, which demonstrated the spatiotemporal dynamics of Akt activation by insulin. [106,132] Finally, the low signal-to-noise ratios observed with many genetically encoded sensors was improved through the development of a bioluminescent Akt reporter. The two domains of luciferase were connected by a Akt substrate, whose phosphorylation sterically constrained their association, thus preventing fluorescence. [133]

Rather than employ a FRET pair, the Covert lab has developed a suite of kinase translocation reporters (KTRs) to assess kinase activity as reported by subcellular localization. Fluorescent kinase substrates were engineered with phosphorylation-sensitive

nuclear export or import sequences, converting kinase activity to localization changes. [134] While a KTR has not been described for Akt, it was shown that the KTR technology is generalizable to several enzyme classes. The dynamic changes in JNK, p38, and ERK pathways in response to anisomycin were modeled with three KTRs.

Overall, genetically encoded sensors enable real-time imaging of dynamic signaling events in single cells. They have direct applications in basic research and drug discovery. However, their utility is severely limited in clinical samples, which are often small and possess numerous cell types. This is rooted in the difficulties of uniformly transfecting primary cells, which can also induce significant stress to the cell and induce survival pathways such as Akt. Furthermore, genetically encoded sensors have notoriously low signal-to-noise ratios and may not accurately reflect the inactivation of the kinase by phosphatases, since the closed confirmation of FRET sensors is often highly stable and inaccessible to phosphatases. These encoded tools require rational design, optimization, and innovative delivery strategies, and in some cases, cell lines are the endpoint.

1.4.2.4 Mass Cytometry

The combination of features from flow cytometry and mass spectrometry led to the development of mass cytometry, which offers multiplexed single cell analysis of up to 120 parameters, including the presence of Akt. Rare, nonbiological earth metals coupled to protein-specific antibodies are used as reporters.[135] Cells are fixed and permeabilized before probing with antibodies and analysis with inductively coupled plasma-mass spectrometry (ICP-MS). The detected abundance of rare earth elements allows determination of protein marker expression in single cells. At an analysis rate of 2 million cells per hour, it is less

rapid than multi-color flow cytometry (25-60 million cells per hour) but boasts more than triple the multiplexing potential.[136] Using mass cytometry, Han and others demonstrated that Akt was not upregulated as expected in some acute myeloid leukemia patients, but rather ERK was potentiating cell survival behaviors.[137] The simultaneous analysis of nodes in multiple signaling pathways is inherently valuable to further understanding of pathway crosstalk in disease, but mass cytometry has several limitations. Since cells are fixed prior to analysis, it suffers from the same drawbacks as IHC in terms of potential measurement artifacts caused by fixation. Most importantly, it provides only an indirect gauge of kinase activity because Akt directed antibodies only measure Akt expression, not the comparative ratios of phosphorylated to native Akt substrates, whose relative amounts are key regulators of cell growth and apoptosis. It is also problematic to analyze small or rare populations of cells from clinical samples since the current technique of nebulizing single-cell droplets into the ICP-MS system is highly inefficient, with greater than 70% sample loss.[136] For this reason, most analyses with mass cytometry have been conducted with blood cancers or other disorders where retrieval of approximately 10^4 cells is facile. [138]

1.5. Chemical Cytometry

Cytometry is simply defined as the characterization of individual cells. Chemical cytometry, defined by Dovichi in 2003, is the use of high sensitivity analytical instrumentation to characterize the components of individual cells.[139,140] These are destructive assays which provide the opportunity to quantify and evaluate an ever-expanding number of compounds from a single cell, including nucleic acids, metabolites, and proteins. Inherent challenges with this type of analysis are twofold: i) small volumes associated with a single cell and ii) the limited mass or concentration of analytes. In the past, these challenges

21

were addressed by increasing the quantity of sample, with the rationale that the more material present, the greater the quantity of chemical entities to be detected. However, this is not necessarily true with heterogeneous populations. For example, if 0.1% of the cells in a tissue express a particular protein, then homogenization of the surrounding cells result in a 1000-fold dilution of the compound of interest, while maintaining the concentration of compounds common to all cells.[141] Thus, detection schemes for chemical cytometry must be adapted to the femtoliter volume and picogram protein content of a single cell. These span a wide array of technologies, including electrochemistry, mass spectrometry, and capillary electrophoresis (CE).

Electrochemical detection of ascorbic acid from single protoplast cells has been accomplished by a microfluidic chip which allows single cell lysis and electrophoretic separation of lysates, but has relatively high detection limits.[142] More recently, electrochemical detection has seen wide application in amperometric detection of neurotransmitters released from single cells via exocytosis.[143,144] In order to access additional biological analytes without derivatization, other methods are preferred. Single cell analysis has been accomplished with mass spectrometry, which is well suited to discovery-driven research. Rather than measuring changes in selective probes, mass spectrometry methods forego *a priori* selection of analytes and instead the mass of all peptides, proteins, oligonucleotides and lipids within a selected mass range are detected. The development of "soft" ionization techniques which limit fragmentation, such as Matrix Assisted Laser Desorption Ionization (MALDI) and Electrospray Ionization (ESI) have significantly contributed to the detection of these biomolecules. For example, Onjiko *et al.* utilized single cell micro-ESI-CE to detect changes in 50 compounds in different localizations of a 16-cell

blastocyte.[145] However, limitations of mass spectrometry lie primarily in the limited analytes

which can be determined within existing detection limits, which mostly linger in the

nanomolar domain. [146-148] Additionally, the ionization of some compounds may be more

efficient than others into the mass spectrometer, complicating the quantification process. For

these reasons, CE-based techniques with laser induced fluorescence detection (CE-LIF) are

perhaps the most well-known methodology for chemical cytometry. CE is capable of

physically separating the contents of an individual cell with very high resolution, peak

capacity, and limits of detection in the yoctomole range.

1.5.1 Principles of Capillary Electrophoresis

CE is an analytical separation technique which resolves analytes based on their

differential mobilities in an electric field. The seminal description of CE was published by

Jorgenson and Lukas in 1981,[149] and the technique has since seen wide application in

biopharmaceutical, clinical, and environmental analyses. CE employs hollow, fused silica

capillaries with small inner diameters ($<150\,\mu m$) which are filled with electrolytic buffer. A

sample is injected at the inlet, voltage is applied, and analytes are detected as they migrate

past a detection window typically located near the outlet (Figure 1.2a). The migration

velocity for a solute, specific for the ion and medium, is described in Equation 1.1. The

effective mobility of the ion is the sum of its electrophoretic mobility (μ_{ep}) and the

electroosmotic mobility of the electrolytic buffer (μ_{eof}).

The factors governing $\mu_{ep,}$, described in Equation 1.3 as a spherical analyte, includes

the net charge, which is opposed by frictional forces due to the hydrodynamic radius of the

analyte and the viscosity of the buffer (η). From this equation, it is evident that small, highly

23

charged molecules possess greater mobilities relative to large, minimally charged species. Neutral species have no inherent mobility in an electric field.

Equation 1.1 $$v = \mu_{eff}E$$

v = migration velocity

μ_{eff} = effective mobility

E= electric field (V/cm)

Equation 1.2 $$\mu_{eff} = \mu_{ep} + \mu_{eof}$$

μ_{eff} = effective mobility

μ_{ep} = electrophoretic mobility

μ_{eof} = electroosmotic flow mobility

Equation 1.3 $$\mu_{ep} = \frac{q}{6\pi\eta a}$$

q = net charge

η = buffer viscosity

a = hydrodynamic radius

The surface charge, or zeta potential (ζ), of the capillary also plays a large role in CE. The fused silica surface possesses silanol groups (SiOH), which have pKa values ranging from 2.5 to 6 and can be ionized to their anionic form (SiO⁻) through pretreatment with base.[150] The anionic surface results in the formation of an electrical double layer (Figure

1.2b). Cations, attracted from the bulk electrolyte, first form an adsorbed layer. This region, also known as the Stern layer, is immobile even in the presence of an electric field.[151] Beyond the Stern layer is a compact and mobile region occupied primarily by cations. Finally, the diffuse region, or Gouy-Chapman layer, extends past the mobile region. Beyond this electrical double layer (approximated at 100 Angstrom thickness) the zeta potential from the capillary wall is no longer sensed and the solution is effectively neutral. When a voltage is applied, the mobile cations near the wall migrate to the cathode. Since the ions are solvated, the bulk fluid in the Gouy-Chapman layer is dragged along as well. This electroosmotic flow (EOF; μ_{eof}) extends past the thin electrical double layer, presumably through hydrogen bonding of water molecules, to establish a flow of buffer through the entire capillary. Smoluchowski first described the EOF in 1903 with Equation 1.4.

Equation 1.4 $$\mu_{eof} = \frac{\zeta\varepsilon}{4\pi\eta}$$

μ_{eof} = migration of the electroosmotic flow

ζ = zeta potential

ε = dielectric constant

η = buffer viscosity

A key advantage of flow driven by electroosmosis rather than pressure is that it results in a plug-like, flat fluid velocity profile. When compared to the parabolic profile that arises in pressure driven flow due to interactions of the mobile phase with the tubing, electroosmosis results in increased separation efficiency. [152] Aside from enabling the EOF formation, the small diameter of the capillary has other advantages, including its high

electrical resistance which allows the application of very high electric fields (up to 500 V/cm) with minimal heat generation. Additionally, the lack of a stationary phase in free zone electrophoresis (CZE) eliminates the resistance to mass transfer between stationary and mobile phases, the primary cause of band broadening in traditional liquid chromatography (LC). Under ideal conditions, longitudinal diffusion is the only source of band broadening in CZE. This leads to very high separation efficiencies, which is typically quantified as the number of theoretical plates (N; Equation 1.5). Separations with high plate numbers are considered to be more efficient, and CE separations are known to have unparalleled resolving power. Multiple groups have reported millions of theoretical plates for the separation of synthetic peptides. [153,154]

Equation 1.5
$$N = 5.545 \left(\frac{t_m}{w_h}\right)^2$$

N= number of theoretical plates

t_m = migration time

w_h= peak width at half height

The EOF is a crucial aspect of CE since it sweeps neutral molecules towards the detector, which do not migrate in an electric field. However, the separation of such neutral molecules is often difficult to achieve with CZE alone. Micellar Electrokinetic Capillary Chromatography (MEKC) is a hybrid method which utilizes both electrophoretic and chromatographic separation principles to separate neutral analytes. Surfactant molecules are added to the electrolytic buffer until micelles are formed, which act as a psuedostationary phase. When sodium dodecyl sulfate (SDS) is utilized as a surfactant, micelles possess a

hydrophobic core with a negatively charged outer shell. These micelles experience

electrophoretic migration like any other charged particle in CZE, but they also interact with

analytes through electrostatic and hydrophobic interactions.[155] Owing to their negative

charge, SDS micelles generally migrate against, albeit at a slower velocity than, the EOF

when a positive voltage is applied, and thus are relatively late migrating. The dynamic

partitioning that occurs with analytes, including neutral molecules, between large micelles

and free solution provides an additional separation dimension that can distinguish between

similar analytes. For example, chiral separations have been successful with MEKC owing to

the affinity of the enantiomers towards the micelles.[156] In general, the fraction of analyte

incorporated into the micelle (n_{mc}) versus the aqueous phase (n_{aq}) is modeled by the capacity

factor (k'), similar to chromatography.

Equation 1.6 $$k' = \frac{n_{mc}}{n_{aq}}$$

k' = capacity factor

n_{mc} = fraction of the analyte incorporated into the micelle

n_{aq} = fraction of the analyte in the aqueous phase

The micelle partitioning process directly affects the resolution (R) for MEKC, which

is given in Equation 1.7. MEKC separations have been performed with theoretical plate

values as high as 900,000.[157] These values are often lower than theoretical plates obtained

with CZE since MEKC separations tend to be longer due to the later migrating micelles.

Since longitudinal diffusion is the defining factor for efficiency, a shorter separation

produces higher efficiency. However, the increased resolution of neutral analytes granted by

MEKC is often a welcome trade-off. For this reason, many of the peptide separations

described in Chapters 2 and 3 of this dissertation were performed with MEKC.

Equation 1.7 $$R = \frac{\sqrt{N}}{4}\left(\frac{\alpha-1}{\alpha}\right)\left(\frac{k_2'}{1+k_2'}\right)\left(\frac{1-t_0/t_{mc}}{1+(t_0/t_{mc})k_1'}\right)$$

N= theoretical plates

α = separation factor

k_1' = capacity factor for analyte 1

k_2' = capacity factor for analyte 2

t_0 = migration time for an analyte experiencing no interaction with micelles

t_{mc} = migration time for an analyte totally incorporated into micelles

There are a variety of detection schemes which are compatible with both MEKC and

CE including absorbance, fluorescence, photothermal refraction, amperometry, and

conductivity.[158] The most sensitive is laser induced fluorescence (LIF), in which fluorescent

molecules are excited by a laser as they pass by the detection window. Since only fluorescent

analytes are excited this technique boasts high selectivity and eliminates potential

contaminants including assay components or cellular debris. LIF also has excellent limits of

detection, with frequent reports of 10^{-21} moles or lower.[159-161]

1.5.2 Using Peptides as Reporters of Kinase Activity

Short peptide sequences are simple to synthesize, relatively inexpensive, and highly

customizable.[162,163] When peptide substrates are based on known consensus sequences and

possess the requisite amino acids for phosphorylation, they are useful tools for assessing

kinase activity. They can also be selectively labeled at the N-terminus with a fluorophore for detection with CE-LIF. Since both the native and phosphorylated versions of the peptide exhibit fluorescence, they can simply be separated by CE or MEKC to quantify the relative amounts of each. The Allbritton lab has extensive experience in the utilization of peptides as reporters of kinase[164-170] protease,[171-177] and phosphatase activity. [178,179] This dissertation will focus on the use of peptides as reporters for kinases and proteases.

One major challenge associated with peptides as intracellular kinase activity reporters involves their delivery to a single cell. Hydrophobic molecules such as steroids are lipid soluble and can enter the cell by passive diffusion across the plasma membrane, while most peptides cannot permeate the membrane. However, there are multiple existing methods for introducing macromolecules into living cells. Microinjection is an effective method for peptide delivery, but is extremely low throughput and requires skilled operators. Pinocytic loading, electroporation, and optoporation have also been utilized to introduce peptides into cells.[180-183] While these methods are useful for high throughput peptide loading, they can induce significant cellular stress that may activate the survival pathways and artificially increase the kinase activity measured, obscuring accurate measurements of normal versus aberrant enzyme activity. Cell permeable peptides such as HIV-TAT and octoarginine have also been reported, but often result in endocytic uptake which can prevent the reporter from interacting with cytosolic enzymes such as Akt.[184-186] Chemical innovations to overcome such peptide delivery challenges are described in Chapter 3.

1.5.3 Single Cell Capillary Electrophoresis

Capillary electrophoresis was first utilized to analyze the contents of individual cells in a series of publications by Jorgenson *et al*, the same group known for the formative publications on CZE. In all cases, giant neurons were the cells of interest. Individual cells were homogenized and their contents injected into a CZE system. Molecules possessing primary amines were labeled with naphthalene-2,3-dicarboxyaldehyde (NDA) for fluorescence detection.[187,188] This enabled the identification of tryptophan, tyrosine, and 5-hydroxytryptophan (5-HT) from a single cell lysate. By 1994, Jorgenson had partnered with Wightman to detect intracellular and excreted catecholamines from single neurons. [189,190] There have since been significant developments in analysis of compounds from individual cells from countless cell types, including primary cells. A large number of proteins have been identified by utilizing a two-dimensional capillary sieving electrophoresis separation combined with MEKC.[191] However, a large remaining challenge associated with single cell-CE is the low throughput. Often up to 15 cells can be manually analyzed with CE per day, owing to the serial nature of analysis, manual positioning of the capillary, and the challenges with delivering reporters to cells. Dovichi has improved throughput for single cell analysis with a multiplexed array of up to 5 capillaries which can simultaneously sample the contents of single cells.[192] Microfluidic platforms also require mention since they are capable of analyzing hundreds of cells per hour, but their use is often limited to nonadherent cell types.[172,193] Recently, Dickinson *et al* reported a fully-automated CE system capable of analyzing 3.2 cells per minute, rivaling microfluidic devices and providing the robust separations of a capillary-based method. [194]

1.6 Scope of Dissertation

The following chapters of this dissertation will describe the development and characterization of an assay for measurement of Akt activity in single cells utilizing chemical cytometry. Chapter 2, which is submitted as a manuscript to *Analytical Chemistry*, describes the characterization of Akt activity in FLS from healthy subjects as well as those suffering from RA. Chapter 3 will discuss the photochemical modification of an Akt peptide reporter, resulting in improvements in the throughput of enzyme activity measurements in pancreatic cancer cells when paired with an automated, high throughput CE system. This chapter is in preparation to be submitted as a manuscript to *Angewandte Chemie International Edition*. Chapter 4 describes preliminary work on the development of a degradation-resistant Akt reporter through a rational design strategy. In chapter 5, methodology to track peptide metabolism in individual cells will be described. This chapter has been published in *Analytical Chemistry*.[195]

1.7 Figures
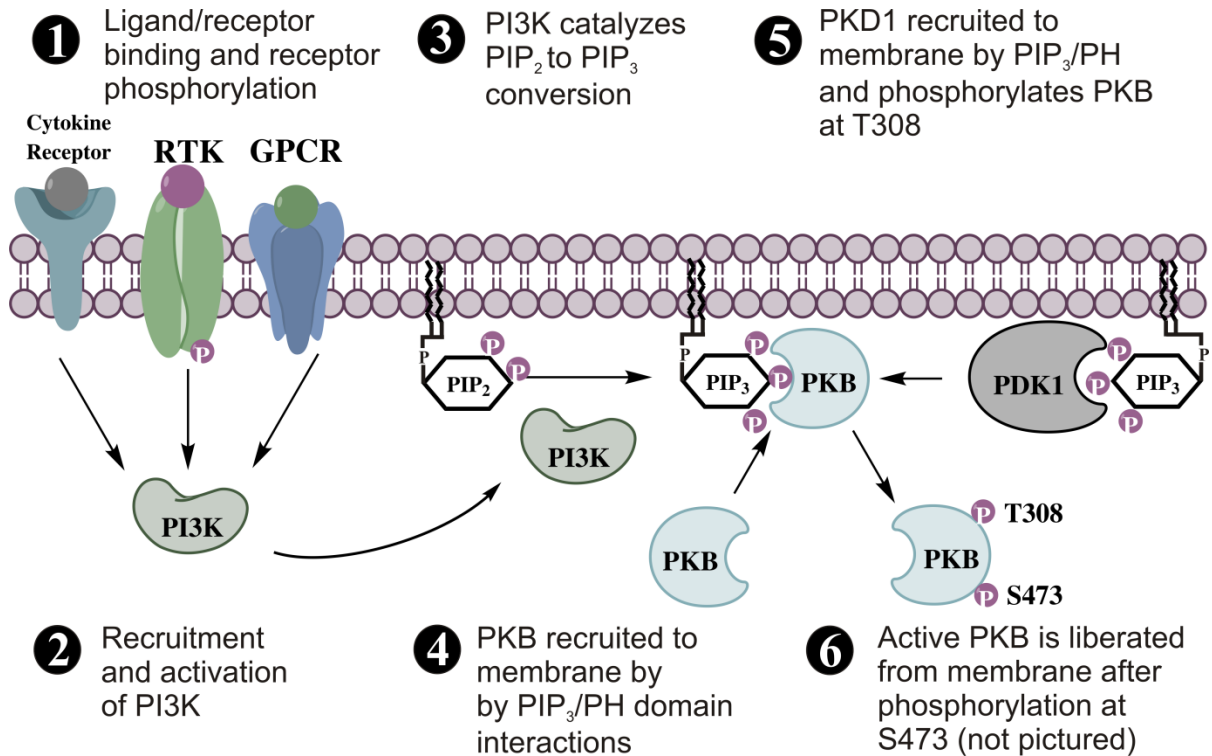
Figure 1.1 A simplified schematic of Akt (*aka* PKB) activation. Akt can be stimulated by binding of growth factors, cytokines, and other ligands which activate PI3K. Akt is recruited to the membrane where it is partially activated by PDK1 (at T308) and fully activated by phosphorylation at S473. Active Akt diffuses away from the membrane to phosphorylate its downstream targets.
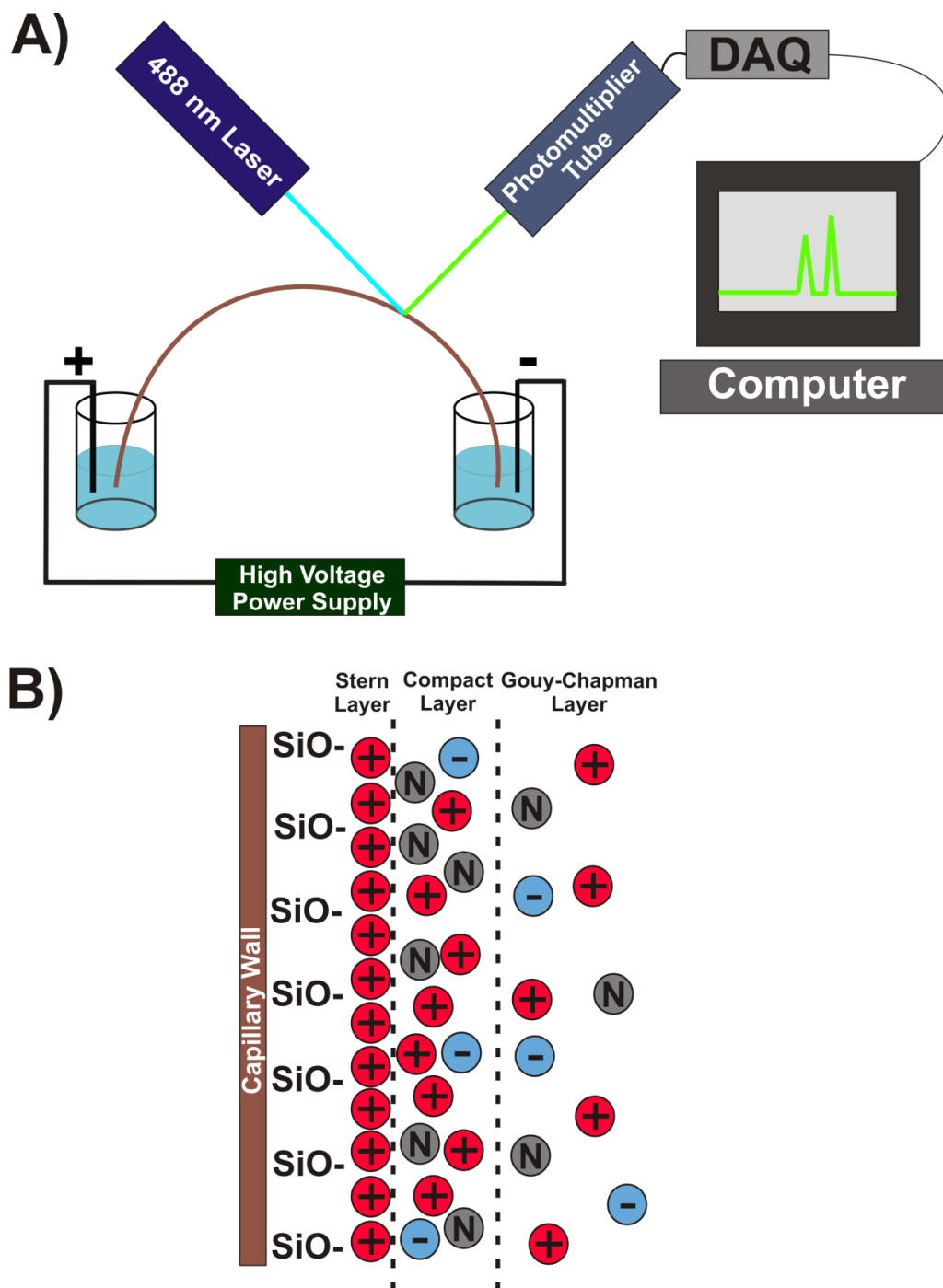
Figure 1.2 Capillary electrophoresis. A) Schematic of a CE system. The capillary is submerged in buffer while a high voltage is applied. Analytes reach the detection window, where they are interrogated with a 488 nm solid state laser. Emission at 530 nm is detected with a photomultiplier tube before processing with a Digital-to-Analog Converter (DAQ) and output onto a computer. B) Formation of the electrical double layer required for electroosmotic flow (EOF).

REFERENCES

1. Mann, M.; Jensen, O. N. Proteomic analysis of post-translational modifications. *Nat. Biotechnol.* 2003*, 21*, 255-261.

2. Fabbro, D.; Cowan-Jacob, S. W.; Moebitz, H. Ten things you should know about protein kinases: IUPHAR Review 14. *Br J Pharmacol* 2015*, 172*, 2675-2700.

3. Komander, D.; Rape, M. The Ubiquitin Code. *Annual Review of Biochemistry* 2012*, 81*, 203-229.

4. Knowles, J. R. Enzyme-Catalyzed Phosphoryl Transfer Reactions. *Annual Review of Biochemistry* 1980*, 49*, 877-919.

5. Cheng, H.; Qi, R. Z.; Paudel, H.; Zhu, H. Regulation and function of protein kinases and phosphatases. *Enzyme Res* 2011*, 2011*, 794089.

6. Graves, J. D.; Krebs, E. G. Protein Phosphorylation and Signal Transduction. *Pharmacology and Therapeutics* 1999*, 82*, 111.

7. Savage, D. G.; Antman, K. H. Imatinib mesylate--a new oral targeted therapy. *N. Engl. J. Med.* 2002*, 346*, 683-693.

8. Fischer, E. H. Phosphorylase and the origin of reversible protein phosphorylation. *Biol. Chem.* 2010*, 391*, 131-137.

9. Cohen, P. The origins of protein phosphorylation. *Nat Cell Biol* 2002*, 4*, E130.

10. Griner, E. M.; Kazanietz, M. G. Protein kinase C and other diacylglycerol effectors in cancer. *Nat Rev Cancer* 2007*, 7*, 281-294.

11. Gschwind, A.; Fischer, O. M.; Ullrich, A. The discovery of receptor tyrosine kinases: targets for cancer therapy. *Nat Rev Cancer* 2004*, 4*, 361-370.

12. Tamaoki, T.; Nomoto, H.; Takahashi, I.; Kato, Y.; Morimoto, M.; Tomita, F. Staurosporine, a potent inhibitor of phospholipid/Ca++dependent protein kinase. *Biochem. Biophys. Res. Commun.* 1986*, 135*, 397-402.

13. Nakano, H.; Omura, S. Chemical biology of natural indolocarbazole products: 30 years since the discovery of staurosporine. *J. Antibiot.* 2009*, 62*, 17-26.

14. Fabian, M. A.; Biggs, W. H.; Treiber, D. K.; Atteridge, C. E.; Azimioara, M. D.; Benedetti, M. G.; Carter, T. A.; Ciceri, P.; Edeen, P. T.; Floyd, M.; Ford, J. M.; Galvin, M.; Gerlach, J. L.; Grotzfeld, R. M.; Herrgard, S.; Insko, D. E.; Insko, M. A.; Lai, A. G.; Lélias, J.; Mehta, S. A.; Milanov, Z. V.; Velasco, A. M.; Wodicka, L. M.; Patel, H. K.;

Zarrinkar, P. P.; Lockhart, D. J. A small molecule–kinase interaction map for clinical kinase inhibitors. *Nat Biotech* 2005, *23*, 329-336.

15. O'Brien, S. G.; Guilhot, F.; Larson, R. A.; Gathmann, I.; Baccarani, M.; Cervantes, F.; Cornelissen, J. J.; Fischer, T.; Hochhaus, A.; Hughes, T.; Lechner, K.; Nielsen, J. L.; Rousselot, P.; Reiffers, J.; Saglio, G.; Shepherd, J.; Simonsson, B.; Gratwohl, A.; Goldman, J. M.; Kantarjian, H.; Taylor, K.; Verhoef, G.; Bolton, A. E.; Capdeville, R.; Druker, B. J. Imatinib Compared with Interferon and Low-Dose Cytarabine for Newly Diagnosed Chronic-Phase Chronic Myeloid Leukemia. *New England Journal of Medicine* 2003, *348*, 994-1004.

16. Wu, P.; Nielsen, T. E.; Clausen, M. H. Small-molecule kinase inhibitors: an analysis of FDA-approved drugs. *Drug Discovery Today* 2016, *21*, 5-10.

17. Fleischmann, R.; Kremer, J.; Cush, J.; Schulze-Koops, H.; Connell, C. A.; Bradley, J. D.; Gruben, D.; Wallenstein, G. V.; Zwillich, S. H.; Kanik, K. S. Placebo-Controlled Trial of Tofacitinib Monotherapy in Rheumatoid Arthritis. *New England Journal of Medicine* 2012, *367*, 495-507.

18. Seiwert, T.; Sarantopoulos, J.; Kallender, H.; McCallum, S.; Keer, H. N.; Blumenschein, G. Phase II trial of single-agent foretinib (GSK1363089) in patients with recurrent or metastatic squamous cell carcinoma of the head and neck. *Invest New Drugs* 2013, *31*, 417-424.

19. Torti, D.; Trusolino, L. Oncogene addiction as a foundational rationale for targeted anti-cancer therapy: promises and perils. *EMBO Mol Med* 2011, *3*, 623-636.

20. Sharma, S. V.; Settleman, J. Oncogene addiction: setting the stage for molecularly targeted cancer therapy. *Genes Dev.* 2007, *21*, 3214-3231.

21. Richeldi, L.; du Bois, R. M.; Raghu, G.; Azuma, A.; Brown, K. K.; Costabel, U.; Cottin, V.; Flaherty, K. R.; Hansell, D. M.; Inoue, Y.; Kim, D. S.; Kolb, M.; Nicholson, A. G.; Noble, P. W.; Selman, M.; Taniguchi, H.; Brun, M.; Le Maulf, F.; Girard, M.; Stowasser, S.; Schlenker-Herceg, R.; Disse, B.; Collard, H. R. Efficacy and Safety of Nintedanib in Idiopathic Pulmonary Fibrosis. *New England Journal of Medicine* 2014, *370*, 2071-2082.

22. Gharwan, H.; Groninger, H. Kinase inhibitors and monoclonal antibodies in oncology: clinical implications. *Nat Rev Clin Oncol* 2016, *13*, 209-227.

23. Brazil, D. P.; Hemmings, B. A. Ten Years of protein kinase B signalling: a hard Akt to follow. *TRENDS in biochemical sciences* 2001, *26*, 657.

24. Datta, S. R.; Brunet, A.; Greenberg, M. E. Cellular survival: a play in three Akts. *Genes Dev.* 1999, *13*, 2905-2927.

25. Jiang, B. H.; Liu, L. Z. AKT signaling in regulating angiogenesis. *Current Cancer Drug Targets* 2008, *8*, 19.

26. Kohn, A. D.; Tekeuchi, F.; Roth, R. A. Akt, a Pleckstrin Homology Domain Containing Kinase, Is Activated Primarily by Phosphorylation. *The Journal of Biological Chemistry* 1996, 21920.

27. Pearce, L. R.; Komander, D.; Alessi, D. R. The nuts and bolts of AGC protein kinases. *Nat Rev Mol Cell Biol* 2010, *11*, 9-22.

28. Kumar, C. C.; Madison, V. AKT crystal structure and AKT-specific inhibitors. *Oncogene* 2005, *24*, 7493-7501.

29. Testa, J. R.; Bellacosa, A. AKT plays a central role in tumorigenesis. *98* 2001, *20*.

30. Hemmings, B. A.; Restuccia, D. F. PI3K-PKB/Akt Pathway. *Cold Spring Harb Perspect Biol* 2012, *4*, a011189.

31. Hart, J. R.; Vogt, P. K. Phosphorylation of AKT: a Mutational Analysis. *Oncotarget* 2011, *2*, 467-476.

32. Guertin, D. A.; Stevens, D. M.; Thoreen, C. C.; Burds, A. A.; Kalaany, N. Y.; Moffat, J.; Brown, M.; Fitzgerald, K. J.; Sabatini, D. M. Ablation in mice of the mTORC components raptor, rictor, or mLST8 reveals that mTORC2 is required for signaling to Akt-FOXO and PKCalpha, but not S6K1. *Dev. Cell* 2006, *11*, 859-871.

33. Bozulic, L.; Hemmings, B. A. PIKKing on PKB: regulation of PKB activity by phosphorylation. *Curr. Opin. Cell Biol.* 2009, *21*, 256-261.

34. Sarbassov, D. D.; Guertin, D. A.; Ali, S. M.; Sabatini, D. M. Phosphorylation and regulation of Akt/PKB by the rictor-mTOR complex. *Science* 2005, *307*, 1098-1101.

35. Feng, J.; Park, J.; Cron, P.; Hess, D.; Hemmings, B. A. Identification of a PKB/Akt hydrophobic motif Ser-473 kinase as DNA-dependent protein kinase. *J. Biol. Chem.* 2004, *279*, 41189-41196.

36. Georgescu, M. PTEN Tumor Suppressor Network in PI3K-Akt Pathway Control. *Genes & Cancer* 2010, *1*, 1170.

37. Yuan, T. L.; Cantley, L. C. PI3K pathway alterations in cancer: variations on a theme. *Oncogene* 2008, *27*, 5497.

38. Siegel, R. L.; Miller, K. D.; Jemal, A. Cancer statistics, 2016. *CA: A Cancer Journal for Clinicians* 2016, *66*, 7-30.

39. Oettle, H.; Post, S.; Neuhaus, P.; Gellert, K.; Langrehr, J.; Ridwelski, K.; Schramm, H.; Fahlke, J. Adjuvant Chemotheraphy with Gemcitabine vs Observation in Patients Undergoing Curative- Intent Resection of Pancreatic Cancer. *Journal of the American Medical Association* 2007*, 297*, 267.

40. Gonzalez, E.; McGram, T. E. The Akt Kinases: isoform specificity in metabolism and cancer. *Cell Cycle* 2009*, 16*, 2502.

41. Eyler, C. E.; Foo, W. C.; LaFiura, F. M. Brain cancer stem cells display preferential sensitivity to Akt inhibition. *Stem Cells* 2008*, 26*, 3027.

42. Mortenson, M.; Galante, J. M.; Schlieman, M.; Bold, R. J. AKT: A novel target in pancreatic cancer therapy. *Cancer Therapy* 2004*, 2*, 227.

43. Ottenhof, N. A.; de Wilde, R. F.; Maitra, A.; Hruban, R. H.; Offerhaus, G. J. A. Molecular Characteristics of Pancreatic Dunctal Adenocarcinoma. *Pathology Research International* 2011*, 2011*.

44. Eser, S.; Schnieke, A.; Schneider, G.; Saur, D. Oncogenic KRAS signalling in pancreatic cancer. *Br J Cancer* 2014*, 111*, 817-822.

45. Altomare, D. A.; Testa, J. R. Perturbations of the AKT signaling pathway in human cancer. *Oncogene* 2005*, 24*, 7455-7464.

46. Surucu; Bozulic; Hynx; Parcellier; Hemmings In Vivo Analysis of Protein Kinase B (PKB)/Akt Regulation in DNA-PKcs-null Mice Reveals a Role for PKB/Akt in DNA Damage Response and Tumorigenesis. *Journal of Biological Chemistry* 2008*, 283*, 30025-30033.

47. Yamamoto, S.; Tomita, Y.; Hoshida, Y.; Morooka, T.; Nagano, H.; Dono, K.; Umeshita, K.; Sakon, M.; Ishikawa, O.; Ohigashi, H.; Nakamori, S.; Monden, M.; Aozasa, K. Prognostic significance of activated Akt expression in pancreatic ductal adenocarcinoma. *Clin. Cancer Res.* 2004*, 10*, 2846-2850.

48. Schlieman, M. G.; Fahy, B. N.; Ramsamooj, R.; Beckett, L.; Bold, R. J. Incidence, mechanism and prognostic value of activated AKT in pancreas cancer. *Br. J. Cancer* 2003*, 89*, 2110-2115.

49. Mohamedali, A.; Lea, N. C.; Feakins, R. M.; Raj, K.; Mufti, G. J.; Kocher, H. M. AKT1 (E17K) mutation in pancreatic cancer. *Technol. Cancer Res. Treat.* 2008*, 7*, 407-408.

50. Albury, T. M.; Pandey, V.; Gitto, S. B.; Dominguez, L.; Spinel, L. P.; Talarchek, J.; Klein-Szanto, A. J.; Testa, J. R.; Altomare, D. A. Constitutively Active Akt1 Cooperates

with KRasG12D to Accelerate In Vivo Pancreatic Tumor Onset and Progression. *Neoplasia* 2015*, 17*, 175-182.

51. Schlieman, M. G.; Fahy, B. N.; Ramsamooj, R.; Beckett, L.; Bold, R. J. Incidence, mechanism and prognostic value of activated AKT in pancreas cancer. *Br J Cancer* 2003*, 89*, 2110-2115.

52. Ying, H.; Elpek, K. G.; Vinjamoori, A.; Zimmerman, S. M.; Chu, G. C.; Yan, H.; Fletcher-Sananikone, E.; Zhang, H.; Liu, Y.; Wang, W.; Ren, X.; Zheng, H.; Kimmelman, A. C.; Paik, J.; Lim, C.; Perry, S. R.; Jiang, S.; Malinn, B.; Protopopov, A.; Colla, S.; Xiao, Y.; Hezel, A. F.; Bardeesy, N.; Turley, S. J.; Wang, Y. A.; Chin, L.; Thayer, S. P.; DePinho, R. A. PTEN is a major tumor suppressor in pancreatic ductal adenocarcinoma and regulates an NF-κB-cytokine network. *Cancer Discov* 2011*, 1*, 158-169.

53. Sun, S.; Rosenberg, L. M.; Wang, X.; Zhou, Z.; Yue, P.; Fu, H.; Khuri, F. R. Activation of Akt and eIF4E Survival Pathways by Rapamycin-Mediated Mammalian Target of Rapamycin Inhibition. *Cancer Research* 2005, 7052.

54. DeFeo-Jones, D.; Barnett, S. F.; Fu, S.; Hancock, P. J.; Haskell, K. M.; Leander, K. R.; McAvoy, E.; Robinson, R. G.; Duggan, M. E.; Lindsley, C. W.; Zhao, Z.; Huber, H. E.; Jones, R. E. Tumor cell sensitization to apoptotic stumuli by selective inhibition of specific Akt/PKB family members. *Molecular Cancer Therapeutics* 2005*, 4*, 271.

55. Matsubara, S.; Ding, Q.; Miyazaki, Y.; Kuwahata, T.; Tsukasa, K.; Takao, S. mTOR plays critical roles in pancreatic cancer stem cells through specific and stemness-related functions. *Scientific Reports* 2013*, 3*, 3230.

56. Xia, P.; Xu, X. PI3K/Akt/mTOR signaling pathway in cancer stem cells: from basic research to clinical application. *Am J Cancer Res* 2015*, 5*, 1602-1609.

57. Sharma, N.; Nanta, R.; Sharma, J.; Gunewardena, S.; Singh, K. P.; Shankar, S.; Srivastava, R. K. PI3K/AKT/mTOR and sonic hedgehog pathways cooperate together to inhibit human pancreatic cancer stem cell characteristics and tumor growth. *Oncotarget* 2015*, 6*, 32039-32060.

58. Helmick, C. G.; Felson, D. T.; Lawrence, R. C.; Gabriel, S.; Hirsch, R.; Kwoh, C. K.; Liang, M. H.; Kremers, H. M.; Mayes, M. D.; Merkel, P. A.; Pillemer, S. R.; Reveille, J. D.; Stone, J. H. Estimates of the prevalence of arthritis and other rheumatic conditions in the United States. Part I. *Arthritis Rheum.* 2008*, 58*, 15-25.

59. Glocker, M. O.; Guthke, R.; Kekow, J.; Thiesen, H. Rheumatoid arthritis, a complex multifactorial disease: on the way toward individualized medicine. *Med Res Rev* 2006, *26*, 63-87.

60. Suresh, E. Diagnosis of early rheumatoid arthritis: what the non-specialist needs to know. *JRSM* 2004, *97*, 421.

61. Bartok, B.; Firestein, G. S. Fibroblast-like synoviocytes: key effector cells in rheumatoid arthritis. *Immunology Review* 2010, *233*, 233.

62. Huber, L. C.; Distler, O.; Tarner, I.; Gay, R. E.; Gay, S.; Pap, T. Synovial fibroblasts: key players in rheumatoid arthritis. *Rheumatology* 2006, *45*, 669-675.

63. Seemayer, C. A.; Kuchen, S.; Kuenzler, P.; Rihoskova, V.; Gay, S. Cartilage destruction mediated by synovial fibroblasts does depend on proliferation in rheumatoid arthritis. *Am J Pathology* 2003, *165*, 1549.

64. Lefevre, S.; Knedla, A.; Tennie, C.; Kampmann, A.; Wunrau, C.; Dinser, R.; Korb, A.; Schnaker, E.; Tarner, I. P., T.; Muller-Ladner, U. N., E. Synovial fibroblasts spread rheumatoid arthritis to unaffected joints. *Nature Medicine* 2009, *15*, 1414.

65. Neumann, E.; Lefèvre, S.; Zimmermann, B.; Geyer, M.; Lehr, A.; Umscheid, T.; Schönburg, M.; Rehart, S.; Müller-Ladner, U. Migratory potential of rheumatoid arthritis synovial fibroblasts: additional perspectives. *Cell Cycle* 2010, *9*, 2286-2291.

66. Malemud, C. J. Intracellular Signaling Pathways in Rheumatoid Arthritis. *Journal of Clinical & Cellular Immunology* 2013, *160*.

67. Lundquist, L. M.; Cole, S. W.; Sikes, M. L. Efficacy and safety of tofacitinib for treatment of rheumatoid arthritis. *World J Orthop* 2014, *5*, 504-511.

68. Mountz, J. D.; Zhang, H.; Wang, Y.; Xie, J. F.; Liang, X.; Hsu, H.; Curiel, D. T. AKT regulates TNF-alpha-mediated apoptosis of rheumatoid arthritis synovial fibroblasts. *Arthritis Res* 2001, *3*, P8.

69. Zhang, H.; Wang, Y.; Xie, J. F.; Liang, X.; Liu, D.; Yang, P.; Hsu, H. C.; Ray, R. B.; Mountz, J. D. Regulation of Tumor Necrosis Factor alpha-mediated Apoptosis of RASF by PKB. *Arthritis and Rheumatism* 2001, *44*, 1555.

70. Camps, M.; Ruckle, T.; Ardissone, V.; Rintelen, F.; Shaw, J.; Ferrandi, C.; Chabert, C.; Gillieron, C.; Fracon, B.; Rommel, C. Blockade of PI3Kgamma suppresses joint inflammation and damage in mouse models of rheumatoid arthritis. *Nature Medicine* 2005, *9*.

71. Neovius, M.; Arkema, E. V.; Olsson, H.; Eriksson, J. K.; Kristensen, L. E.; Simard, J. F.; Askling, J.; Bäcklund, E.; Cöster, L.; Forsblad-d'Elia, H.; Feltelius, N.; Jacobsson, L.; Klareskog, L.; Lindblad, S.; Rantapää-Dahlqvist, S.; Saxne, T.; Vollenhoven, R. v. Drug survival on TNF inhibitors in patients with rheumatoid arthritis comparison of adalimumab, etanercept and infliximab. *Ann Rheum Dis* 2015, *74*, 354-360.

72. Rubbert-Roth, A.; Finckh, A. Treatment options in patients with rheumatoid arthritis failing initial TNF inhibitor therapy: a critical review. *Arthritis Res Ther* 2009, *11*, 1-12.

73. Madge, L. A.; Pober, J. S. A Phosphatidylinositol 3-Kinase/Akt Pathway, Activated by Tumor Necrosis Factor or Interleukin-1, Inhibits Apoptosis but Does Not Activate NFκB in Human Endothelial Cells. *J. Biol. Chem.* 2000, *275*, 15458-15465.

74. García, S.; Liz, M.; Gómez-Reino, J. J.; Conde, C. Akt activity protects rheumatoid synovial fibroblasts from Fas-induced apoptosis by inhibition of Bid cleavage. *Arthritis Res Ther* 2010, *12*, R33.

75. Altschuler, S. J.; Wu, L. F. Cellular Heterogeneity: Do Differences Make a Difference? *Cell* 2010, *141*, 559-563.

76. Turner, N. C.; Reis-Filho, J. S. Genetic heterogeneity and cancer drug resistance. *The Lancet Oncology* 2012, *13*, e185.

77. Samuel, N.; Hudson, T. J. The molecular and cellular heterogeneity of pancreatic ductal adenocarcinoma. *Nature Reviews: Gastroenterology and Hepatology* 2012, *9*, 77.

78. Wu, J.; Tzanakakis, E. S. Deconstructing stem cell population heterogeneity: Single-cell analysis and modeling approaches. *Biotechnol Adv* 2013, *31*, 1047-1062.

79. Navin, N.; Kendall, J.; Troge, J.; Andrews, P.; Rodgers, L.; McIndoo, J.; Cook, K.; Stepansky, A.; Levy, D.; Esposito, D.; Muthuswamy, L.; Krasnitz, A.; McCombie, W. R.; Hicks, J.; Wigler, M. Tumour evolution inferred by single-cell sequencing. *Nature* 2011, *472*, 90-94.

80. Süel, G. M.; Kulkarni, R. P.; Dworkin, J.; Garcia-Ojalvo, J.; Elowitz, M. B. Tunability and noise dependence in differentiation dynamics. *Science* 2007, *315*, 1716-1719.

81. Spencer, S. L.; Gaudet, S.; Albeck, J. G.; Burke, J. M.; Sorger, P. K. Non-genetic origins of cell-to-cell variability in TRAIL-induced apoptosis. *Nature* 2009, *459*, 428-432.

82. Stegle, O.; Parts, L.; Durbin, R.; Winn, J. A Bayesian framework to account for complex non-genetic factors in gene expression levels greatly increases power in eQTL studies. *PLoS Comput. Biol.* 2010, *6*, e1000770.

83. Eldar, A.; Elowitz, M. B. Functional roles for noise in genetic circuits. *Nature* 2010, *467*, 167-173.

84. Kikkawa, U.; Kishimoto, A.; Nishizuka, Y. The Protein Kinase C Family: Heterogeneity and its Implications. *Annual Review of Biochemistry* 1989, *58*, 31-44.

85. Voliotis, M.; Perrett, R. M.; McWilliams, C.; McArdle, C. A.; Bowsher, C. G. Information transfer by leaky, heterogeneous, protein kinase signaling systems. *PNAS* 2014, *111*, E333.

86. Anselmetti, D. *Wiley-VCH - Anselmetti, Dario (ed.) - Single Cell Analysis;* Wiley-VCH: Weinheim, Germany, 2009; .

87. Yuan, T. L.; Wulf, G.; Burga, L.; Cantley, L. C. Cell-to-Cell Variability in PI3K Protein Level Regulates PI3K-AKT Pathway Activity in Cell Populations. *Current Biology* 2011, *21*, 173-183.

88. Meyer, R.; D'Alessandro, L. A.; Kar, S.; Kramer, B.; She, B.; Kaschek, D.; Hahn, B.; Wrangborg, D.; Karlsson, J.; Kvarnström, M.; Jirstrand, M.; Lehmann, W.; Timmer, J.; Höfer, T.; Klingmüller, U. Heterogeneous kinetics of AKT signaling in individual cells are accounted for by variable protein concentration. *Front Physiol* 2012, *3*, 451.

89. Dickson, L. M.; Lingohr, M. K.; McCuaig, J.; Hügl, S. R.; Snow, L.; Kahn, B. B.; Myers, J. M. G.; Rhodes, C. J. Differential Activation of Protein Kinase B and p70S6K by Glucose and Insulin-like Growth Factor 1 in Pancreatic β-Cells (INS-1). *Journal of Biological Chemistry* 2001, *276*, 21110-21120.

90. Torsvik, A.; Stieber, D.; Enger, P. Ø; Golebiewska, A.; Molven, A.; Svendsen, A.; Westermark, B.; Niclou, S. P.; Olsen, T. K.; Chekenya Enger, M.; Bjerkvig, R. U-251 revisited: genetic drift and phenotypic consequences of long-term cultures of glioblastoma cells. *Cancer Med* 2014, *3*, 812-824.

91. Briske-Anderson, M. J.; Finley, J. W.; Newman, S. M. The influence of culture time and passage number on the morphological and physiological development of Caco-2 cells. *Proc. Soc. Exp. Biol. Med.* 1997, *214*, 248-257.

92. Lee, H.; Yoon, T.; Figueiredo, J.; Swirski, F. K.; Weissleder, R. Rapid detection and profiling of cancer cells in fine-needle aspirates. *PNAS* 2009, *106*, 12459-12464.

93. Lai, K.; Chen, H.; Wen, M.; Chen, Y.; Lan, J.; Chen, D. Minimally Invasive Ultrasound-guided Synovial Biopsy Using SuperCore Biopsy Instrument. *Journal of Medical Ultrasound* 2013, *21*, 132-137.

94. Turner, A. H. Epidermal Growth Factor Receptor Tyrosine Kinase Assays in Single Intact Cells Using Capillary Electrophoresis, University of North Carolina, 2015.

95. Gopalakrishna, R.; Chen, Z. H.; Gundimeda, U.; Wilson, J. C.; Anderson, W. B. Rapid filtration assays for protein kinase C activity and phorbol ester binding using multiwell plates with fitted filtration discs. *Anal. Biochem.* 1992*, 206*, 24-35.

96. Morrow, C. J.; Gray, A.; Dive, C. Comparison of phosphatidylinositol-3-kinase signalling within a panel of human colorectal cancer cell lines with mutant or wild-type PIK3CA. *FEBS Letters* 2005*, 579*, 5123-5128.

97. Reuveni, H.; Livnah, N.; Geiger, T.; Klein, S.; Ohne, O.; Cohen, I.; Benhar, M.; Gellerman, G.; Levitzki, A. Toward a PKB inhibitor: modification of a selective PKA inhibitor by rational design. *Biochemistry* 2002*, 41*, 10304-10314.

98. Hastie, C. J.; McLauchlan, H. J.; Cohen, P. Assay of protein kinases using radiolabeled ATP: a protocol. *Nat. Protocols* 2006*, 1*, 968-971.

99. Park, Y.; Cummings, R. T.; Wu, L.; Zheng, S.; Cameron, P. M.; Woods, A.; Zaller, D. M.; Marcy, A. I.; Hermes, J. D. Homogeneous Proximity Tyrosine Kinase Assays: Scintillation Proximity Assay versus Homogeneous Time-Resolved Fluorescence. *Analytical Biochemistry* 1999*, 269*, 94-104.

100. Koresawa, M.; Okabe, T. High-Throughput Screening with Quantitation of ATP Consumption: A Universal Non-Radioisotope, Homogeneous Assay for Protein Kinase. *ASSAY and Drug Development Technologies* 2004*, 2*, 153-160.

101. Quercia, A. K.; LaMarr, W. A.; Myung, J.; Ozbal, C. C.; Landro, J. A.; Lumb, K. J. High-throughput screening by mass spectrometry: comparison with the scintillation proximity assay with a focused-file screen of AKT1/PKB alpha. *J Biomol Screen* 2007*, 12*, 473-480.

102. AnonymousFluorescence Anisotropy. In *Principles of Fluorescence Spectroscopy*; Lakowicz, J. R., Ed.; Springer US: 2006; pp 353-382.

103. Jameson, D. M.; Ross, J. A. Fluorescence Polarization/Anisotropy in Diagnostics and Imaging. *Chem. Rev.* 2010*, 110*, 2685-2708.

104. Martić, S.; Kraatz, H. Chemical biology toolkit for exploring protein kinase catalyzed phosphorylation reactions. *Chem. Sci.* 2012*, 4*, 42-59.

105. Seethala, R.; Menzel, R. A Homogeneous, Fluorescence Polarization Assay for Src-Family Tyrosine Kinases. *Analytical Biochemistry* 1997*, 253*, 210-218.

106. Tarrant, M. K.; Cole, P. A. The Chemical Biology of Protein Phosphorylation. *Annual Review of Biochemistry* 2009*, 78*, 797-825.

107. Li, Y.; Xie, W.; Fang, G. Fluorescence detection techniques for protein kinase assay. *Analytical and Bioanalytical Chemistry* 2008*, 390*, 2049-57.

108. Jill Coffin, M. L. Detection of phosphopeptides by fluorescence polarization in the presence of cationic polyamino acids: application to kinase assays. Anal Biochem. *Analytical biochemistry* 2000*, 278*, 206-12.

109. Scott, J. E.; Carpenter, J. W. A homogeneous assay of kinase activity that detects phosphopeptide using fluorescence polarization and zinc. *Analytical Biochemistry* 2003*, 316*, 82-91.

110. Sportsman, J. R.; Gaudet, E. A.; Boge, A. Immobilized metal ion affinity-based fluorescence polarization (IMAP): advances in kinase screening. *Assay Drug Dev Technol* 2004*, 2*, 205-214.

111. Tammy C Turek-Etienne, Ming Lei Use of Red-Shifted Dyes in a Fluorescence Polarization AKT Kinase Assay for Detection of Biological Activity in Natural Product Extracts. *Journal of biomolecular screening* 2004*, 9*, 52-61.

112. Levi, V.; González Flecha, F. L. Labeling of proteins with fluorescent probes: Photophysical characterization of dansylated bovine serum albumin. *Biochem. Mol. Biol. Educ.* 2003*, 31*, 333-336.

113. McIlroy, B. K.; Walters, J. D.; Johnson, J. D. A continuous fluorescence assay for protein kinase C. *Analytical Biochemistry* 1991*, 195*, 148-152.

114. Rininsland, F.; Stankewicz, C.; Weatherford, W.; McBranch, D. High-throughput kinase assays with protein substrates using fluorescent polymer superquenching. *BMC Biotechnol* 2005*, 5*, 16.

116. United States Patent , 2009.

117. Ma, H.; Deacon, S.; Horiuchi, K. The challenge of selecting protein kinase assays for lead discovery optimization. *Expert Opin Drug Discov* 2008*, 3*, 607-621.

118. Burns, S.; Travers, J.; Collins, I.; Rowlands, M. G.; Newbatt, Y.; Thompson, N.; Garrett, M. D.; Workman, P.; Aherne, W. Identification of Small-Molecule Inhibitors of Protein Kinase B (PKB/AKT) in an AlphaScreen™ High-Throughput Screen. *J Biomol Screen* 2006*, 11*, 822-827.

119. Eglen, R. M.; Reisine, T.; Roby, P.; Rouleau, N.; Illy, C.; Bossé, R.; Bielefeld, M. The Use of AlphaScreen Technology in HTS: Current Status. *Curr Chem Genomics* 2008*, 1*, 2-10.

120. Berney, C.; Danuser, G. FRET or No FRET: A Quantitative Comparison. *Biophys J* 2003*, 84*, 3992-4010.

121. Wegener, A. D.; Jones, L. R. Phosphorylation-induced mobility shift in phospholamban in sodium dodecyl sulfate-polyacrylamide gels. Evidence for a protein structure consisting of multiple identical phosphorylatable subunits. *J. Biol. Chem.* 1984*, 259*, 1834-1841.

122. Seethala, R.; Zhang, L. *Handbook of Drug Screening, Second Edition;* CRC Press: 2009; .

123. Puchi, M.; Garcia-Huidobro, J.; Cordova, C.; Aguilar, R.; Dufey, E.; Imschenetzky, M.; Bustos, P.; Morin, V. A new nuclear protease with cathepsin L properties is present in HeLa and Caco-2 cells. *J Cell Biochem* 2010*, 5*, 1099.

124. Ramos-Vara, J. A. Technical aspects of immunohistochemistry. *Vet Pathology* 2005*, 4*, 105.

125. Seelig, S. Fluorescence In Situ Hybridization Versus Immunohistochemistry: Importance of Clinical Outcome. *Journal of Clinical Oncology* 1999*, 17*, 3690.

126. Burns, J. M.; Cuschieri, A.; Campbell, P. A. Optimisation of Fixation Period on Biological Cells via Time-Lapse Elasticity Mapping. *Japanese Journal of Applied Physics* 2006*, 45*.

127. Xiao, Y.; Liddle, J. C.; Pardi, A.; Ahn, N. G. Dynamics of Protein Kinases: Insights from Nuclear Magnetic Resonance. *Acc Chem Res* 2015*, 48*, 1106-1114.

128. Mahmood, T.; Yang, P. Western Blot: Technique, Theory, and Trouble Shooting. *N Am J Med Sci* 2012*, 4*, 429-434.

129. Hughes; Spelke; Xu; Kang; Schaffer; Herr Single-cell western blotting. *Nature Methods* 2014*, 11*, 749-755.

130. Hughes, A. J.; Herr, A. E. Microfluidic Western blotting. *PNAS* 2012*, 109*, 21450-21455.

131. Sasaki, K.; Sato, M.; Umezawa, Y. Fluorescent Indicators for Akt/Protein Kinase B and Dynamics of Akt Activity Visualized in Living Cells. *J. Biol. Chem.* 2003*, 278*, 30945-30951.

132. Gao, X.; Zhang, J. Akt signaling dynamics in plasma membrane microdomains visualized by FRET-based reporters. *Commun Integr Biol* 2009, *2*, 32-34.

133. Zhang, L.; Lee, K. C.; Bhojani, M. S.; Khan, A. P.; Shilman, A.; Holland, E. C.; Ross, B. D.; Rehemtulla, A. Molecular imaging of Akt kinase activity. *Nat Med* 2007, *13*, 1114-1119.

134. Regot, S.; Hughey, J. J.; Bajar, B. T.; Carrasco, S.; Covert, M. W. High-sensitivity measurements of multiple kinase activities in live single cells. *Cell* 2014, *157*, 1724-1734.

135. Bendall, S. C.; Nolan, G. P. From single cells to deep phenotypes in cancer. *Nature Biotechnology* 2012, *30*, 639.

136. Bendall, S. C.; Nolan, G. P.; Roederer, M.; Chattopadhyay, P. K. A deep profiler's guide to cytometry. *Trends Immunol.* 2012, *33*, 323-332.

137. Han, L.; Qiu, P.; Zeng, Z.; Jorgensen, J. L.; Mak, D. H.; Burks, J. K.; Schober, W.; McQueen, T. J.; Cortes, J.; Tanner, S. D.; Roboz, G. J.; Kantarjian, H. M.; Kornblau, S. M.; Guzman, M. L.; Andreeff, M.; Konopleva, M. Single-cell mass cytometry reveals intracellular survival/proliferative signaling in FLT3-ITD-mutated AML stem/progenitor cells. *Cytometry* 2015, *87*, 346-356.

138. Bodenmiller, B.; Zunder, E. R.; Finck, R.; Chen, T. J.; Savig, E. S.; Bruggner, R. V.; Simonds, E. F.; Bendall, S. C.; Sachs, K.; Krutzik, P. O.; Nolan, G. P. Multiplexed mass cytometry profiling of cellular states perturbed by small-molecule regulators. *Nat Biotech* 2012, *30*, 858-867.

139. Turner, E. H.; Cohen, D.; Pugsley, H. R.; Gómez, D. G.; Whitmore, C. D.; Zhu, C.; Dovichi, N. J. Chemical cytometry: the chemical analysis of single cells. *Anal Bioanal Chem* 2007, *390*, 223-226.

140. Cohen, D.; Dickerson, J. A.; Whitmore, C. D.; Turner, E. H.; Palcic, M. M.; Hindsgaul, O.; Dovichi, N. J. Chemical Cytometry: Fluorescence-Based Single-Cell Analysis. *Annual Review of Analytical Chemistry* 2008, *1*, 165-190.

141. Romanova, E. V.; Rubakhin, S. S.; Monroe, E. B.; Sweedler, J. V. Single Cell Mass Spectrometry. In *Single Cell Analysis*; Anselmetti, D., Ed.; Wiley-VCH Verlag GmbH & Co. KGaA: 2009; pp 109-133.

142. Xia, F.; Jin, W.; Yin, X.; Fang, Z. Single-cell analysis by electrochemical detection with a microfluidic device. *J Chromatogr A* 2005, *1063*, 227-233.

143. Mellander; Trouillon; Svensson; Ewing Amperometric post spike feet reveal most exocytosis is via extended kiss-and-run fusion. *Scientific Reports* 2012*, 2*.

144. Wittenberg, N.; Maxson, M.; Eves, D.; Cans, A.; Ewing, A. G. Electrochemistry at the Cell Membrane/Solution Interface. In *Electrochemical Methods for Neuroscience*; Michael, A. C., Borland, L. M., Eds.; CRC Press/Taylor & Francis: Boca Raton (FL), 2007; .

145. Onjiko, R. M.; Moody, S. A.; Nemes, P. Single-cell mass spectrometry reveals small molecules that affect cell fates in the 16-cell embryo. *Proc. Natl. Acad. Sci. U. S. A.* 2015*, 112*, 6545-6550.

146. Yu, J.; Li, C.; Shen, S.; Liu, X.; Peng, Y.; Zheng, J. Mass spectrometry based detection of glutathione with sensitivity for single-cell analysis. *Rapid Commun. Mass Spectrom.* 2015*, 29*, 681-689.

147. Nemes, P.; Rubakhin, S. S.; Aerts, J. T.; Sweedler, J. V. Qualitative and quantitative metabolomic investigation of single neurons by capillary electrophoresis electrospray ionization mass spectrometry. *Nat Protoc* 2013*, 8*, 783-799.

148. Rubakhin; Churchill; Greenough; Sweedler Profiling Signaling Peptides in Single Mammalian Cells Using Mass Spectrometry. *Analytical Chemistry* 2006*, 78*, 7267-7272.

149. Jorgenson, J. W. J.; Lukas, K. D. Zone Electrophoresis in Open-Tubular Glass Capillaries. *Analytical Chemistry* 1981*, 53*, 1298.

150. Pfeiffer-Laplaud, M.; Costa, D.; Tielens, F.; Gaigeot, M.; Sulpizi, M. Bimodal Acidity at the Amorphous Silica/Water Interface. *J. Phys. Chem. C* 2015*, 119*, 27354-27362.

151. Weinberger, R. *Practical Capillary Electrophoresis;* Academic Press: San Diego, 2000; .

152. Lunte, S. M.; Radzik, D. M. *Pharmaceutical & Biomedical Applications of Capillary Electrophoresis;* Elsevier: 1996; .

153. Yang, Y.; Boysen, R. I.; Hearn, M. T. W. Analysis of synthetic peptides by capillary electrophoresis: Effect of organic solvent modifiers and variable electrical potentials on separation efficiencies. *Journal of Chromatography A* 2004*, 1043*, 91-97.

154. Jorgenson, J. W.; Lukacs, K. D. Capillary zone electrophoresis. *Science* 1983*, 222*, 266-272.

155. Hancu, G.; Simon, B.; Rusu, A.; Mircia, E.; Gyéresi, Á Principles of Micellar Electrokinetic Capillary Chromatography Applied in Pharmaceutical Analysis. *Adv Pharm Bull* 2013*, 3*, 1-8.

156. Carlavilla, D.; Moreno-Arribas, M. V.; Fanali, S.; Cifuentes, A. Chiral MEKC-LIF of amino acids in foods: analysis of vinegars. *Electrophoresis* 2006*, 27*, 2551-2557.

157. Shih, C.; Lin, C. Comparison of the use of single capillaries and coupled capillaries based on micellar electrokinetic chromatography (MEKC) and sweeping-MEKC modes. *Electrophoresis* 2005*, 26*, 962-969.

158. Swinney, K.; Bornhop, D. J. Detection in capillary electrophoresis. *Electrophoresis* 2000*, 21*, 1239-1250.

159. Zhang, H.; Jin, W. Determination of different forms of human interferon-gamma in single natural killer cells by capillary electrophoresis with on-capillary immunoreaction and laser-induced fluorescence detection. *Electrophoresis* 2004*, 25*, 1090-1095.

160. Ireland, I. D.; Lewis, D. F.; Li, X. F.; Renborg, A.; Kwong, S.; Chen, M.; Dovichi, N. J. Double coupling Edman chemistry for high-sensitivity automated protein sequencing. *J. Protein Chem.* 1997*, 16*, 491-493.

161. Liu, K. J.; Rane, T. D.; Zhang, Y.; Wang, T. Single Molecule Analysis Enables Free Solution Hydrodynamic Separation Using Yoctomole Levels of DNA. *J Am Chem Soc* 2011*, 133*, 6898-6901.

162. Chan, W. C.; White, P. D. *Fmoc Solid Phase Peptide Synthesis: A Practical Approach;* Oxford University Press, Inc: New York, 2000; .

163. Rothman; Vázquez; Vogel; Imperiali General Method for the Synthesis of Caged Phosphopeptides: Tools for the Exploration of Signal Transduction Pathways. *Organic Letters* 2002*, 4*, 2865-2868.

164. Turner, A. Epidermal Growth Factor Receptor Tyrosine Kinase Assays in Single Intact Cells Using Capillary Electrophoresis, University of North Carolina at Chapel Hill, 2015.

165. Proctor, A.; Wang, Q.; Lawrence, D.; Allbritton, N. Development of a Peptidase-Resistant Substrate for Single-Cell Measurement of Protein Kinase B Activation. 2012*, 84*, 7195.

166. Proctor, A.; Herrera-Loeza, G.; Wang, Q.; Lawrence, D. S.; Yeh, J.; Allbritton, N. L. Measurement of Protein Kinase B Activity in Single Primary Human Pancreatic Cancer Cells. *Analytical Chemistry* 2014*, 86*, 4573-4580.

167. Proctor, A.; Wang, Q.; Lawrence, D. S.; Allbritton, N. L. Metabolism of peptide reporters in cell lysates and single cells. *The Analyst* 2012, *137*.

168. Meredith, G. D.; Sims, C. E.; Soughayer, J. S.; Allbritton, N. L. Measurement of kinase activation in single mammalian cells. *Nature Biotechnology* 2000, *18*, 309.

169. Nelson, A.; Borland, L.; Allbritton, N.; Sims, C. Myristoyl-Based Transport of Peptides into Living Cells. *Biochemistry* 2007, *46*, 14771.

170. Li, H.; Sims, C. E.; Kaluzova, M.; Stanbridge, E. J.; Allbritton, N. L. A quantitative single-cell assay for protein kinase B reveals important insights into the biochemical behavior of an intracellular substrate peptide. *Biochemistry* 2004, *43*, 1599-1608.

171. Mainz, E. R.; Dobes, N. C.; Allbritton, N. L. Pronase E-Based Generation of Fluorescent Peptide Fragments: Tracking Intracellular Peptide Fate in Single Cells. *Anal. Chem.* 2015, *87*, 7987-7995.

172. Kovarik; Shah; Armistead; Allbritton Microfluidic Chemical Cytometry of Peptide Degradation in Single Drug-Treated Acute Myeloid Leukemia Cells. *Analytical Chemistry* 2013, *85*, 4991-4997.

173. Kovarik, M. L.; Dickinson, A. J.; Roy, P.; Poonnen, R. A.; Fine, J. P.; Allbritton, N. L. Response of single leukemic cells to peptidase inhibitor therapy across time and dose using a microfluidic device. *Integrative Biology* 2014, *6*, 164-174.

174. Yang, S.; Proctor, A.; Cline, E.; Houston, K.; Waters, M.; Allbritton, N. L. β-Turn sequences promote stability of peptide substrates for kinases within the cytosolic environment. *The Analyst* 2013, *138*.

175. Melvin, A. T.; Woss, G. S.; Park, J. H.; Dumberger, L. D.; Waters, M. L.; Allbritton, N. L. A comparative analysis of the ubiquitination kinetics of multiple degrons to identify an ideal targeting sequence for a proteasome reporter. *PLoS ONE* 2013, *8*, e78082.

176. Melvin, A. T.; Dumberger, L. D.; Woss, G. S.; Waters, M. L.; Allbritton, N. L. Identification of a p53-based portable degron based on the MDM2-p53 binding region. *Analyst* 2016, *141*, 570-578.

177. Melvin, A. T.; Woss, G. S.; Park, J. H.; Waters, M. L.; Allbritton, N. L. Measuring activity in the ubiquitin-proteasome system: from large scale discoveries to single cells analysis. *Cell Biochem. Biophys.* 2013, *67*, 75-89.

178. Phillips; Dailey; Bair; Samet; Allbritton Ex Vivo Chemical Cytometric Analysis of Protein Tyrosine Phosphatase Activity in Single Human Airway Epithelial Cells. *Analytical Chemistry* 2014, *86*, 1291-1297.

179. Phillips, R.; Bair, P.; Lawrence, D. S.; Sims, C. E.; Allbritton, N. L. Measurement of Protein Tyrosine Phosphatase Activity in Single Cells by Capillary Electrophoresis. *Analytical Chemistry* 2013*, 85*, 6136-6142.

180. Okada, C. Y.; Rechsteiner, M. Introduction of macromolecules into cultured mammalian cells by osmotic lysis of pinocytic vesicles. *Cell* 1982*, 29*, 33.

181. Daukas, G.; Lauffenburger, D. A.; Zigmond, S. Reversible Pinocytosis in Polymorphonuclear Leukocytes. *Journal of Cell Biology* 1983*, 96*, 1642.

182. Tsong, T. Electroporation of cell membranes. *Biophysical Journal* 1991*, 60*, 297.

183. Soughayer, J.; Krasieva, T.; Jacobson, S.; Ramsey, J. M.; Tromberg, B. J.; Allbritton, N. A. Characterization of Cellular Optoporation with Distance. *Anal. Chem* 2000*, 72*, 1342.

184. Jones, A. T.; Sayers, E. J. Cell entry of cell penetrating peptides: tales of tails wagging dogs. *Journal of Controlled Release* 2012*, 161*, 582.

185. Mann, D. A.; Frankel, A. D. Endocytosis and targeting of exogenous HIV-1 Tat protein. *The EMBO Journal* 1991*, 10*, 1733.

186. Chauhan, A.; Tikoo, A.; Kapur, A. K.; Singh, M. The taming of the cell penetrating domain of the HIV Tat: Myths and realities. *Journal of Controlled Release* 2007*, 117*, 148.

187. Kennedy, R. T.; Iii, Robert L St Claire; White, J. G.; Jorgenson, J. W. Chemical analysis of single neurons by open tubular liquid chromatography. *Mikrochim Acta* 1987*, 92*, 37-45.

188. Kennedy, R. T.; Oates, M. D.; Cooper, B. R.; Nickerson, B.; Jorgenson, J. W. Microcolumn Separations and the Analysis of Single Cells. *Science* 1989*, 246*, 57.

189. Ciolkowski, E. L.; Cooper, B. R.; Jankowski, J. A.; Jorgenson, J. W.; Wightman, R. M. Direct observation of epinephrine and norepinephrine cosecretion from individual adrenal medullary chromaffin cells. *J. Am. Chem. Soc.* 1992*, 114*, 2815-2821.

190. Cooper, B. R.; Jankowski, J. A.; Leszczyszyn, D. J.; Wightman, R. M.; Jorgenson, J. W. Quantitative determination of catecholamines in individual bovine adrenomedullary cells by reversed-phase microcolumn liquid chromatography with electrochemical detection. *Anal. Chem.* 1992*, 64*, 691-694.

191. Dickerson, J. A.; Dovichi, N. J. Capillary sieving electrophoresis and micellar electrokinetic capillary chromatography produce highly correlated separation of tryptic digests. *Electrophoresis* 2010*, 31*, 2461-2464.

192. Zhu, C.; He, X.; Kraly, J. R.; Jones, M. R.; Whitmore, C. D.; Gomez, D. G.; Eggertson, M.; Quigley, W.; Boardman, A.; Dovichi, N. J. Instrumentation for Medium-Throughput Two-Dimensional Capillary Electrophoresis with Laser-Induced Fluorescence Detection. *Anal. Chem.* 2007*, 79*, 765-768.

193. Metto, E. C.; Evans, K.; Barney, P.; Culbertson, A. H.; Gunasekara, D. B.; Caruso, G.; Hulvey, M. K.; Fracassi da Silva, Jose Alberto; Lunte, S. M.; Culbertson, C. T. An integrated microfluidic device for monitoring changes in nitric oxide production in single T-lymphocyte (Jurkat) cells. *Anal. Chem.* 2013*, 85*, 10188-10195.

194. Dickinson, A. J.; Meyer, M.; Pawlak, E. A.; Gomez, S.; Jaspers, I.; Allbritton, N. L. Analysis of sphingosine kinase activity in single natural killer cells from peripheral blood. *Integr Biol (Camb)* 2015*, 7*, 392-401.

195. Mainz, E. R.; Dobes, N. C.; Allbritton, N. L. Pronase E-Based Generation of Fluorescent Peptide Fragments: Tracking Intracellular Peptide Fate in Single Cells. *Anal. Chem.* 2015*, 87*, 7987-7995.

Chapter 2: Single Cell Chemical Cytometry of Akt Activity in Fibroblast-like Synoviocytes Reveals Heterogeneity in Responses of Rheumatoid Arthritis Subjects to Tumor Necrosis Factor α

2.1 Overview

The etiology of rheumatoid arthritis (RA) is poorly understood, and 30% of patients are unresponsive to established treatments targeting Tumor Necrosis Factor α (TNFα). Akt kinase is implicated in TNFα signaling, and may act as a barometer of patient responses to biologic therapies. Fluorescent peptide sensors and chemical cytometry were employed to directly measure Akt activity as well as proteolytic activity in individual fibroblast-like synoviocytes (FLS) from RA and normal subjects. The specificity of the peptide reporter was evaluated and shown to be a valid measure of Akt activity in single cells. The effect of TNFα treatment on Akt activity was highly heterogeneous between normal and RA subjects, which was not observable in bulk analyses. In 2 RA subjects, a bimodal distribution of Akt activity was observed, primarily due to a subpopulation (21.7%: RA Subject 5 and 23.8%: RA Subject 6) of cells in which >60% of the reporter was phosphorylated. These subjects also possessed statistically elevated proteolytic cleavage of the reporter relative to normal subjects, suggesting heterogeneity in Akt and protease activity that may play a role in the RA-affected joint. We expect that chemical cytometry studies pairing peptide reporters with capillary electrophoresis will provide valuable data regarding aberrant kinase activity from small samples of clinical interest.

2.2 Introduction

The advent of biologic therapies for treatment of rheumatoid arthritis (RA) signaled a shift towards precision medicine for treatment of rheumatologic disorders. Three very successful RA biologics include etanercept, adalimumab, and infliximab, all targeting TNFα, an inflammatory cytokine commonly upregulated in RA.[1] Though considered revolutionary, these engineered proteins yield no clinically measurable benefit in 30% of patients; coined 'primary nonresponders'.[2] Due to the cost and potential co-morbidities associated with these drugs, the rheumatology community has worked for over a decade to identify biomarkers which may be predictive of patient response to anti-TNFα therapies. Clinical factors such as sex, smoking, and the presence of anti-cyclic citrullinated peptide antibodies as well as TNFα itself have not been predictive of patient response to anti-TNFα biologics; thus, the focus has shifted towards identification of molecular biomarkers or biochemical response profiles.[3]

One potential biomarker is the serine/threonine protein kinase Akt (also called protein kinase B), which is downstream of the TNFα receptor and is a component of TNF biochemical signaling. Both upregulated expression[4] and constitutive activation[5-7] of Akt in FLS have been linked to chronic inflammation, increased efflux of matrix metalloproteinases (MMPs), and resistance to apoptosis, resulting in pseudo-tumoral proliferation of FLS and the irreversible cartilage damage characteristic of RA. These Akt abnormalities appear to exist primarily in FLS rather than macrophages or other cell types, suggesting that overactive Akt in FLS may be a component of disease progression.[7] Thus, this signaling arm is being pursued as a therapeutic target for novel therapies and inhibitors with anti-inflammatory effects.[8] With Akt mediating multiple downstream effects of TNFα signaling, the biochemical activity of this kinase in cells may also act as a barometer of the downstream

effects of upregulated TNFα, with potential applications in patient classification as anti-TNFα therapy responsive or non-responsive.

A complicating factor in the analysis of these cells is the heterogeneity expected in RA FLS that possess this aggressive phenotype.[9] Since only a fraction of the FLS population may have aberrant Akt activity, with even fewer present at early stages of the disease, it becomes imperative to analyze these cells with single-cell resolution. Traditional methodologies to determine the presence of Akt, such as immunohistochemistry, are valuable in determining the location of the kinase in tissue, but they are generally qualitative and do not provide compelling evidence that the labeled kinase's biochemical activity is aberrant.[10] Western blotting is another useful technique to garner gene expression information, but the detection of distinct subpopulations is not possible as the blot returns an ensemble average of the bulk population. Moreover, it is often difficult to obtain sufficient cells in biopsy samples for assay performance. Hughes and co-authors demonstrated a multiplexed solution capable of single-cell Western blots[11], but the nature of their antibody-based kinase detection did not allow detection of constitutively or transiently active enzymes through quantification of substrate and products. These protein-only detection schemes are the primary limitations of other single-cell techniques, including Phospho-flow and mass cytometry.[12,13] Liquid chromatography coupled tandem mass spectrometry (LC-MS/MS) has been reported to more accurately measure the stoichiometry of Akt phosphorylation in biological samples, but it requires immunoprecipitation, resulting in substantial samples losses.[14] Furthermore, the low sensitivity necessitates large sample sizes. Meaningful measurement of Akt activity within RA FLS instead requires single-cell resolution, excellent limits of detection, quantification of

substrate and products (as well as differentiation between any additional metabolites) and head-to-head comparison with normal FLS cells.

Chemical cytometry in the form of capillary electrophoresis with laser induced fluorescence detection (CE-LIF) routinely attains excellent (10^{-20} mol) limits of detection, as is required when analyzing intracellular metabolites of single mammalian cells which are typically $\leq$1 pL in volume. When coupled with peptide based probes, this separation based technology can directly assess kinase activity[15-17], and is highly quantitative with the inclusion of internal standards. In this study we performed the first evaluation of Akt and peptidase activity in single FLS cells with direct comparison to normal controls. Prior to single-cell analysis, the specificity of the peptide based Akt reporter was characterized to ensure rigorous measurements of the intended pathway. The Akt activity was then quantified in single cells from normal and RA FLS cells by chemical cytometry, and compared to traditional bulk analyses, which revealed novel information about the heterogeneity of this pathway in RA FLS.

2.3 Materials and Methods

2.3.1 Cell Culture

Hela (human cervical cancer) and OPM2 (human multiple myeloma) cell lines were obtained from the American Type Culture Collection and maintained in a humidified atmosphere of 37°C in 5% CO_2. Hela cells were cultured in Dulbecco's Modified Eagle Medium (DMEM) supplemented with 10% Fetal Bovine Serum (FBS), penicillin (100 units/mL) , and streptomycin (100 µg/mL), while OPM2 cells were maintained in RPMI-1640 media with the same supplements.

2.3.2 FLS Cell Culture

FLS from 6 individuals were collected at the time of synovectomy or total joint replacement. Three were biologic-naïve RA patients which fulfilled the American College of Rheumatology 1997 criteria for RA classification. Three were individuals who were undergoing surgical resection of tissue for reasons unrelated to rheumatologic disorders. Tissues were stored under liquid N_2 until the time of FLS culture. Synovial tissue was minced and immobilized in a tissue culture plate and covered with Dulbecco's Modified Eagle Medium (DMEM) supplemented with 10% Fetal Bovine Serum (FBS) and 1% PenStrep Solution (Gibco, Grand Island, NY) and were maintained in a humidified atmosphere of 37°C in 5% CO_2. Media was changed regularly until the FLS expanded to fill the entire plate. These cell lines from primary FLS were utilized from the third to ninth passage.

2.3.3 Small Interfering RNA transfection in FLS

Akt and scrambled non-targeting siRNA were purchased from Dharmacon Research, Inc. (Lafayette, CO, USA). The FLS cells were seeded in culture plates and grown to 80% confluence. FLS cells (3×10^5) were transfected with a variety of siRNA concentrations utilizing the Amaxa Human Dermal Fibroblast Nucleofector kit (NHDF-adult) with high efficiency program U-023 for human cells. After transfection, cultures were incubated at 37°C for 12 h and then placed in fresh culture media. Forty eight hours after transfection, the cells were harvested and the Akt protein expression levels were determined by Western blot analysis.

2.3.4 Western Blot Analysis

FLS from normal or rheumatic human samples were obtained and cultured. Cells were either not stimulated or stimulated with 100 nM TNFα for 30 min and then lysed in ice cold RIPA buffer plus protease and phosphatase inhibitors (10 mM Tris-Cl (pH 8.0), 1 mM ethylenediaminetetraacetic acid (EDTA), 0.5 mM ethyleneglycoltetraacetic acid (EGTA), 1% Triton X-100, 0.1% sodium deoxycholate, 0.1% sodium dodecyl sulfate (SDS), 140 mM NaCl, 1X cOmplete ULTRA Protease Inhibitor and 1X PhosSTOP Phosphatase Inhibitor Cocktail (Roche, Indianapolis, IN)). Protein lysates were normalized using a BCA assay (Thermo Scientific, Rockford, IL) and run on a Mini-PROTEAN TGX™ gel (Any kD™, 15-well comb, 15 µl) (Bio-Rad, Hercules, CA). Between 6-10 µg total protein was run per independent experiment. All lysates for an independent experiment were run on the same blot for direct comparison of signaling strength. Antibodies were from Cell Signaling Technology (Danvers, MA) or Trevigen (Gaithersburg, MD): P-Akt (S473) (D9E) XP® Rabbit mAb), anti-G3PDH/GAPDH, Akt Rabbit Ab, and anti-rabbit IgG, HRP-linked Antibody. All antibodies were diluted in 1x Tris-Buffered Saline with Tween 20 (Cell Signaling, Danvers, MA) + 3% Bovine Serum Albumin (BSA). Images were scanned and imported into ImageJ where images were converted into an 8-bit black and white image.

2.3.5 Cell Loading and Single-Cell Analysis by Capillary Electrophoresis

FLS from normal and rheumatoid arthritis subjects were separately cultured in custom cell chambers as described previously.[18] Chambers were placed on the stage of a custom-built single-cell CE-LIF system (fluorescence excitation at 473 nm, emission at 530 nm).[19] Cells were microinjected with 100 µM peptide VI-B (6FAM-GRP-MeArg-AFTF-

MeAla-Amide) using a Transjector 5246 microinjection system (Eppendorf AG, Hamburg, Germany) and bathed in a continuous flow of extracellular buffer (ECB; 10 mM HEPES, 135 mM NaCl, 5 mM KCl, 1 mM $CaCl_2$, pH 7.4, 37°C) during incubation and analysis. After microinjection (5 min), individual cells were rapidly lysed with a 9 ns pulse from a Nd:YAG laser (New Wave Research, Bozeman, MT) and the cellular contents simultaneously electrokinetically injected (5 s at -125 V/cm) into an overlying 30 µm inner diameter (Polymicro Technologies, Phoenix, AZ). Electrophoresis was performed in 100 mM borate, 15 mM SDS, pH 11.6 with a field strength of -250 V/cm. Electropherograms were integrated using customized software written in MATLAB (Natick, MA).[17] Detailed information regarding peptide fragment nomenclature and identification is available in supplemental information.

2.3.6 Identification of Peptide Fragmentation Products

Synthetic standards of all possible fluorescent peptide fragments of VI-B were synthesized as described previously.[2] Under the electrophoretic conditions used, the phosphorylated peptide was fully resolved from the parent peptide and each potential fragment. Thus, the fragments formed and their identities were identifiable as described previously.[2] Each peak present in the individual cells were readily matched by migration time to a fluorescent peptide fragment or the intact or phosphorylated reporter.

2.3.7 Flow Cytometry

Antibodies conjugated with AlexaFluor 647 (AF647) were utilized for flow cytometry. CD120a (Tumor Necrosis Factor Receptor 1)–AF647 and isotype control immunoglobulin (Ig)G2a-AF647 were purchased from BioRad (Hercules, CA). For washes,

incubation and data acquisition, cells were suspended in incubation buffer (137 mM NaCl, 2.7 mM KCl, 10 mM Na_2HPO_4, 1.8 mM KH_2PO_4, 20 mM 4-(2-hydroxyethyl)-1-piperzineethanesulfonic acid, 5 mM EDTA, 2% FBS). FLS cells were removed from tissue culture dishes with Accutase (Sigma Aldrich, St. Louis, MO) per manufacturer's instructions. CD120a-AF647 antibody and 500 nM SYTOX Green (ThermoFisher Scientific, Waltham, MA) was added to FLS cells (0.1 µg/mL) and incubated for 30 min in the dark at 25°C. Cells were washed twice with incubation buffer by centrifugation at 300 x g for 5 min. For an isotype control, FLS cells were stained with (Ig)G2a-AF647 (0.1 µg/mL) and 500 nM SYTOX Green. Positive control staining was performed with HeLa cells. Data were acquired on a FACSAria II Flow Cytometer (BD Biosciences, San Jose, CA) and analysis was performed using BD FACSDiva 8.0 software.

2.3.8 Statistical Analysis

To analyze single cells in these chemical cytometry experiments, the distribution of the difference between the mean percentage of phosphorylated peptide or intact full length reporter in each single-cell analysis treatment and control group was calculated utilizing bootstrapping.[20] 10,000 bootstrap replicates (with replacement) were generated from each group and the means of each bootstrap replicate group were calculated. The distribution of the differences between the appropriate pairs of bootstrap replicates was utilized to estimate the distribution of the mean differences. The p-value for testing the null hypothesis of no difference in mean between the control and treatment groups was estimated by dividing the number of bootstrap differences which possessed values of 0 or less by the number of bootstrap replicates (10,000).

Boxplots were utilized to represent the non-normal distribution of the reporter phosphorylation from individual cells. Within the boxplots, squares represent the mean value from all cells. The middle bar indicates the median, while the upper and lower boxes showed the 75% and 25% percentile of the data, respectively. Whiskers extend to the 5th and 95th percentiles. Any individual data points outside of the whiskers are outliers.

2.4 Results and Discussion

2.4.1 Evaluating Peptide Reporter Specificity

In order to measure Akt activity in single FLS, a phosphorylatable-threonine-containing peptide, herein after referred to as VI-B (6FAM-GRP-MeArg-AFTF-MeAla-Amide), was utilized. The sequence was determined using an iterative design strategy originating from the consensus sequence of Akt.[16] VI-B possessed favorable phosphorylation kinetics as well as demonstrated degradation resistance, and has been employed to measure Akt activity in single tissue-cultured cells and pancreatic adenocarcinoma patient-derived xenografts.[21,22]

Since many eukaryotic protein kinases possess similar catalytic domains,[23] we sought to evaluate whether the majority of VI-B phosphorylation was due to Akt or other analogous, potentially interfering kinases. A basal level of phosphorylation was established by depriving FLS cells of serum for 12 h, loading VI-B, and analyzing cells by single-cell CE-LIF. Basal phosphorylation varied between cells (0-37%), but was similar between normal and RA subjects (p = 0.31) (Figure 2.1A,B). To determine whether VI-B phosphorylation was a result of Akt activity or due to other kinases within the intracellular environment, reporter phosphorylation in response to physiologic stimulation or pharmacologic inhibition of the Akt pathway was measured. Insulin stimulates cell growth and protein synthesis by

activation of Akt.[24] When FLS were treated with 100 ng/mL insulin, significantly increased

mean VI-B phosphorylation was observed in both normal (n = 16; 38.2 ± 31%) and RA

subjects (n = 11; 39.5 ± 37.7%). Conversely, when cells were treated with 10 µM LY294002,

a reversible inhibitor of PI3K, the kinase directly upstream of Akt,[25] mean VI-B

phosphorylation was less than 5% of the basal level. These data supported that the majority

of the reporter phosphorylation observed was the result of Akt activity (Figure 2.1A,B).

In a second experiment, Akt protein was transiently knocked down in FLS by

administering a specific siRNA for Akt. The presence of the kinase was monitored 48 h post

siRNA-transfection by western blot (Figure 2.1C), which demonstrated a dose-dependent

reduction in Akt expression. The transfection process did not disrupt Akt expression, as

demonstrated by similar expression of Akt between un-transfected cells (0 nM Akt siRNA)

and 500 nM of a non-targeting (NT) scrambled siRNA. Using chemical cytometry, VI-B

phosphorylation was assessed in single cells 48 h following transfection with 300 and 500

nM Akt-targeting siRNA. Cells were serum starved and stimulated with insulin (100 ng/mL)

prior to analysis as described above. Significant reduction in reporter phosphorylation was

seen in comparison to FLS transfected with non-targeting scrambled siRNA (Figure 2.1D),

again supporting that a dominant portion of reporter phosphorylation was due to Akt activity.

These data from physiologic and pharmacological perturbation of the Akt pathway indicated

that VI-B phosphorylation was a valid measure of Akt activity in FLS.

2.4.2 Akt Activity within Single FLS from RA and Normal Subjects

Individual FLS cells (analyzed: n=107) were stimulated with TNFα to determine

whether this factor would activate Akt in FLS from normal and RA subjects (Figure 2.2).

TNFα is known to be elevated in the joints of RA patients; therefore, addition of TNFα to

FLS is expected to partially mimic the inflammatory environment of the RA-affected joint.

FLS obtained from RA patients and normal subjects were plated on glass cell chambers.

Cells were serum-starved overnight, then stimulated with 100 ng/mL TNFα for 30 min and

loaded with VI-B. After a 5-min incubation, individual cells were assayed for

phosphorylation of VI-B. When cells originating from normal subjects 1-3 (N1-N3) were

stimulated with TNFα, minimal phosphorylation of the reporter was detected (Figure 2.2D).

N1-N3 demonstrated 0.8±2.5% (n=14), 1.6±6.1% (n=16), and 0.8±2.6% (n=15)

phosphorylation, respectively (Figure 2.3B). When individual FLS were analyzed from RA

Subject 4 under identical conditions s (Figure 2.3A), a similar level of phosphorylation was

detected (0.5±2.1% [n=18]), suggesting that in this particular subject, TNFα contributed

minimally to Akt activation. In contrast, when single FLS were analyzed from RA subjects 5

and 6, the mean phosphorylation rose to 25.6±36.4% (n=23) and 27.1±37.8% (n=21),

respectively. This was primarily due to a subpopulation (21.7% of cells: RA Subject 5 and

23.8% of cells: RA Subject 6) which phosphorylated >60% of the reporter within the 5 min

incubation period.

2.4.3 Active Akt Determined by Western Blot Analysis in Lysates from FLS

Western blot analysis was performed on FLS from all subjects to compare the amount

of active Akt detected between single cells and ensemble population level measurements

(Figure 2.3C). Cells were unstimulated or stimulated with TNFα as described above prior to

lysis. The amount of endogenous Akt was determined with an anti-Akt antibody competent

to bind to Akt1, Akt2, and Akt3. Phospho-Akt was estimated utilizing a monoclonal antibody

against phosphorylated serine at location 473. In all cases, TNFα treatment resulted in

increased amounts of p473, but there were no differences detectable between normal and RA subjects.

2.4.4 Tumor Necrosis Factor Receptor 1 (TNFR1) Expression in FLS

TNFα signaling is initiated by binding to receptors expressed on nucleated cells. Of two distinct receptors, Akt is thought to be regulated by the 55-kDa type 1 receptor (TNFR1).[8] To evaluate whether differences in TNFR1 expression between RA and normal subjects might be due to receptor expression, we probed FLS with antibodies specific for the receptor and analyzed the FLS by flow cytometry (Figure 2.4). Positive, negative, and isotype controls were also performed (Figure 2.5). Cells were concomitantly stained with SYTOX green (50 µM) to detect non-viable cells. All subjects possessed TNFR1 positive populations with few TNFR1-negative cells. Statistical analysis (Kruskal Wallis one-way ANOVA) performed on live cells determined TNFR1-positive revealed that normal subjects 2 and 3 possessed elevated expression of TNFR1 ($p = 0.009$ and 0.012, respectively), relative to RA cells. This is in agreement with reports of decreased membrane TNFR1 expression on RA FLS, which may occur due to receptor internalization or to increased rates of cleavage of membrane TNFR1 to form soluble extracellular 17 kDa TNFα, not detected by flow cytometry.[26-28] The mechanism of Akt activation in cells with decreased TNFR1 expression remains debated, but it is possible that the increased TNFα ligand generated by cleavage of the receptor,[29] or that shuttling of TNFα by the soluble receptor[7] plays a role.

2.4.5 Degradation of VI-B in Single FLS from Normal and RA Subjects

It is well known that within the RA-affected joint, FLS secrete potent MMPs and cathepsins which act extracellularly to degrade collagen and bone.[9] Intracellular protease and peptidase activity constitutes a mostly unexplored area of FLS research, but correlations have

been shown between advanced (>10 yr duration) RA and highly active intracellular

proteolysis pathways involving cysteine and aspartate proteinases.[30] As shown in Figure

2.2A,F, we generated standards of all potential fluorescent fragments of VI-B, which are

well-resolved from phosphorylated VI-B by CE-LIF. Thus, we have the capability to identify

the fluorescent proteolysis products of VI-B via chemical cytometry as previously

described[16], and therefore characterize the proteolysis rate as well as the primary sites of VI-

B cleavage within FLS from RA as well as normal subjects. Normal subjects 1-3 and RA

Subject 4 possessed similar (p = 0.11) rates of VI-B degradation (Figure 2.6A,B): 0.14 ± 0.76,

0.35 ± 0.78, 0.75 ± 0.46, and $0.71\pm.69$ zmol $pg^{-1} s^{-1}$ for Subjects 1-4, respectively. However,

RA Subjects 5 (2.99 ± 0.52 zmol $pg^{-1} s^{-1}$) and 6 (3.27 ± 0.60 zmol $pg^{-1} s^{-1}$) demonstrated

significantly more rapid degradation of the reporter (p = .013), providing evidence that at

least some RA subjects have significantly greater proteolytic capability, which may correlate

with intracellular Akt activity.

Interestingly, fragment identities between RA and normal cells also differed (Figure

2.6C,D). Fragment F1 corresponds to the shortest possible fluorescent fragment (6FAM-G),

which extends C-terminally to the longest fragment F8 (6FAM-GRP-MeArg-AFTF). RA

Subjects 5 and 6 were the only group to cleave between phenylalanine and threonine (F6),

with an average frequency of $19.4\pm5.8\%$ (RA5) and $22.5\pm9.8\%$ (RA6). Both RA and normal

subjects often possessed the fragments arising due to cleavage C-terminal of arginine (F2)

and N-methylarigine or alanine (F4/5) (RA: $52.2\pm22\%$ Normal: $46.6\pm14\%$). RA Subjects

rarely produced fragments due to cleavage after proline (F3), penultimate phenylalanine (F7),

or glycine (F1), which were frequently observed in small quantities from the FLS of normal

subjects (Figure 2.6D, F).

2.5 Conclusions

While prior reports have indicated that Akt activity can be elevated in RA FLS cells in response to TNFα,[31] this is the first demonstration of the heterogeneity of this response, both within and between RA subjects. Such differential upregulation of Akt between patients may indicate differences in the responsiveness of the Akt pathway in these cells, for example, in the ability to transmit the downstream signal after TNFα binding to modify cell behavior, *i.e.* apoptosis resistance and/or secretion of MMPs.[32] With respect to the heterogeneity of Akt activity within RA Subjects 5 and 6, such cell-to-cell variation in Akt activity is not unprecedented in the literature; it is relatively common in cancers[33], Proteus syndrome[34], and other diseases[35,36] that hijack this pathway to promote survival of cells under stressful conditions. Importantly, bulk analyses by western blotting was unable to resolve these differences in activation, solidifying the concept that single cell analysis is necessary to observe the intra- and inter-subject heterogeneity in Akt signaling upon TNFα stimulation.

It was also determined that RA subjects 5 and 6 possessed more rapid degradation of the reporter and that fragmentation occurred in locations not detected in normal subjects. It is possible that these findings are due to the differential activity and/or different types of proteases or peptidases found in FLS of RA and normal subjects. For example, the protease cathepsins B and L are known for their role in extracellular degradation of collagen, but are also overexpressed intracellularly as a result of increased TNFα stimulation.[37,38] Specificity studies indicate their canonical preference for aromatic residues including phenylalanine.[39] The increased cleavage at hydrophobic residues (F6) observed in RA subjects 5 and 6 could potentially be due to contributions from such cathepsins B and L.

FLS cells within the RA afflicted joint are unique in their dependence on kinases such as Akt, which allow for unfettered growth, but also proteases, which catalyze the destruction of cartilage, therefore the simultaneous measurement of both these parameters may be clinically valuable. Tracking the Akt upregulation within single cells from many RA patients following treatment to inhibit TNFα should help inform our understanding as to whether the activity of this kinase might be a predictive marker of patient response to biologic therapies. Importantly, cells possessing elevated Akt and protease activity could be identified in difficult-to-analyze small clinical samples, such as a fine needle biopsy or synovial fluid collection[40]; samples that current methodologies struggle to analyze.

2.6 Figures and Tables
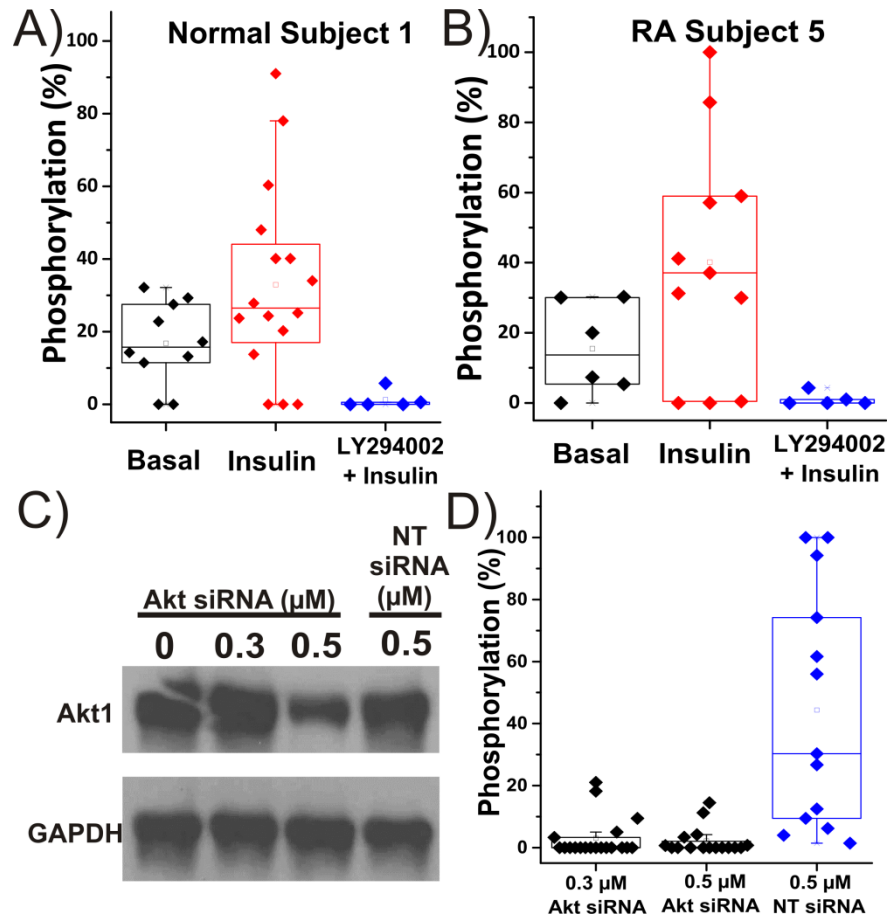
Figure 2.1 Specificity Evaluation of Akt Reporter VI-B. Basal measurements, physiologic stimulation, and pharmacologic inhibition of the Akt pathway in single FLS cells from a A) normal subject 1 or B) RA subject 5. Before microinjection with VI-B, cells were either serum starved for 12 h for basal measurements, stimulated with 100 ng/mL insulin, or were treated with 10 µM LY294002 prior to insulin treatment (100 ng/mL). C) Western blot results from siRNA knockdown of Akt in RA Subject 5. The housekeeping protein GAPDH was probed as a loading control. Cells underwent no transfection as a control or were transfected with various concentrations of Akt-targeting siRNA or non-targeting, scrambled siRNA (NT siRNA). D) Individual FLS cells analyzed for Akt activity 48 hrs after siRNA transfection with Akt-targeting siRNA or non-targeting, scrambled siRNA (NT siRNA).
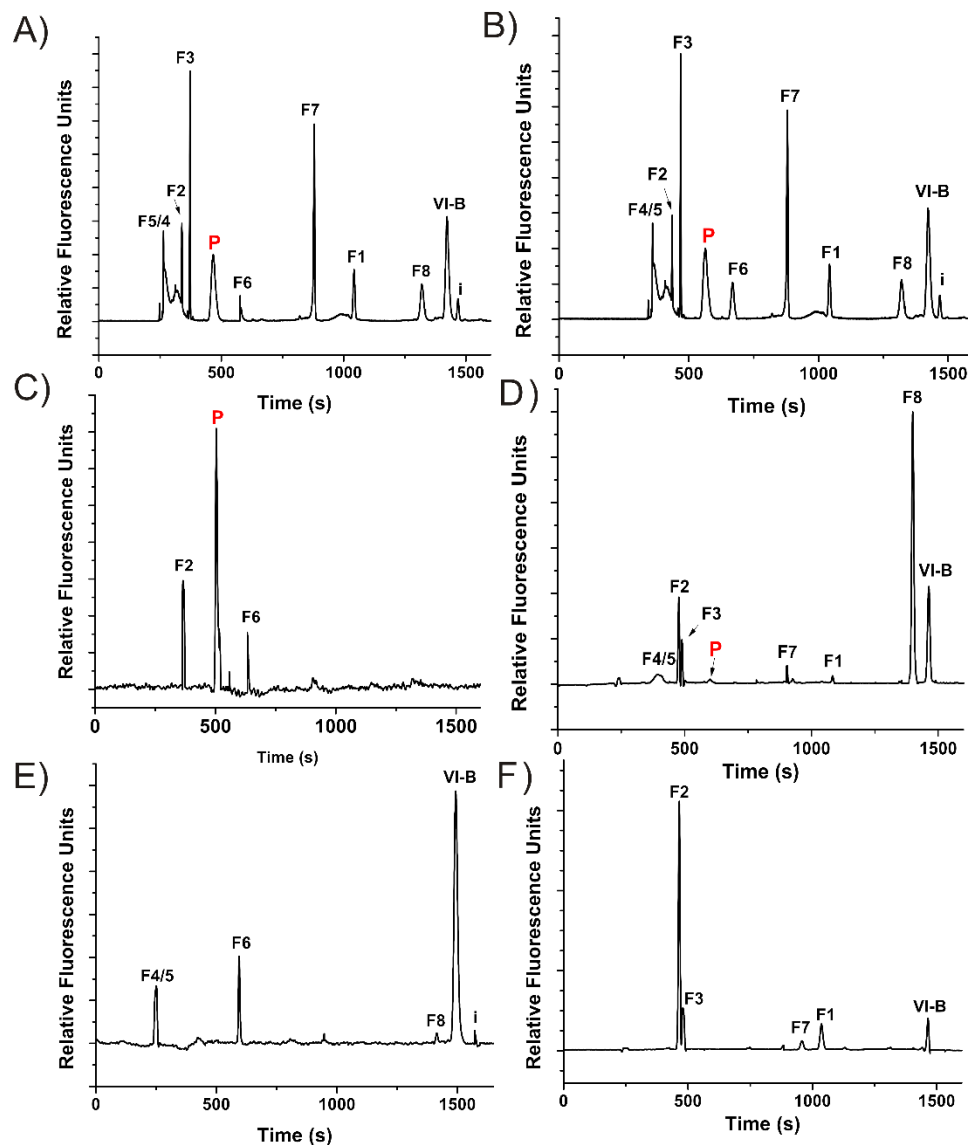
Figure 2.2 Akt Activity Measurements in Single FLS. CE-LIF analysis from individual cells originating from RA subject 5 (A,C,E) and normal subject 1 (B,D,F). Migration time standards of parent peptide (VI-B), phosphorylated peptide (P) and all possible fluorescent fragments (F1-8, Table 2.1) were loaded into the capillary after loading the contents of single cells not loaded with VI-B (A,B). Individual cells were stimulated with 100 ng/mL TNFα for 30 min (C,D) or treated with 10 µM LY294002 for 25 min prior to TNFα stimulation (E,F) and subsequently analyzed with CE-LIF. Each trace represents CE-LIF analysis of a single cell.
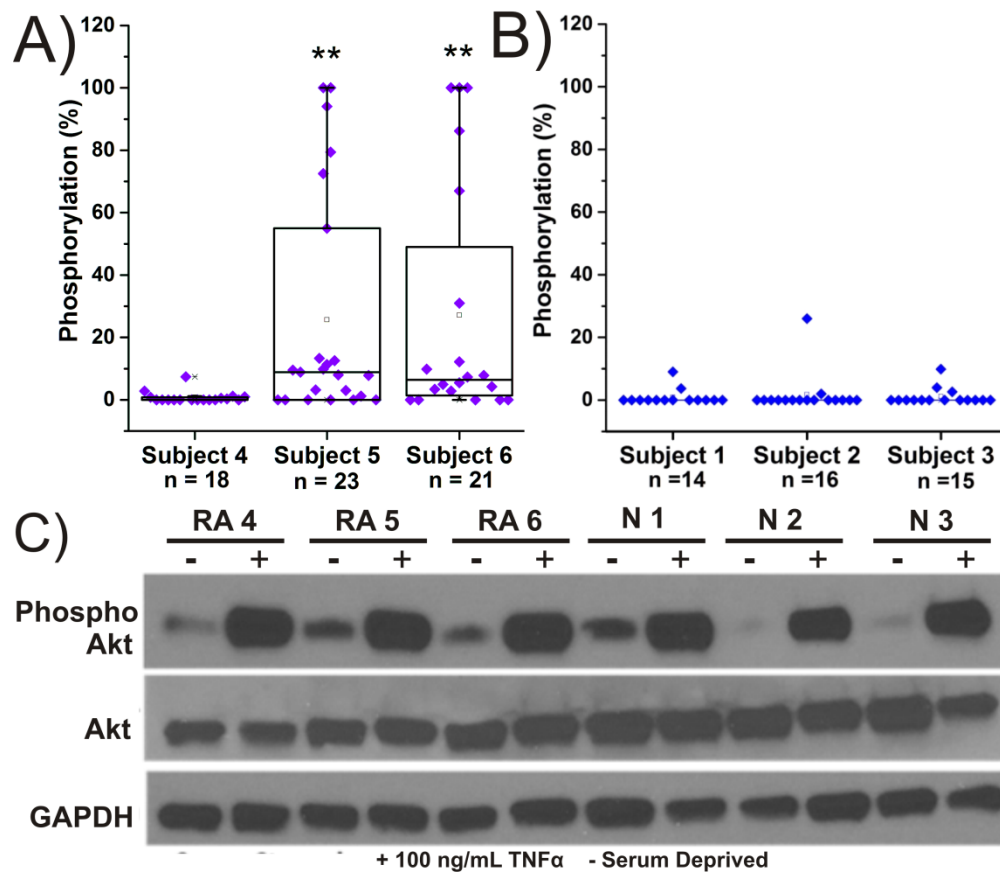
Figure 2.3 Akt Activity in FLS from Normal and RA Subjects after Stimulation with TNFα. Each data point represents a single cell analyzed for Akt activity from A) RA subjects or B) normal subjects. All cells were serum deprived overnight and subsequently stimulated with 100 ng/mL TNFα for 30 min before analysis with chemical cytometry. C) Western blotting was performed in lysates prepared from cells with and without TNFα stimulation (100 ng/mL).
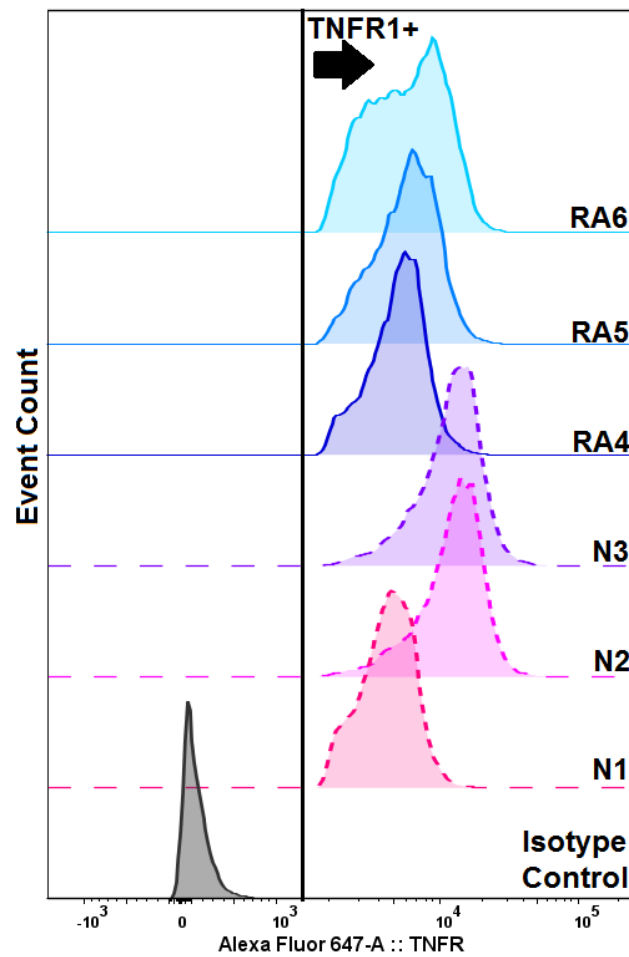
Figure 2.4 Tumor Necrosis Factor Receptor 1 (TNFR1) Expression in FLS. Normal subjects 1-3 (N1-N3, dashed lines) and RA subjects 4-6 (RA4-6, solid lines) FLS were co-stained with a monoclonal antibody to detect TNFR1 and the dead-cell indicator SYTOX Green (10 µM), then were analyzed by flow cytometry. TNFR1 positive, viable cells are depicted to the right of the arrow and possess a minimum relative fluorescence intensity of 1500.
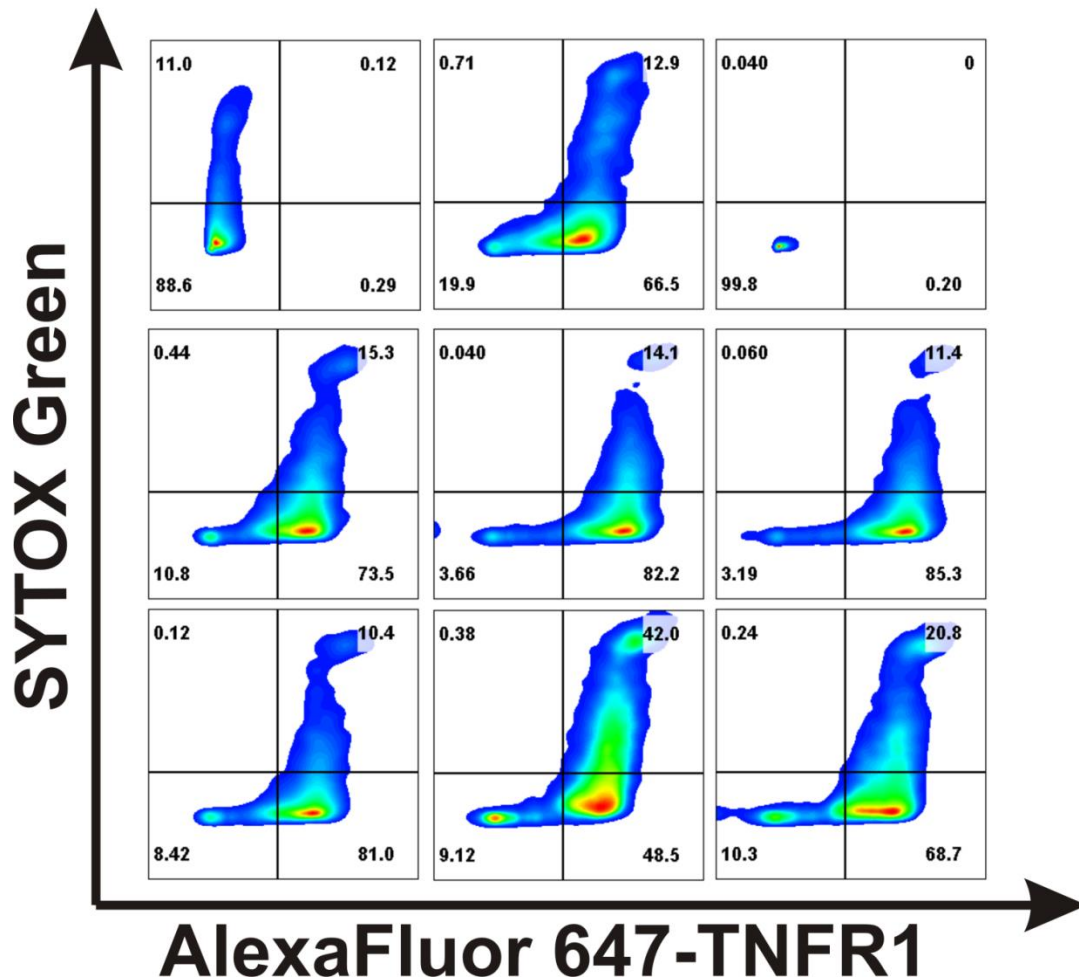
Figure 2.5. Analysis of FLS Cells by Flow Cytometry. Tumor Necrosis Factor Receptor 1 (TNFR1) positive, viable cells are present in the right hand lower quadrant (Q3) of each cell density plot A) Isotype control antibody IgG2a-AF647 was incubated with RA Subject 6 cells prior to analysis, demonstrating minimal nonspecific binding. B) HeLA cells stained for TNFR1 C) OPM2 cells stained for TNFR1 D-F) Normal subjects N1-N3 and G-I) RA subjects RA4-6 were stained for TNFR1. All cells we co-stained with SYTOX Green to identify nonviable cells.
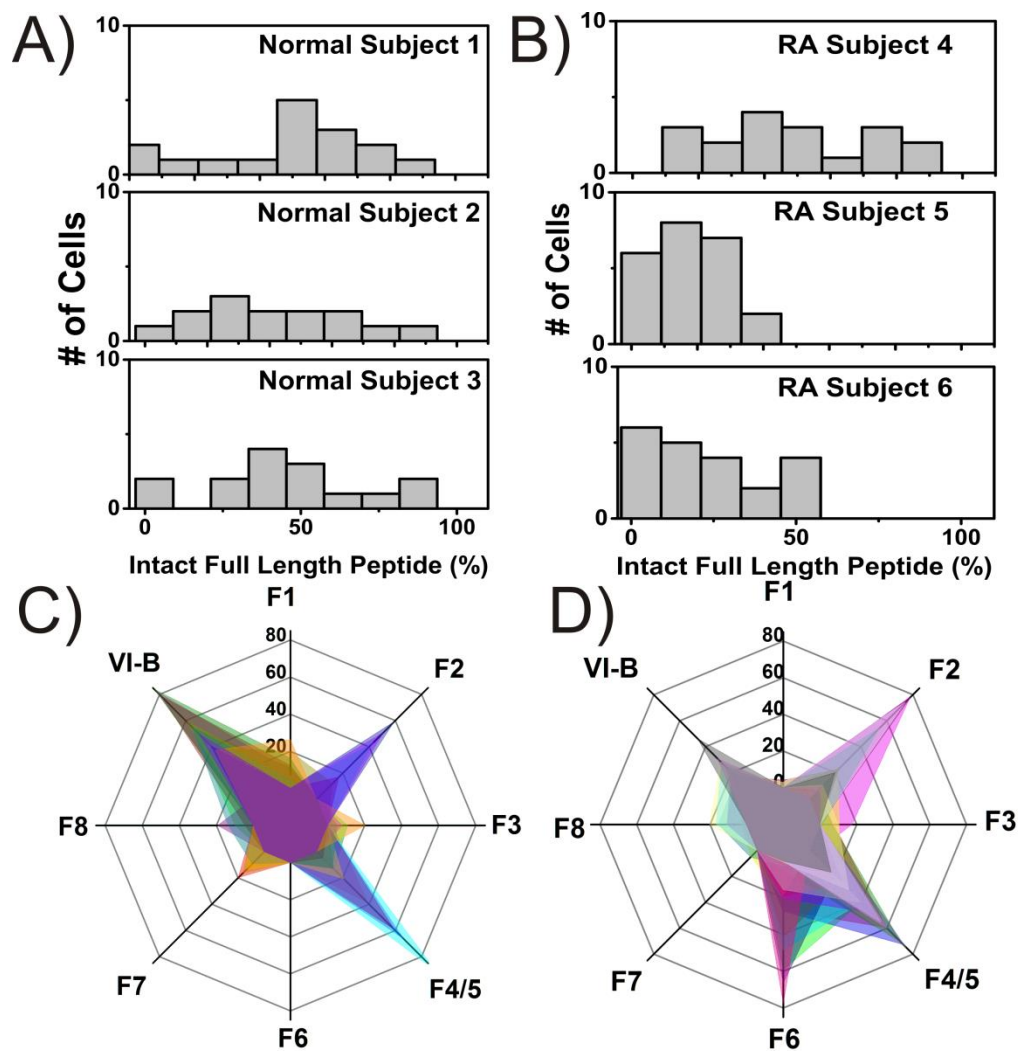
Figure 2.6 Proteolysis of VI-B in Single FLS cells from Normal and RA Subjects.
Histograms illustrating the percentage of intact, un-degraded reporter (VI-B) from each
TNFα-stimulated cell analyzed by chemical cytometry from A) normal and B) RA subjects.
Fragmentation profiles for C) normal subject 1 (n=14 cells each depicted as a different color)
and D) RA subject 5 (n=23). VI-B represents the full length peptide, while F1-F8 indicates
the 1 to 8 amino-acid fluorescent fragments, respectively. Fragment identities can be found in
Table 2.1.

Table 2.1 Fragment nomenclature for reporter VI-B

Name	Proteolytic Fragment
F1	6FAM-G-OH
F2	6FAM-GR-OH
F3	6FAM-GRP-OH
F4	6FAM-GRP-MeR-OH
F5	6FAM-GRP-MeR-A-OH
F6	6FAM-GRP-MeR-AF-OH
F7	6FAM-GRP-MeR-AFT-OH
F8	6FAM-GRP-MeR-AFTF-OH

REFERENCES

1. Neovius, M.; Arkema, E. V.; Olsson, H.; Eriksson, J. K.; Kristensen, L. E.; Simard, J. F.; Askling, J.; Bäcklund, E.; Cöster, L.; Forsblad-d'Elia, H.; Feltelius, N.; Jacobsson, L.; Klareskog, L.; Lindblad, S.; Rantapää-Dahlqvist, S.; Saxne, T.; van Vollenhoven, R. *Ann Rheum Dis* **2015***,74*, 354-360.

2. Rubbert-Roth, A.; Finckh, A.. *Arthritis Res Ther* **2009***, 11*, 1-12.

3. Potter, C.; Hyrich, K. L.; Tracey, A.; Lunt, M.; Plant, D.; Symmons, D. P. M.; Thomson, W.; Worthington, J.; Emery, P.; Morgan, A. W.; Wilson, A. G.; Isaacs, J.; Barton, A. *Ann. Rheum. Dis.* **2009***, 68*, 69-74.

4. García, S.; Liz, M.; Gómez-Reino, J. J.; Conde, C. *Arthritis Res Ther* **2010***, 12*, R33.

5. García, S.; Mera, A.; Gómez-Reino, J. J.; Conde, C. *Rheumatology (Oxford)* **2009***, 48*, 483-489.

6. Miyashita, T.; Kawakami, A.; Tamai, M.; Izumi, Y.; Mingguo, H.; Tanaka, F.; Abiru, S.; Nakashima, K.; Iwanaga, N.; Aratake, K.; Kamachi, M.; Arima, K.; Ida, H.; Migita, K.; Origuchi, T.; Tagashira, S.; Nishikaku, F.; Eguchi, K. *Biochem. Biophys. Res. Commun.* **2003***, 312*, 397-404.

7. Zhang, H. G.; Wang, Y.; Xie, J. F.; Liang, X.; Liu, D.; Yang, P.; Hsu, H. C.; Ray, R. B.; Mountz, J. D. *Arthritis Rheum.* **2001***, 44*, 1555-1567.

8. Ozes, O. N.; Akca, H.; Gustin, J. A.; Mayo, L. D.; Pincheira, R.; Korgaonkar, C. K.; Donner, D. B. *Cell Signaling in Vascular Inflammation*; DPhil, J. B. M., Ed.; Humana Press: 2005; pp 13-22.

9. Bartok, B.; Firestein, G. S. *Immunology Review* **2010***, 233*, 233.

10. Ramos-Vara, J. A. *Vet Pathology* **2005***, 4*, 105.

11. Hughes; Spelke; Xu; Kang; Schaffer; Herr *Nature Methods* **2014***, 11*, 749-755.

12. Lujan, E.; Zunder, E. R.; Ng, Y. H.; Goronzy, I. N.; Nolan, G. P.; Wernig, M. *Nature* **2015***, 521*, 352-356.

13. Davey, H. M.; Kell, D. B. *Microbiol Rev* **1996***, 60*, 641-696.

14. Atrih, A.; Turnock, D.; Sellar, G.; Thompson, A.; Feuerstein, G.; Ferguson, M. A. J.; Huang, J. T. -. S*J Proteome Res* **2010***, 9*, 743-751.

15. Dickinson, A. J.; Armistead, P. M.; Allbritton, N. L. *Anal Chem* **2013**,85, 4797.

16. Proctor, A.; Wang, Q.; Lawrence, D.; Allbritton, N.L., *Anal Chem* **2012**, *84*, 7195.

17. Phillips; Dailey; Bair; Samet; Allbritton, N.L., *Analytical Chemistry* **2014**, *86*, 1291-1297.

18. Turner, A. H. Epidermal Growth Factor Receptor Tyrosine Kinase Assays in Single Intact Cells Using Capillary Electrophoresis, University of North Carolina, 2015.

19. Mainz, E. R.; Dobes, N. C.; Allbritton, N. L. *Anal. Chem.* **2015**, *87*, 7987-7995.

20. Efron, B. Bootstrap Methods: Another Look at the Jackknife. *Breakthroughs in Statistics*; Kotz, S., Johnson, N. L., Eds.; Springer New York: 1992; pp 569-593.

21. Proctor, A. Development of Peptidase-Resistant Peptide Substrates for measurement of Protein Kinase B and Bcr-Abl Kinase Activity, University of North Carolina at Chapel Hill, 2012.

22. Proctor, A.; Herrera-Loeza, G.; Wang, Q.; Lawrence, D. S.; Yeh, J.; Allbritton, N. L. *Analytical Chemistry* **2014**, *86*, 4573-4580.

23. Ubersax, J. A.; Ferrell Jr, J. E. *Nat Rev Mol Cell Biol* **2007**, *8*, 530-541.

24. Haar, E. V.; Lee, S.; Bandhakavi, S.; Griffin, T. J.; Kim, D. *Nat Cell Biol* **2007**, *9*, 316-323.

25. Gharbi, S.; Zvelebil, M. J.; Shuttleworth, S. J.; Hancox, T.; Saghir, N.; Timms, J. F.; Waterfield, M. D. *Biochemical Journal* **2007**, *404*, 15.

26. Wong, C. K.; Chen, D. P.; Tam, L. S.; Li, E. K.; Yin, Y. B.; Lam, C. W. *Arthritis Res Ther* **2010**, *12*, 1-15.

27. Arend, W. P.; Dayer, J. *Arthritis & Rheumatism* **1995**, *38*, 151-160.

28. Levine, S. J. *J Biol Chem* **2008**, *283*, 14177-14181.

29. Offermanns, S. *Encyclopedia of Molecular Pharmacology;* Springer Science & Business Media: .

30. Tak, P. P.; Bresnihan, B. *Arthritis Rheum.* **2000**, *43*, 2619-2633.

31. Reddy, S. A. G.; Huang, J. H.; Liao, W. S. *J Immunol* **2000**, *164*, 1355-1363.

32. Mountz, J. D.; Zhang, H.; Wang, Y.; Xie, J. F.; Liang, X.; Hsu, H.; Curiel, D. T. *Arthritis Res* **2001**, *3*, P8.

33. Lei, Q.; Jiao, J.; Xin, L.; Chang, C.; Wang, S.; Gao, J.; Gleave, M. E.; Witte, O. N.; Liu, X.; Wu, H. *Cancer Cell* **2006***, 9*, 367-378.

34. Lindhurst, M. J.; Sapp, J. C.; Teer, J. K.; Johnston, J. J.; Finn, E. M.; Peters, K.; Turner, J.; Cannons, J. L.; Bick, D.; Blakemore, L.; Blumhorst, C.; Brockmann, K.; Calder, P.; Cherman, N.; Deardorff, M. A.; Everman, D. B.; Golas, G.; Greenstein, R. M.; Kato, B. M.; Keppler-Noreuil, K. M.; Kuznetsov, S. A.; Miyamoto, R. T.; Newman, K.; Ng, D.; O'Brien, K.; Rothenberg, S.; Schwartzentruber, D. J.; Singhal, V.; Tirabosco, R.; Upton, J.; Wientroub, S.; Zackai, E. H.; Hoag, K.; Whitewood-Neal, T.; Robey, P. G.; Schwartzberg, P. L.; Darling, T. N.; Tosi, L. L.; Mullikin, J. C.; Biesecker, L. G. *New England Journal of Medicine* **2011***, 365*, 611-619.

35. Lindhurst, M. J.; Parker, V. E. R.; Payne, F.; Sapp, J. C.; Rudge, S.; Harris, J.; Witkowski, A. M.; Zhang, Q.; Groeneveld, M. P.; Scott, C. E.; Daly, A.; Huson, S. M.; Tosi, L. L.; Cunningham, M. L.; Darling, T. N.; Geer, J.; Gucev, Z.; Sutton, V. R.; Tziotzios, C.; Dixon, A. K.; Helliwell, T.; O'Rahilly, S.; Savage, D. B.; Wakelam, M. J. O.; Barroso, I.; Biesecker, L. G.; Semple, R. K. *Nat Genet* **2012***, 44*, 928-933.

36. Hevner, R. F. *Semin. Perinatol.* **2015***, 39*, 36-43.

37. Hou, W.; Li, Z.; Gordon, R. E.; Chan, K.; Klein, M. J.; Levy, R.; Keysser, M.; Keyszer, G.; Brömme, D. *Am J Pathol* **2001***, 159*, 2167-2177.

38. Lemaire, R.; Huet, G.; Zerimech, F.; Grard, G.; Fontaine, C.; Duquesnoy, B.; Flipo, R. M. *Br. J. Rheumatol.* **1997***, 36*, 735-743.

39. Biniossek, M. L.; Nägler, D. K.; Becker-Pauly, C.; Schilling, O. *J. Proteome Res.* **2011***, 10*, 5363-5373.

40. McNally, E. G. *Skeletal Radiol* **2008***, 37*, 99-113.

Chapter 3: Cell Permeable, Photoactivated Peptide Reporters: Shining a Light on Akt Activity in Single Cells

3.1 Overview

Akt kinase is a known contributor to tumor formation, and tools to evaluate the activity of this kinase in small clinical samples may eventually guide precision medicine. Microinjected or genetically encoded peptide sensors are powerful tools to detect aberrant kinase activity, but generally preclude high-throughput studies with primary cells. To address these limitations, we developed a cell permeable, photoactivated peptide reporter which can be delivered *en masse* to a population of cells. Since the 2-4,5-dimethoxy 2-nitrobenzyl (DMNB)-caged probe becomes active upon light stimulation, it enables programmable reaction times. We demonstrated that this strategy may be generalizable, and when paired with an automated capillary electrophoresis analysis system, significant improvements in throughput are achieved while retaining the ability to quantify all fluorescent metabolites from single cells.

3.2 Introduction

Protein kinases are arguably the largest driver of intracellular signal transduction. When regulatory control of this family of enzymes is usurped by disease, the relative amounts of phosphorylated product and substrate become unbalanced. This is true of protein kinase Akt *aka* protein kinase B, whose dysregulation is a key step in tumor formation and maintenance.[1] As such, this enzyme and the pathway (phosphoinositide 3-kinase (PI3K)) to

which it belongs are targets for therapeutics and companion diagnostics. Selection of patients for treatment with Akt inhibitors will rely on development of analytical platforms to identify aberrant kinase activity in clinical samples, but this remains a challenge due to the small tumor sample sizes attainable and their mixed cellular composition. Single cell analysis is necessary due to the presence of rare subpopulations which may be masked in bulk analysis only to drive drug resistance at a later point.[2]

Fluorescent peptide reporters have been utilized as reporters to directly assess kinase activity, and stand to bridge the gap between small molecules which are poor substrates and of limited specificity and genetically engineered proteins which often preclude use with primary and other difficult to transfect cells.[3,4] Peptide reporters are phosphorylated by kinases within intact cells and the relative ratios of unphosphorylated peptide and phosphorylated product obtained from single cells is quantified by microelectrophoretic techniques such as capillary electrophoresis (CE).[5] While these measurements are highly sensitive, quantitative, and possess great multiplexing potential, a continuing bottleneck for *ex vivo* applications is the delivery of fluorescent reporters into the cell cytoplasm. To date, delivery of these reporters has relied on low throughput methods such as microinjection or cell-penetrating peptides (CPPs) which predominantly deliver cargo to endosomal compartments.[6] Overcoming these limitations would be beneficial particularly when assaying clinical samples. Delivering a reporter *en masse* into the cytosol of a population of cells would dramatically improve overall throughput when coupled to an automated analysis system, enabling sampling from sufficient numbers of cells for statistical analyses and inference of aberrant phenotypes.

We aimed to address such challenges through chemical and instrumentation innovations. Specifically, we have developed a cell permeable, photoactivatable (i.e. "caged") reporter which is masked as a substrate until UV light induces a photochemical conversion of the molecule into its substrate form (Figure 3.1). When the programmable reaction time of the caged reporter is paired with automated single cell-CE, significantly higher throughput measurements of kinase activity from single cells are achieved, which has the potential to circumvent current technological gaps in biosensor development.

3.3 Materials and Methods

3.3.1 Materials

O-(6-chlorobenzotriazol-1-yl)-N,N,N′,N′-tetramethyluronium hexafluorophosphate(HCTU), 6-carboxyfluorescein (6FAM), Fmoc-protected amino acids, and NovaSyn TGR resin were purchased from Chempep and NovaBiochem. Purified recombinant Akt was purchased from EMD Millipore (14-276). PANC-1 cells were supplied from ATCC. All other reagents and solvents were purchased from Sigma-Aldrich or Fisher.

3.3.2 Peptide Synthesis

Peptides described in this chapter were synthesized by Dr. Qunzhao Wang in the laboratory of Professor David Lawrence.

3.2.2.1 Synthesis of Caged Threonine: *N*-(9-Fluorenylmethyloxycarbonyl)-*O*-(4,5-dimethoxy-2-nitrobenzyl)-L-threonine (Fmoc-Thr(O-(4,5-dimethoxy-2-nitrobenzyl))-OH)

Triflic anhydride (18 µL, 0.2 mmol) in 1 mL anhydrous methylene chloride was added slowly to a solution of *N*-(9-Fluorenylmethyloxycarbonyl)-L-threonine allyl ester (Figure 3.2, S1a) (1.3 g, 3.4 mmol, prepared following reported method[7] from Fmoc-Thr-

OH) and 4,5-dimethoxy-2-nitrobenzyl trichloroacetimidate (1.2 g, 3.4 mmol, prepared following reported method[6] in 40 mL anhydrous methylene chloride kept under nitrogen at room temperature.[8] The resulting dark green solution was stirred overnight in the dark. The resulting solution was filtered, concentrated, dissolved in small amount of methylene chloride and run through a 50 g silica column with 30-40% ethyl acetate in hexane. The desired fraction was collected, concentrated (0.89 g) and treated with Pd(PPh$_3$)$_4$ (1.7 g, 1.5 mmol) in 40 mL chloroform containing 1 mL acetic acid and 4 mL N-methylmorphorline for 4 h. The reaction was treated with 0.1 N HCl until pH around 3-4, and extracted with ethyl acetate, dried (Na$_2$SO$_4$), concentrated, and purified on silica gel column (0-3% methanol in methylene chloride) to yield S1c (Figure 3.2) (210 mg, 12% yield in two steps). ^{1}H NMR (400 MHz, CHLOROFORM-d) δ ppm 1.36 (d, J=6.27 Hz, 3 H) 3.93 (s, 3 H) 3.95 (s, 3 H) 4.26 (t, J=7.03 Hz, 1 H) 4.30-4.38 (m, 1 H) 4.48 (d, J=6.78 Hz, 1 H) 4.55 (dd, J=9.29, 2.51 Hz, 1 H) 4.86 (AB quartet, Δ δ =0.28, J=14.56 Hz, 2 H) 5.55 (d, J=9.79 Hz, 1 H) 7.11 (s, 1 H) 7.28 (s, 1 H) 7.32 (t, J=7.40 Hz, 2 H) 7.42 (t, J=7.40 Hz, 2 H) 7.57 - 7.67 (m, 3 H) 7.78 (d, J=7.53 Hz, 2 H). ESI MS calculated for C$_{28}$H$_{28}$N$_2$O$_9$ + H$^+$ (M$^+$) m/z: 537.2, found 537.2.

3.2.2.2 Synthesis of Caged Threonine-Containing Peptide 1: 6FAM-Gly-Arg-Pro-MeArg-Ala-Phe-Thr(O-(4,5-dimethoxy-2-nitrobenzyl))-Phe-MeAla-amide

Coupling was achieved with two 5-min incubations in dimethylformamide (DMF) with 5 equivalents (eq) Fmoc amino acid, 5 eq HCTU, and 10 eq N,N-Diisopropylethylamine (DIPEA). Fmoc-Thr(O-(4,5-dimethoxy-2-nitrobenzyl)), Fmoc-MeArg(Pbf)-OH, Fmoc-MeAla-OH and other regular protected amino acids were used. Fmoc deprotection was performed with two 2.5-min incubations with 20% piperidine in DMF. For couplings of aminos next to N-methylated amino acid (Attaching Phe to MeAla and attaching Pro to

MeArg), HATU in place of HCTU was used and the coupling was repeated for three times of 1 h, then Capped with acetic anhydride. The N-terminus of all peptides was reacted with 5 eq 6FAM, 5 eq diisopropylcarbodiimide (DIC), and 5 eq Oxyma in DMF overnight, and then treated with 20% piperidine in DMF for 30 min. The peptide was cleaved with trifluoroacetic acid: water: triisopropylsilane (TFA: H_2O: TIS) in a ratio of 95 : 2.5 : 2.5, and purified by HPLC using H_2O/Acetonitrile containing 0.1% TFA solvent system. $C_{79}H_{95}N_{17}O_{20}$, exact mass calculated 1601.7 (M), found (ESI+, m/z) 535.4 (M+3H$^+$), 802.5 (M+2H$^+$).

3.2.2.3 Synthesis of Fmoc-L-serine allyl ester (S2a)

150 mL water containing N-Fmoc-L-Serine (10.22 g, 31.2 mmol) and NaHCO$_3$ (14.36 g, 31.8 mmol) were combined with 60 mL CH_2Cl_2 containing tricaprylmethylammonium chloride (~11g) and allyl bromide (16 mL, 184.89 mmol), and the suspension was vigorously stirred at room temperature for 24 h. Water (300 mL) was added to the reaction mixture, and the suspension was extracted with methylene chloride (3 x 200 mL). The combined organics were dried (Na$_2$SO$_4$) and the solvent was removed under reduced pressure. The crude residue was purified by silica flash chromatography (65:35 hexanes:ethyl acetate) to yield S2a (Figure 3.3) as a white solid: ^{1}H NMR (400MHz, CDCl$_3$) $\square$ = 7.77 (d, J = 7.3 Hz, 2 H), 7.62 (br.d., J = 4.6 Hz, 2 H), 7.41 (t, J = 7.5 Hz, 2 H), 7.32 (t, J = 7.5 Hz, 2 H), 5.92 (tdd, J = 5.6, 11.0, 16.9 Hz, 1 H), 5.84 (d, J = 7.8 Hz, 1 H), 5.35 (d, J = 17.1 Hz, 1 H), 5.27 (dd, J = 1.1, 10.4 Hz, 1 H), 4.69 (d, J = 5.4 Hz, 2 H), 4.53 - 4.46 (m, 1 H), 4.46 - 4.37 (m, 2 H), 4.23 (t, J = 7.0 Hz, 1 H), 4.04 (dd, J = 3.1, 11.1 Hz, 1 H), 3.94 (dd, J = 2.9, 11.2 Hz, 1 H), 2.37 (br. s., 1 H). Exact mass calculated for $C_{21}H_{21}NO_5$ 367.14; found (ESI+) 368.1 (M + H)$^+$, 390.1 (M + Na)$^+$.

3.2.2.4 Synthesis of 4,5-dimethoxy-2-nitrobenzyl trichloroacetimidate (S2b)

4,5-dimethoxy-2-nitrobenzyl alcohol (8.97 g, 42.08 mmol) and anhydrous K_2CO_3 (14.2 g, 102.74 mmol) were stirred in 120 mL of anhydrous methylene chloride under nitrogen atmosphere. To the above mixture, trichloroacetonitrile (10 mL, 99.73 mmol) and anhydrous triethylamine (6 mL, 43.01 mmol mmol) were added and the reaction mixture stirred at room temperature for 24 h. Methylene chloride (300 mL) was added to the reaction mixture. Organic layer was collected and washed with 0.5 N HCl followed by solvent removal. The dried crude residue was purified by silica flash chromatography (75:25 hexanes:ethyl acetate) to yield S2b (Figure 3.3): ^{1}H NMR (400MHz, CDCl$_3$) □ = 8.51 (s, 1 H), 7.75 (s, 1 H), 7.23 (s, 1 H), 5.78 (s, 2 H), 3.97 (s, 3 H), 3.96 (s, 3 H). Exact mass calculated for $C_{11}H_{11}Cl_3N_2O_5$ 355.97; found (ESI+) 374.9 (M + H$_3$O)$^+$.

3.2.2.5 Synthesis of *N*-(9-fluorenylmethyloxycarbonyl)-*o*-(4,5-dimethoxy-2-nitrobenzyl)-L-serine allyl ester (S2c)

Fmoc-serine allyl ester (1.74 g, 4.75 mmol) and the 4,5-dimethoxy-2-nitrobenzyl trichloroacetimidate (3.22 g, 9.04 mmol) were dissolved in methylene chloride (40 mL) and mixed under nitrogen atmosphere at room temperature. To the above solution was slowly added solution of triflic acid in methylene chloride (75 uL triflic in 5 mL methylene chloride). The reaction mixture was stirred at room temperature for 30 min after the completion of the triflic acid addition. *N,N*-Diisopropylethylamine (150 uL) in methylene chloride (10 mL) and silica gel were added to the reaction mixture and then concentrated under reduced pressure. The crude residue, adsorbed on silica, was purified by silica flash chromatography (67:33 hexanes:ethyl acetate) to afford S2c (Figure 3.3) : ^{1}H NMR (400MHz, CDCl$_3$) □ = 7.77 (d, *J* = 7.5 Hz, 2 H), 7.72 (s, 1 H), 7.61 (t, *J* = 6.7 Hz, 2 H), 7.41

(t, J = 7.3 Hz, 2 H), 7.31(t, J = 6.6 Hz, 2 H), 7.18 (s, 1 H), 5.97 - 5.82 (m, 1 H), 5.71 (d, J = 8.4 Hz, 1 H), 5.33 (d, J = 17.1 Hz, 1 H), 5.23 (d, J = 10.4 Hz, 1 H), 4.98, 4.92 (ABq, J_{AB} = 15.4 Hz, 2 H), 4.71 (d, J = 5.1 Hz, 2 H), 4.68 - 4.62 (m, 1 H), 4.48, 4.39 (ABX$_{qd}$, J_{AB} = 10.5 Hz, J_{AX} = 6.8 Hz, J_{BX} = 6.9 Hz, 2 H), 4.24 (t, J = 7.1 Hz, 1 H), 4.18 - 4.04 (m, 2 H), 3.96 (s, 3 H), 3.95 (s, 3 H), 3.94 - 3.89 (m, 1 H). Exact mass calculated for $C_{30}H_{30}N_2O_9$ 562.20; found (ESI+) 563.2 (M + H)$^+$, 585.2 (M + Na)$^+$.

3.2.2.6 Synthesis of *N*-(9-Fluorenylmethyloxycarbonyl)-*O*-(4,5-dimethoxy-2-nitrobenzyl)-L-serine (S2d)

The caged serine allyl ester (1.00 g, 1.78 mmol) was dissolved in chloroform (40 mL) containing acetic acid (21 mL) and n-methylmorpholine (3 mL). To the above solution was added Pd(Ph$_3$P)$_4$ (0.97 g, 0.84 mmol). The reaction mixture was stirred for 4 h at room temperature and neutralized by the addition of 0.1 N HCl till pH 4. The suspension was extracted by CH_2Cl_2 (x 2) and ethyl acetate (x 3). The organic extracts were dried (Na$_2$SO$_4$), and concentrated under reduced pressure. The crude residue was purified by silica flash chromatography (methylene chloride and then 48:2 methylene chloride:methanol) to yield S2d: ^{1}H NMR (400MHz,CDCl$_3$) $\square$ = 7.76 (d, J = 7.6 Hz, 2 H), 7.66 (s, 1 H), 7.60 (t, J = 5.9 Hz, 2 H), 7.40 (t, J = 7.5 Hz, 2 H), 7.31 (dt, J = 1.2, 6.4 Hz, 2 H), 7.10 (s, 1 H), 5.69 (d, J = 8.3 Hz, 1 H), 4.97, 4.87 (ABq, J_{AB} = 15.29, 2 H), 4.68 (br.s., 1 H), 4.53 - 4.37 (m, 2 H), 4.23 (t, J = 6.7 Hz, 1 H), 4.12 (d, J = 9.2 Hz, 1 H), 3.93 (s, 3 H), 3.90 (s, 3 H), 3.89 - 3.83 (m, 1 H). Exact mass calculated for $C_{27}H_{26}N_2O_9$ 522.16; found (ESI+) 523.2 (M + H)$^+$, 545.1 (M + Na)$^+$.

3.3.3 Peptide Characterization Protocols

3.3.3.1 *In vitro* Photoactivation Studies

Benchtop photolysis was performed using a Nikon TE300 inverted microscope equipped with a Nikon 75W Xenon arc and an ultraviolet excitation filter (Nikon UV-2E/C) delivering a bandwidth of 360 ± 20 nm to the sample. 40 µL samples were contained within O-rings glued to No. 1 glass coverslips (Fisherbrand: 12-544-F) using polydimethylsiloxane (PDMS). UV power was measured with a ultra-violet radiometer (VWR, Radnor, PA). UV attenuation by the borosilicate glass coverslip was minimal, but accounted for by obtaining measurements with an identical glass coverslip in place between the light source and sensor. Varying light intensities were attained by placing Nikon neutral density filters between the sample and light source. Samples were exposed to UV light for up to 10 min, collected and stored in the dark, and diluted 20X before analysis with capillary electrophoresis with laser-induced fluorescence (CE-LIF) detection.

3.3.3.2 *In Vitro* Kinase Assay

To ensure that the photoactivated peptide **2** possessed similar phosphorylation kinetics to that of the native substrate (**NS**), which had never been caged with DMNB, both were subjected to an *in vitro* phosphorylation assay using recombinant Aktα. Fully caged peptide **1** was also included in the assay to determine if it might be phosphorylated by the kinase. Following benchtop photolysis, photoactivated reporter **2** (15 µM) was mixed with recombinant Aktα (5.6 nM) in 8 mM MOPS (pH 7.0) with 4 mM $MgCl_2$ and 1 mM ATP. Fully caged reporter **1** and **NS** peptide were separately incubated with Aktα under identical conditions. In negative control experiments, ATP was omitted from the reaction mixture. Assays were performed at 30 °C. After the addition of ATP to start the reaction, 6 µL

aliquots were removed at various times and the enzymatic reactions terminated by rapidly heating to 90°C for 4 min. Samples were then diluted 20x and analyzed by CE-LIF.

3.3.3.3 Enzymatic Generation of Peptide 3 (Phosphorylated Reporter)

Standards of phosphorylated reporter **3** were enzymatically generated by incubating 30 µM of peptide **2** with 6 nM recombinant Aktα, 2 mM ATP in 8 mM MOPS (pH 7.0) with 4 mM $MgCl_2$. Assays were incubated at 30 °C for 5 h. The molecular mass of phosphorylated peptide was confirmed by MALDI-MS with an AB SCIEX 4800 Plus instrument equipped with a 337 nm laser.

3.3.3.4 Cell Culture

PANC-1 cells were obtained from the American Type Culture Collection and maintained in a humidified environment atmosphere with 5% CO_2 at 37 °C. The purity of the cell line was authenticated by the Human Cell Line Authentication (CLA) Analysis Facility at Duke University. Cells were grown in Dulbecco's Modified Eagle Medium (DMEM) supplemented with 10% fetal bovine serum (FBS), streptomycin (100 µg mL^{-1}), and penicillin (100 units mL^{-1}).

3.3.3.5 Lysate Phosphorylation Assay

PANC-1 lysates were prepared in the presence of phosphatase and protease inhibitors. Cells were detached from the tissue culture surface with 0.5% trypsin and the reaction stopped by addition of DMEM containing FBS, and the cells were pelleted by centrifugation. The pellet was washed twice in phosphate buffered saline (PBS; 137 mM NaCl, 2.7 mM KCl, 10 mM Na_2HPO_4, 1.8 mM KH_2PO_4) and the cells brought to a pellet by centrifugation. Lysates were prepared by resuspending the cell pellet in 400 µL lysis buffer and rapidly

freezing and thawing the pellet in liquid nitrogen for three cycles. Lysis buffer was comprised of 50 mM MOPS, pH 7.6, 200 mM NaCl, 4 mM pervanadate, 100 mM glycerophosphate, 12 mM sodium pyrophosphate, 40 mM NaF, 2 mM EDTA, 2 mM EGTA, 4 µg/mL aprotinin, 4 µg/mL leupeptin, 2% Triton X-100, 20% glycerol, and 2 mM DTT. The protein content of cell lysates was 3.0 mg/mL. Protein concentration was determined by reaction with fluorescamine and bovine serum albumin was used to generate a calibration curve.

3.3.3.6 Loading Cells with Caged Peptide 1

PANC-1 cells were removed from tissue culture flasks with 0.5% trypsin. Cells (10^6) were incubated with Peptide **1** (10 µM, 10 µL) at the temperature indicated for 10 min. The cell suspension was then washed once with 0.5% trypsin, 2X with extracellular buffer (ECB; 135 mM NaCl, 5 mM KCl, 1mM $MgCl_2$ 1 mM $CaCl_2$ and 10 mM HEPES, pH 7.4) before photoactivation, lysis, or single cell analysis.

3.3.3.7 Confocal Microscopy

Confocal images were obtained at 37°C on an Olympus FV1000 scanning confocal system. All imaging was performed with a 40X (N.A.:1.3) or 60x (N.A.: 1.4) objective using a 488 nm laser for illumination. Image J was employed for image analysis.[9]

3.3.3.8 Cytotoxicity Assay

A colorimetric WST-8 cytotoxicity assay (Dojindo, Inc.) was utilized to detect the activity of intracellular lactate dehydrogenase (LDH) from cells after incubation with peptide and exposure to UV illumination. An absence of LDH activity from cells is an indicator of cellular toxicity and cytolysis.[10] PANC-1 cells were plated in 96-well plates and allowed to

adhere overnight. Cells were incubated with caged peptide **1** (0, 1, or 10 µM) at 4°C for 10 min. Cells were rinsed 1X with 0.5% trypsin, 2X with ECB and exposed to 4.2 mW/cm^2 UV light (360±20 nm) for 4 min and rinsed 2X with ECB. Negative-control wells with cells but without peptide or UV irradiation underwent the same wash steps. ECB was replaced with 100 µL DMEM containing penicillin, streptomycin (100 units mL^{-1}, respectively) and 10% FBS. The cells were returned to the incubator for 2 h. WST-8 (10 µL) reagent was added to each well and the plate returned to the incubator. At 6 h, absorption at 450 nm was measured The colorimetric agents were removed and replaced with the indicated DMEM formulation. Measurements were repeated at 36 h Multiple comparison of means via One-way ANOVA with *post-hoc* Tukey multiple comparison of means demonstrated that no groups were statistically different from one other. (p = 0.50, 6 h; p = 0.28, 36 h)

3.3.3.9 UV-Induced DNA Damage Assessed by Cyclobutane-Dimer ELISA

Cyclobutane dimers (CBD) formed by adjacent pyrimidines in DNA are a common type of UV-induced DNA damage.[11] The UV-Induced DNA Damage ELISA Kit (Cell Biolabs: STA-322) was utilized to assess the presence CBDs in PANC-1 cells exposed to UV light. Cells were plated overnight in tissue culture treated 96 well plates and exposed to varying UV power as indicated in the text. Cells were rinsed 2x with Dulbecco's Phosphate Buffered Saline (DPBS; 137 mM NaCl, 2.7 mM KCl, 8.1 mM Na$_2$HPO$_4$, 1.47 mM KH$_2$PO$_4$, 0.9 mM CaCl$_2$, 0.49 mM MgCl$_2$). Cells were fixed with 75% MeOH, 25% acetic acid for 30 min, and 70% EtOH for 30 min at 25 °C. Samples were denatured and washed according to the manufacturer's instructions. The samples were then incubated with anti-CPD antibody, followed by a horseradish peroxidase (HRP) conjugated secondary antibody. The reaction was terminated with the addition of acid, and the absorbance was measured at 450 nm. The

CPD content sample was determined by comparing with a standard curve that was prepared from predetermined CPD-DNA standards . Comparison of groups by one-way ANOVA indicated that at least one group was statistically different (*p ≤ 0.05), and *post hoc* analysis by Tukey's multiple comparison analysis illustrated that the amount of CBD detected after a 22 min exposure to UV irradiation was statistically different (*p≤ 0.05) from that detected at all other time points, including those used for single cell analysis (4 min exposure).

3.3.3.10 Capillary Electrophoresis

CE-LIF separations of caged and photoactivated peptide samples were performed on a commercial instrument (ProteomeLab PA 800) in 30-μM inner-diameter, fused silica capillaries (30 cm total length, 20 cm length from inlet to detection window). Sample injection was initiated by applying 0.5 psi for 5 s to the inlet of the capillary. Electrophoresis was performed at 333 V/cm in CE buffer (100 mM borate, 15 mM SDS, pH 11.4). Analytes were detected with a solid state laser (excitation at 488 nm, emission at 520 nm). The capillary was sequentially rinsed for 2 min at 20 psi with 1 M NaOH, H_2O, and CE buffer prior to each separation. Photoactivated peptide (%) or phosphorylation (%) or was measured as the ratio of the peak areas of phosphorylated and total reporter.

3.3.3.11 Single Cell Capillary Electrophoresis

Cells were cultured in glass-bottomed chambers which were then placed on the stage of a customized single-cell CE system with LIF. Cells were incubated with 10 μM peptide **1** and photoactivated at 4.2 mW/cm^2 for 4 min while in the cell chamber. Cells were maintained at 37°C using a constant flow of warmed ECB throughout the time for single cell analysis. After peptide uncaging, cells were incubated for an additional 20 min followed by cell lysis with a focused pulse from a Nd:YAG laser. Simultaneously the cell contents were loaded

into an overlying capillary (30 µm) by electrokinetic injection (5 s at 79 V/cm). Separations were performed at 250 V/cm and fluorescence excited at 488 nm with emission collected at 525 ± 25 nm.

To determine the identity of peptides formed as a result to photoactivation or incubation within a cell, peptide standards were loaded into the capillary following the contents of a cell previously loaded with peptide **1** and photoactivated. In order to achieve optimal resolution between peaks, standards of varying concentration were loaded. Peptides **1** and **3:** 100 nM, peptides **2**, iii, viii, i: 50 nM, vi, iv/v, ii: 25 nM . A voltage was then applied across the capillary to initiate electrophoretic separation. These electropherograms were compared to electropherograms with no standard co-injected to determine if that peptide fragment was formed. To calibrate the amount of peptide on the electropherograms, a known concentration (as described above) of standard of each intact peptide was loaded into the capillary, electrophoresed, and the area under the peak calculated. Spontaneous fluid displacement was experimentally determined to contribute to 20.2% ((0.10 nL) of the total volume injected, bringing the total injection volume to 0.48±0.02 nL . Poiseuille's equation was utilized to estimate the moles of peptide injected due to gravity and spontaneous fluid displacement. The moles of peptide injected for each standard were as follows: Peptides **1** and **3:** 4.77×10^{-20} mol, peptides **2**, iii , viii, i: 2.385×10^{-20} mol, vi, iv/v, ii: 1.19×10^{-20} mol .

3.3.3.12 Fabrication of Cell Traps

Cell traps were fabricated from 1002F-50 negative photoresist as described previously.[12] Coverslips were spin-coated (Laurell Model WS-650-23, Laurell Technologies) with 1002F-50 photoresist, and baked at 95°C for 55 min (Table 3.2). A chrome photomask

was placed over the photoresist-coated coverslip and exposed to UV light (650 mJ/cm^2),
crosslinking the exposed photoresist. The photoresist-coated coverslip was then developed
using SU-8 developer for 3 min, rinsed with isopropanol, and sequentially hard baked. Well
depth (44 ± 1 µm) was measured using a profilometer (KLA Tencor model P-15; San Jose,
CA).

3.3.3.13 Cell Trap Loading

Prior to trapping cells within the microwells, photoresist traps were plasma cleaned
(Harrick Plasma) for 10 min to promote wetting of the wells. Having observed a large
distribution in the diameter of PANC-1 cells (15-40 µm), we also optimized the size the
photoresist wells to enable trapping single cells of all sizes to prevent inadvertent
subpopulation profiling. 20 µL caged peptide **1**-loaded PANC-1 cells (1 million cells mL^{-1})
were deposited directly over the traps and allowed to settle for 2 min. Excess cells were
removed by rinsing with ECB buffer. The trapped PANC-1 cells were continuously bathed in
ECB (37°C, flow rate of 1 mm s^{-1}) for the duration of automated CE analysis. The entire
array of cells were simultaneously photoactivated by exposure at 4.2 mW/cm^2 for 4 min
before transfer onto the automated capillary electrophoresis system.

3.3.3.14 Automated Single-Cell Capillary Electrophoresis

A glass-PDMS cassette housing the cell traps similar to that described previously was
used for the automated, single-cell analysis by CE.[13] A 3-D printed housing held the cassette,
electrodes and buffer inlet/outlets securely on the stage of an automated, inverted microscope
(Ti-E, Nikon, Melville, NY). Since the buffer utilized for separations of caged reporter had a
low surface tension relative to that used previously, a 130 µM height difference was
fabricated between the two liquid channel pieces to safeguard against CE buffers spilling into

the air gap and mixing, which would negatively affect cell viability. Cells were maintained at 37 °C by the flowing buffer as well as a heated microscope stage insert. Customized software (Python, Wolfeboro Falls, NH and MicroManager, Vale Lab, UCSF) identified the address of each cell trap and moved the motorized stage as described previously.[13] Each cell trap that did not contain a single cell was removed from the program's list of well addresses to be interrogated, so that only wells with single-cells were analyzed. All other tasks were automated using LabVIEW (National Instruments, Austin, TX).

During automated single-cell analysis, the following events occurred sequentially under computer control. The microscope stage moved to the address of the first cell to be analyzed, placing the cell directly below the inlet of a capillary. The capillary was aligned 35 μm above the plane of the microwells. A focused laser pulse lysed the cell by creating a cavitation bubble and the cell's contents were then electrokinetically loaded into the capillary. Electrokinetic injections were performed by the application of 8 kV across the capillary for 1 s. The voltage was then set to zero as the stage moved through the air channel to the center of the electrophoretic buffer channel. A voltage of 10 kV (0.25 kV cm^{-1}) was applied across the capillary for 500 s to separate the cellular contents. The voltage was then set to zero for 1 s as the stage moved back to place the capillary at the address of the next cell to be assayed. The next cell was lysed, then injected, and this entire process was repeated until all of the cells in the array were analyzed. The capillary was interrogated 4 cm from the inlet end by the focused beam of a fiber-coupled diode-pumped solid-state 473 nm laser and the fluorescence of the analytes detected with a photomultiplier tube. The analytes were identified by comparison of their migration times to that of standards. The peak areas of known quantities (moles) of each above mentioned peptide were used to calculate the moles

of peptide contained in each cell. A brightfield image of each cell, taken immediately prior to the single-cell experiment, was used to measure cell diameter.

3.4 Results and Discussion

3.4.1 In vitro Characterization of Caged Peptide Reporter 1

The native substrate (**NS**) Akt peptide reporter 6FAM-GRP-(MeR)-AFTF-(MeA)-Amide (where MeR and MeA represent N-methylated versions of native amino acids) has favorable phosphorylation kinetics and demonstrated resistance to intracellular degradation.[14,15] **NS** possesses a single hydroxyl group that when coupled to a photoremovable DMNB group should block phosphorylation by Akt and render the reporter inactive as a substrate. As demonstrated by Figure 3.4 and Figure 3.5 (A,B) the photochemical conversion of this caged reporter can be controlled by varying both illumination duration and intensity, enabling investigator-controlled activation of the reporter including tuning its concentration. Predictably, photolysis kinetics are attenuated in cell lysates due to the absorption of UV wavelengths by intracellular molecules. Importantly, uncaged reporter **2** is phosphorylated at a rate indistinguishable to that of **NS**, both *in vitro* and in cell lysates (Figure 3.5C). The caged version **1** was not phosphorylated and did not spontaneously uncage to a measureable degree during assays.

3.4.2 Cell Loading of Caged Reporter 1

Having demonstrated that **1** was photoactivated and phosphorylated by Akt, we explored the delivery options for this reporter. Since **NS** is excluded from PANC-1 cells, prior work required microinjection of the reporter into cells, a slow and difficult process. A variety of CPPs exist for intracellular peptide delivery, but these strategies often utilize endosomal pathways resulting in significant peptide degradation or entrapment in the

90

endosome with little to no delivery to the cytosol, the primary location of endogenous Akt.[16-18] These challenges were manifested in our initial attempts to render **NS** cell permeable, with multiple CPPs[19,20] appended to the reporter resulting in punctate uptake indicative of an non-cytoplasmic location (Figure 3.6). However, **NS** when caged with DMNB to generate **1** was sufficiently hydrophobic to enter into the cytosol when incubated with PANC-1 cells (Figure 3.7, 3.8A). The uncaged peptide was not identified in cells after loading the caged peptide (n=12) indicating that entry into the cytosol did not result in cleavage of the protecting DMNB group (Figure 3.9). Additionally the diffuse (rather than punctate) appearance of the fluorescence after loading peptide into the cells (Figure 3.7) combined with the observed phosphorylation of the reporter (post photoactivation) (Figure 3.8D) suggested delivery into cytosol rather than a cytosolic subcompartment.

Quantification of intracellular peptide by CE revealed a correlation ($R^2 = 0.79$) between the total moles of fluorescent reporter ($n_{total} = n_{caged} + n_{phosphorylated} + n_{degraded}$) and the cell diameter (Figure 3.8E). Interestingly, when **NS** was modified with a DMNB-caged serine moiety rather than threonine, it retained cell permeable properties (Figure 3.10), suggesting that the addition of DMNB may be competent to render peptides of similar hydrophobicity cell permeable. This is consistent with recent studies which generated an angiotensin II analogue which was capable of entering cells upon linkage with DMNB.[21]

3.4.3 Monitoring Intracellular Akt Activity Utilizing Caged Reporter Peptide 1

We next evaluated the ability of this reporter to sense Akt activation after photolysis within intact PANC-1 cells. Akt is upstream of DNA repair mechanisms and is known to be a stress-activated kinase. Consequently, it was important to understand whether the UV

exposure needed for uncaging itself might cause DNA damage or activate the enzyme. CE-LIF analysis revealed that in intracellular photolysis experiments, 96±2.2% the reporter was uncaged when illuminated for 4 min with 4.2 mW cm^{-1} of UV light, an energy that did not induce cytotoxicity (Figure 3.11) or DNA pyrimidine lesions (Figure 3.12). Using these uncaging conditions, we assessed Akt activation and inhibition in single PANC-1 cells (Figure 3.8 D,F). After photolysis, the contents of single cells were assayed by CE and the phosphorylated sensor was quantified. Minimal Akt activity as indicated by very little peptide phosphorylation was detected in the absence of exogenous stimuli (Figure 3.8F), which agrees with prior reports utilizing **NS** and suggests that uncaging did not activate Akt.[15] Pathway stimulation or inhibition in response to TNFα, or TNFα + LY294002 was then assayed We observed significant heterogeneity of reporter phosphorylation in response to TNFα stimulation (0-100%), which is consistent with ours and others' observations of mosaic Akt activation across cell populations.[22-24] Treatment with LY294002 blocked reporter phosphorylation in response to TNFα, as expected since PI3K is downstream of the TNFα receptor. We were also capable of identifying all degradation products of the reporter (i-viii, nomenclature in Table 3.1)

3.4.3 Improved Throughput of Kinase Activity Measurement with Caged Peptide 1 Paired with an Automated Capillary Electrophoresis System

Having produced a cell permeable and photoactivated Akt reporter, we next sought to harness these unique properties to enhance the rate of single-cell protein-kinase analysis. Our prior work utilizing microinjection of **NS** possessed a very limited throughput of 0.5 cell h^{-1}.[14,15] We've recently reported an automated system that can quantify kinase activity as rapidly as 3.5 cells min^{-1}, which rivals microfluidic separation systems while still offering

92

excellent (10^{-20} mol) detection limits.[13,25] A limitation for this system, however, is that reporters are acted upon during the loading process into the cell so that the reaction time in the cell is unknown. These challenges are uniquely addressed by the Akt reporter **1,** which is membrane permeant with a programmable reaction start time (uncaging).

We conducted a pilot study utilizing the automated single-cell CE system in which all cells in a population were simultaneously photoactivated to assess Akt activity as a function of time. Prior to single cell experiments, the cell traps housing individual PANC-1 cells were optimized. Traps were fabricated according to the process parameters in Table 3.2 with a range of diameters, and it was found that plasma treatment for 10 min was optimal to wet wells, and that 45 µm diameter wells were most effective at trapping individual cells (Figure 3.13). Cells were loaded with caged reporter **1**, photoactivated, and serially analyzed (n =109) (Figure 3.14). Among the cells assayed, the photoactivation efficiency was 97±2.8%, and the amount of reporter loaded was 42.4±42.7 amol. The lack of correlation ($R^2 = 0.018$, Figure 3.15) between the total peptide (amol) detected and the dwell time within an intact cell suggests that the reporter was not exported over the analysis period.

An oft overlooked commonality among peptides and sensor proteins, even those engineered for stability, is their eventual degradation within the intracellular context. Since phosphorylation and degradation can have similar effects on sensor fluorescence, this is a particular challenge with many protein-based sensors using fluorescence-resonance energy transfer or lifetime imaging which rely on molecular proximity and/or fluorescence decay rate to readout probe phosphorylation.[3,26] In contrast, the single-cell CE system measures intact and degraded reporter as well as that phosphorylated to accurately quantify

phosphorylation rate (Figure 3.14B). When peptide standards of known concentration are also paired with single-cell CE utilized, the moles of the different peptide species are readily quantified (Figure 3.14C,D). Rather than simply increasing as a function of reporter incubation time, we found that Akt reporter phosphorylation was highly heterogeneous at all times measured. This may suggest that the peptide phosphorylation reaches equilibrium between kinases and their opposing phosphatases, and the balance point is unique for each cell. Since the most frequent aberration resulting in elevated Akt activity in cancer is deactivation of the downstream phosphatases PTEN, the measurement of this equilibrium point is also a valuable snapshot of the entire signaling node.

Measurement of peptide degradation provided insight into how peptides were modified over time within single cells (Figure 3.14D**;** fragment nomenclature in Table 3.1). For cells analyzed at 15±1 min (n=11) after reporter uncaging, both phosphorylated reporter **3** and full length reporter **2** were present as well as the 8-,4-and 5-amino acid proteolysis products, viii and iv/v. At 29±1 min (n=14), cells contained **2** and significant amounts of **3**, but with substantial quantities of peptide fragments iv/v. By 45±1 min (n=10) **3** and **2** remained, but the dominant peptide forms were 5 amino acids or less. The formation of key fragments such as ii, iv/v, and viii indicate that the reporter is acted upon by peptidases targeting basic and hydrophobic amino acids such as arginine and phenylalanine, respectively.

3.5 Conclusions

The generation of a cell permeable, photoactivated reporter enabled analysis (7.2 cells h^{-1}) of kinase activity in a population of cells; a considerable benefit considering similar

caged kinase reporters have required microinjection or transfection. Photoactivation of DMNB-caged peptide enabled investigator control of reporter concentration as well as programmable reaction times. The membrane-permeant qualities imparted by the DMNB group, which may be generalizable beyond the peptides tested here, are highly valuable in the development of peptide sensors, and enable measurement from sufficient cells for meaningful statistical analysis. Overall, throughput was improved 14.4-fold with this reporter and we expect that outfitting peptide sensors with DMNB will shine a light on the role of aberrant kinase activity in small samples of clinical interest.
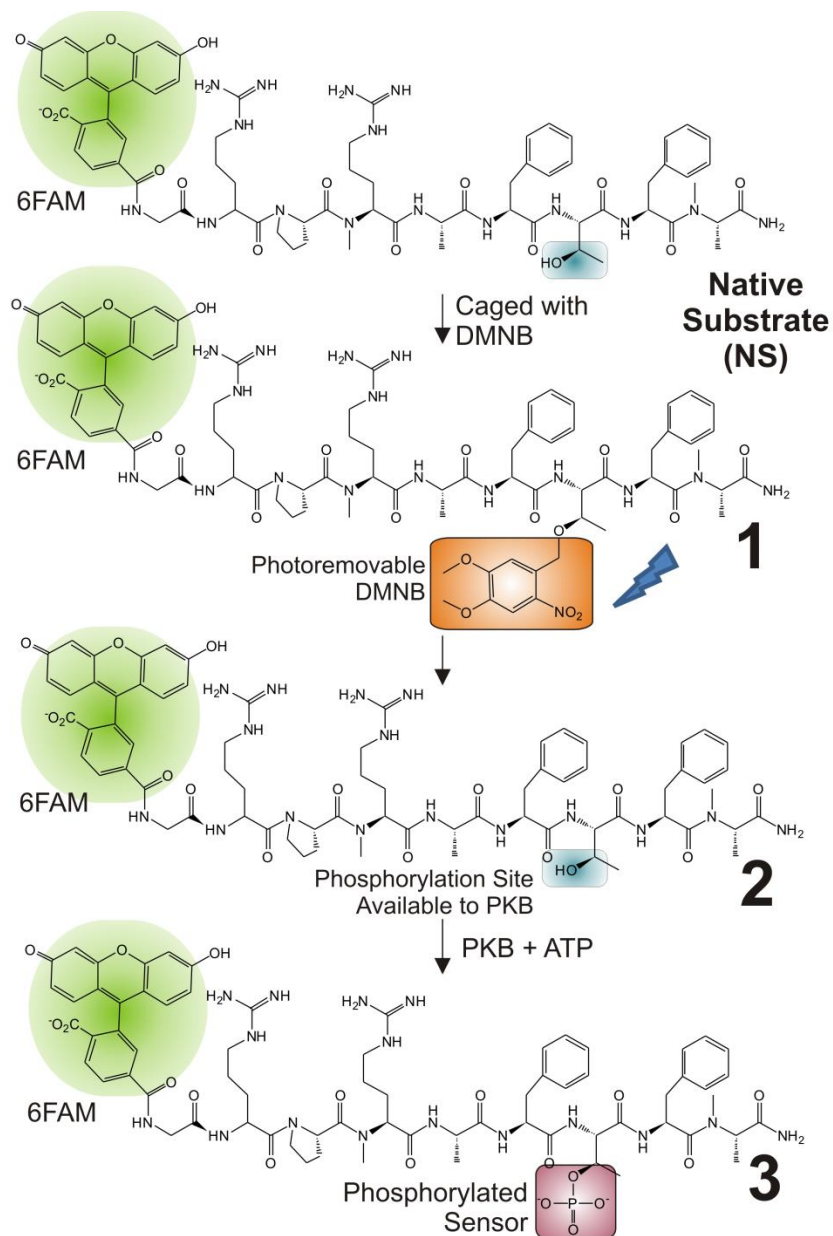
3.6 Figures and Tables

Figure 3.1 Schematic of Peptide Caging and Photoactivation. Native substrate **(NS)** was chemically caged with DMNB to generate **1,** which is delivered intracellularly. Photolysis releases the active sensor **2** which is phosphorylated (**3**) and measured in single cells by automated single-cell, capillary electrophoresis.
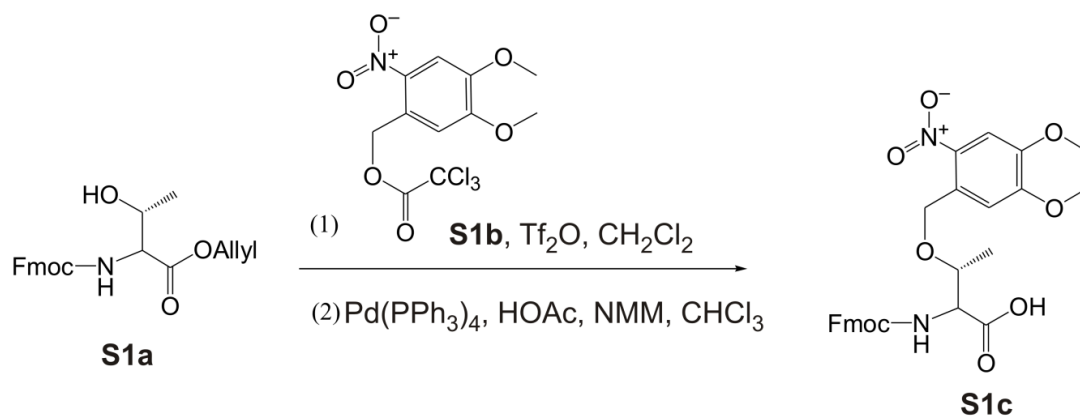
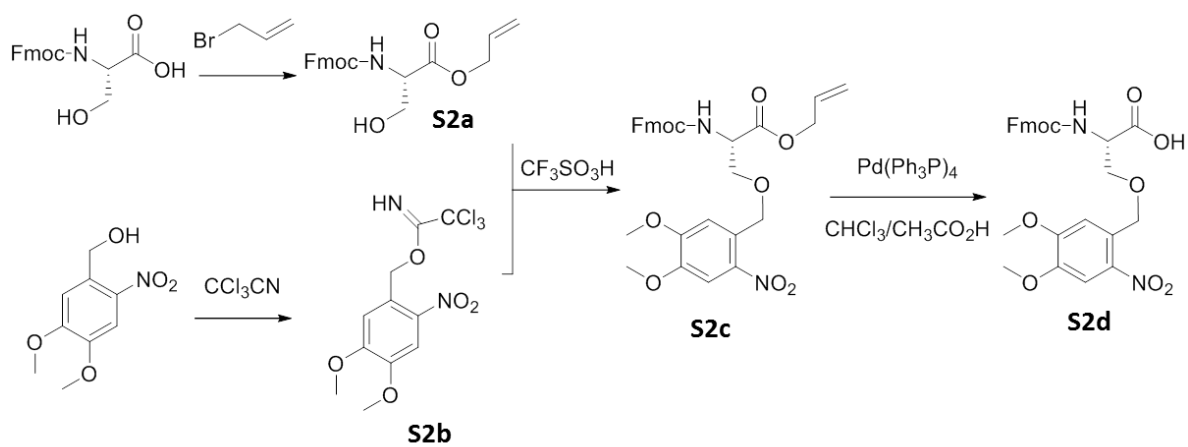**Figure 3.2 Synthesis of Fmoc-Thr(DMNB)-OH.**

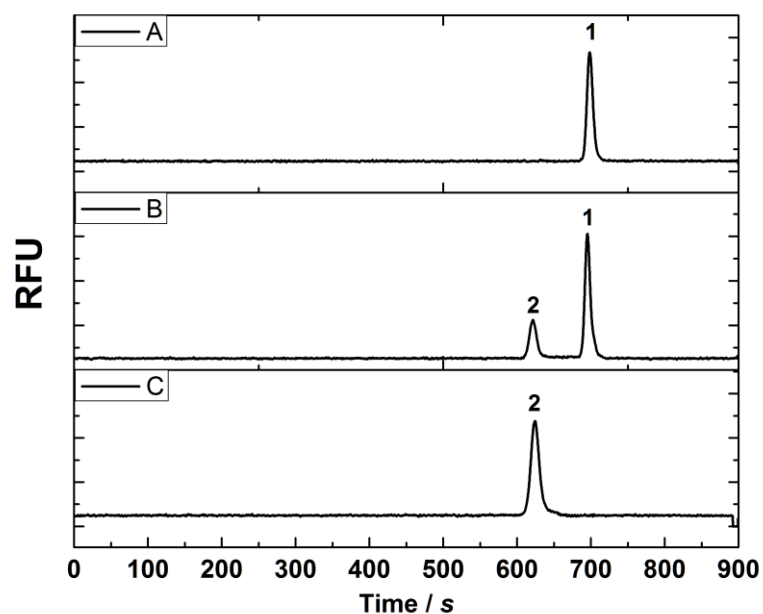**Figure 3.3 Synthesis of Fmoc-Ser(DMNB)-OH.**

Figure 3.4 *In Vitro* Photoactivation of Caged Reporter 1. 10 µM **peptide 1** was exposed to 360 ± 20 nm light at an intensity of 1.5 mW/cm^2 for 0 (A), 2 (B) or 10 (C) min and the sample separated by CE-LIF. Peak labels correspond to the caged reporter **1** and the photoactivated (uncaged) reporter **2,** respectively.
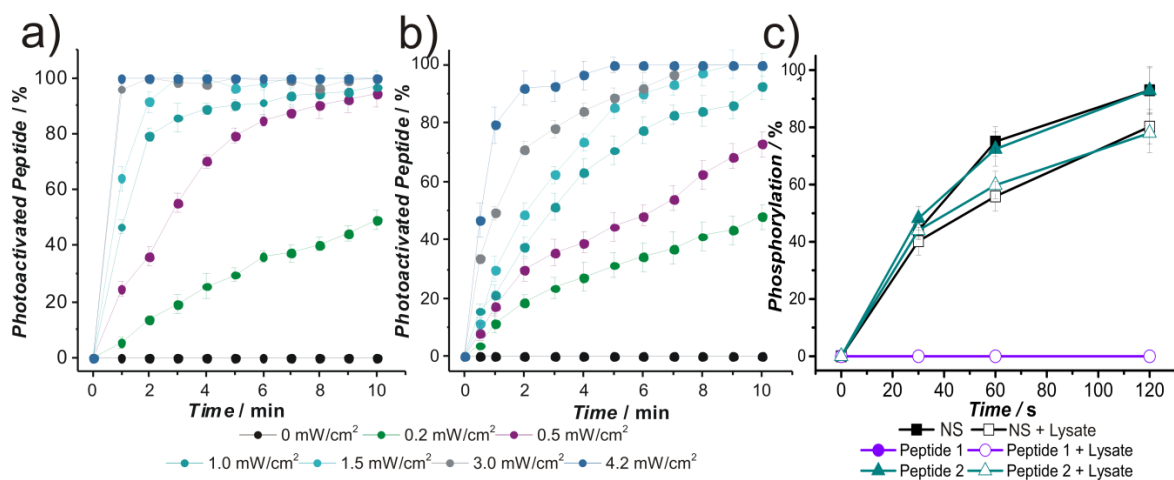
Figure 3.5 *In Vitro* **Characterization of Caged Akt Reporter 1.** A) Photolysis of 10 µM **1** in extracellular buffer (ECB) and B) PANC-1 lysate at varying intensities. C) Phosphorylation assays with recombinant Akt. Closed symbols: *in vitro* assays, open symbols: experiments performed in PANC-1 lysates.
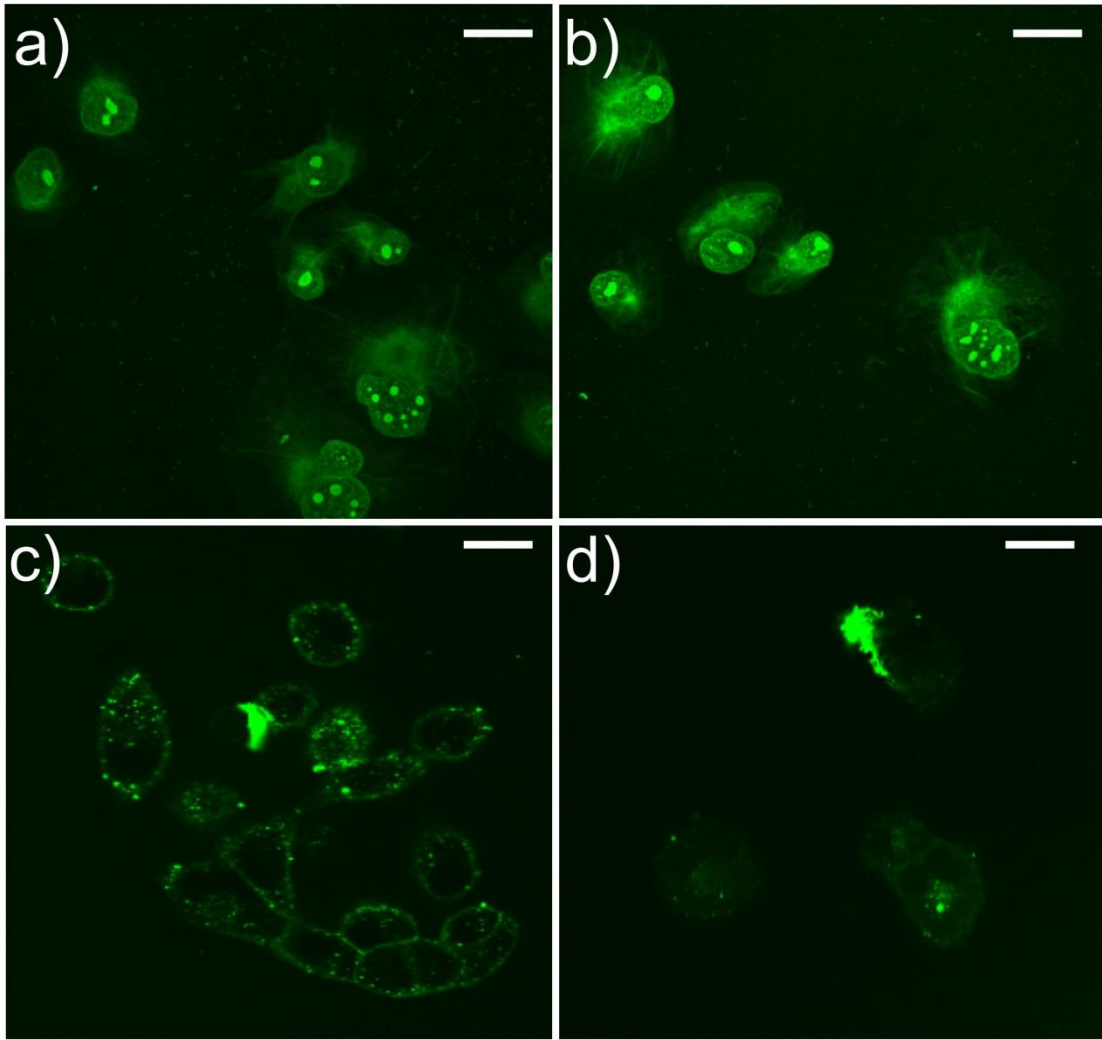
Figure 3.6 Loading Reporter Conjugated to Cell Penetrating Peptides (CPPs) into PANC-1 Cells. Shown are confocal fluorescence images of *Xentry*-peptide **NS** (A,B) and *TP2*-peptide **NS** (C,D) incubated with PANC-1 cells for 20 min at 37 °C (A,C) or 4°C (B,D). *Xentry*-peptide **NS** represents Ac-lclrpvg-Lys(6FAM)-GRP-Me*R*-AFTF-Me*A* while *TP2*-peptide **NS** denotes NH$_2$-pliylrllrgqf-Cys-SS-Cys(NH-6FAM)-GRP-Me*R*-AFTF-Me*A*-Amide. Lower case amino acid abbreviations indicate D-stereoisomer amino acids. Scale bar is 15 µm.
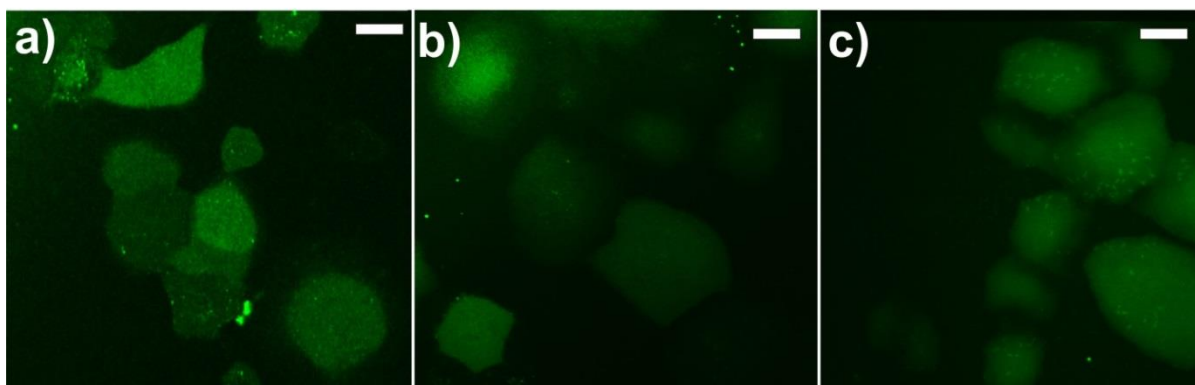
Figure 3.7 Loading of Caged Peptide 1 at Various Temperatures. Confocal images of PANC-1 cells after incubation with 10 µM peptide **1** for 10 min at a) 37°C, b) 25°C c) 4 °C. The scale bar is 10 µm.
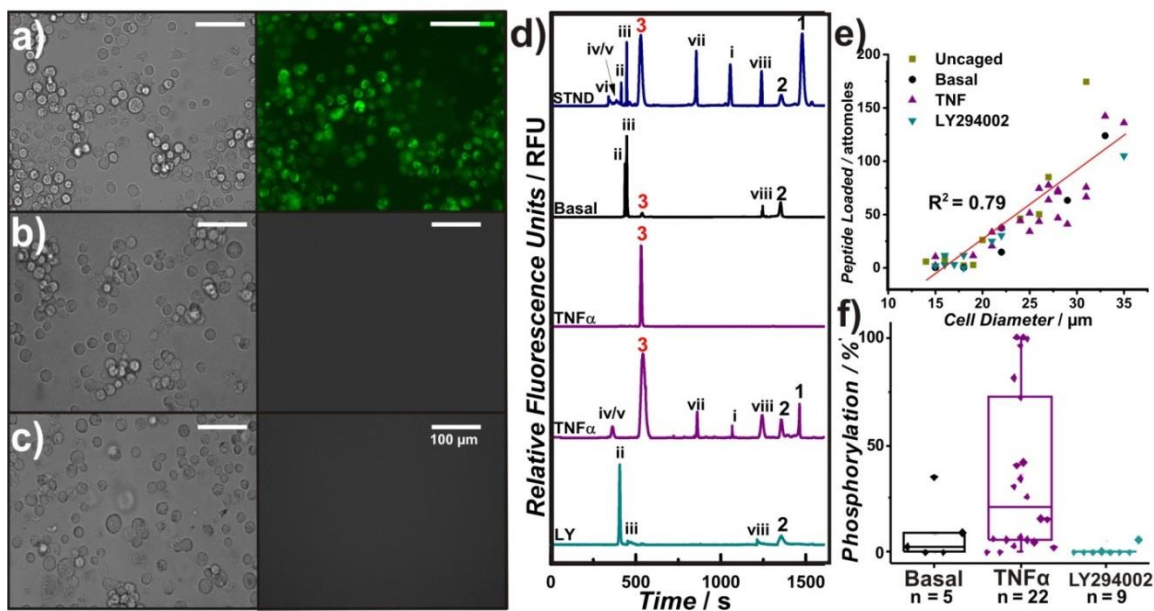
Figure 3.8 Intracellular Characterization of Peptide 1. Images of cells incubated at 4 °C with a) reporter **1,** b) reporter **2** c), or without peptide d) Single-cell Akt activity measured by chemical cytometry with the electrophoretic peaks labeled as **1**, **2**, and **3** for caged, photoactivated, and phosphorylated reporter, respectively. 6FAM-labeled proteolytic products of **1** are marked as i-viii (Table 3.2). The trace labeled (STND) demonstrates the migration time of a standard solution of the peptides. e) The attomoles of reporter loaded as a function of cell diameter ($R^2 = 0.79$). f) Akt activity for a population of single cells analyzed 20-min post-photolysis. Prior to loading with **1,** photolysis and analysis, cells were serum starved (labeled as basal) or pretreated with 100 nM TNFα or 10 μM LY294002.
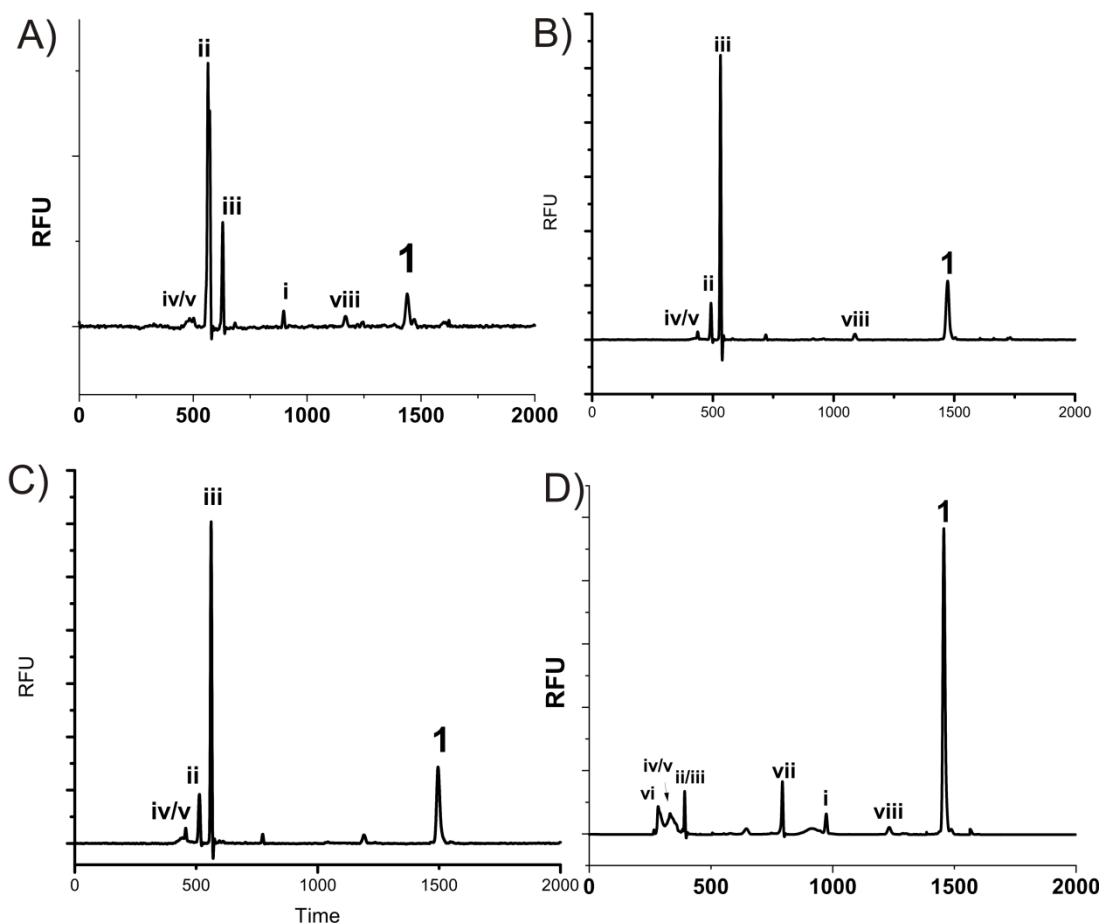
Figure 3.9 Caged Peptide 1 Does Not Spontaneously Photoactivate in the Intracellular Environment. (A-D) PANC-1 cells were loaded with peptide **1**, incubated for 20 min and analyzed by chemical cytometry. In all cases, no free peptide **2** was detected, indicating that DMNB is not liberated into the intracellular environment without UV illumination.
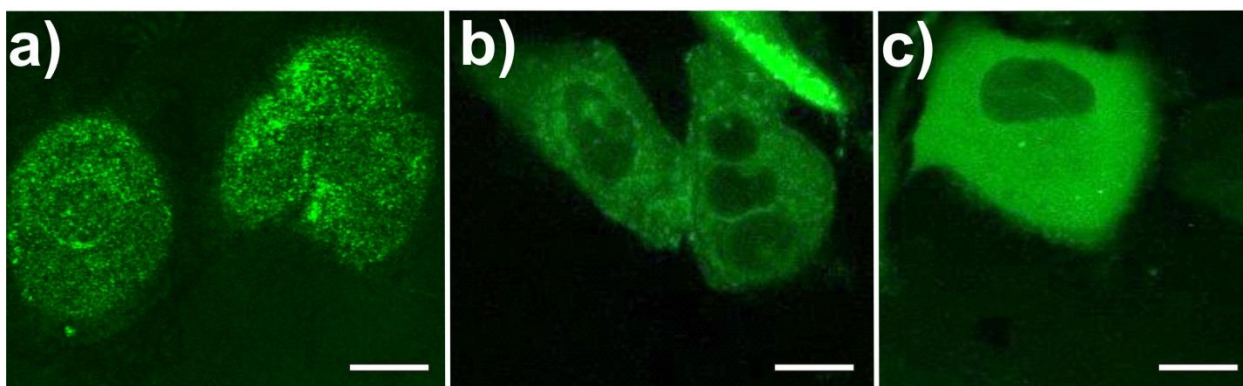
Figure 3.10 Loading of Caged Serine Reporter at Various Temperatures.
Confocal fluorescence images of PANC-1 incubated with 10 µM caged serine peptide
(6FAM-GRP-MeR-AF(DMNB-S)F-MeA-Amide) for 10 min at a) 37°C, b) 25°C c) 4 °C.
The scale bar is 20 µm.
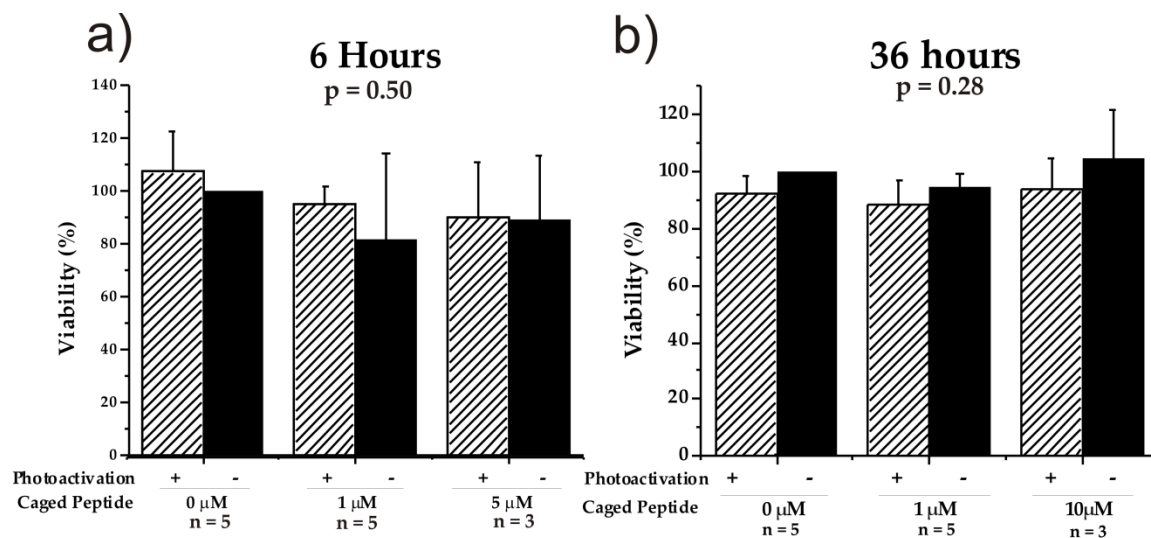
Figure 3.11 PANC-1 Cell Cytotoxicity Assessment After Loading with Peptide 1 Followed by Photoactivation. PANC-1 cells were incubated with peptide **1** (0-10 µM) and then illuminated with 4.2 mW/cm^2 of UV light for 0 min (solid bars) or 4 min (hashed bars). Lactate dehydrogenase (LDH) activity was measured as a metric of cell viability after a) 6 and b) 36 h. Multiple comparison of means via One-way ANOVA with *post-hoc* Tukey multiple comparison of means demonstrated that no groups were statistically different from one other. ($p = 0.50$, 6 h; $p = 0.28$, 36 h).
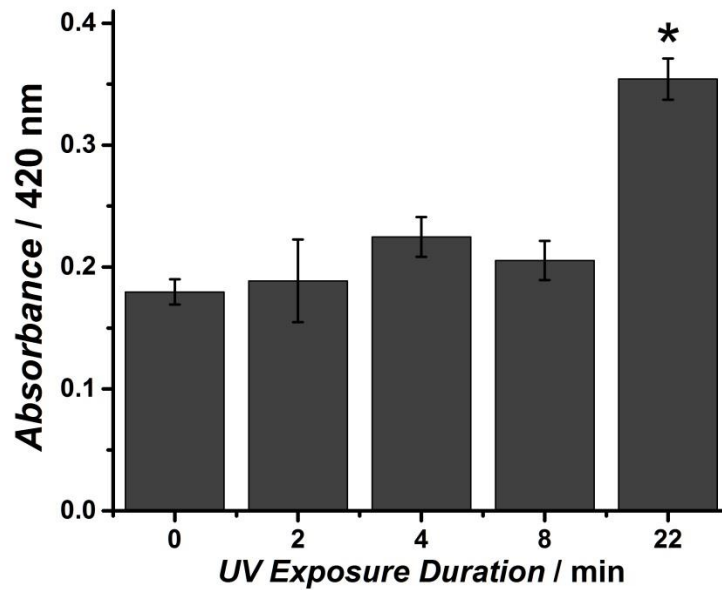
Figure 3.12 DNA Damage as a Result of UV Irradiation. PANC-1 cells were exposed to 360 ± 20 nm at 4.2 mW/cm^2 for 0-22 min. DNA damage was assessed by fixing cells and assaying for pyrimidine cyclobutane dimers. N=3. Comparison of groups by one-way ANOVA indicated that at least one group was statistically different (*$p \leq 0.05$), and *post hoc* analysis by Tukey's multiple comparison analysis illustrated that the amount of CBD detected after a 22 min exposure to UV irradiation was statistically different (*$p \leq 0.05$) from that detected at all other time points.
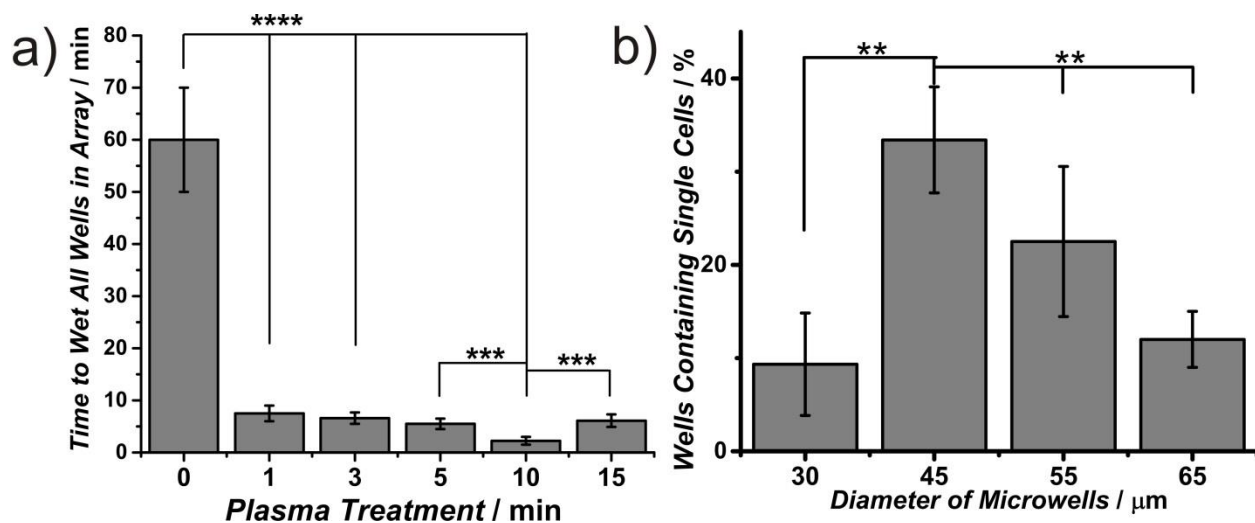
Figure 3.13 Optimization of Cell Traps. a) Effect of plasma cleaning on the time necessary to completely wet an array of photoresist cell traps with ECB. b) The percentage of wells trapping a single cell is depicted for various trap diameters. Multiple comparison of means via one-way ANOVA with *post-hoc* Tukey method analysis was utilized to evaluate statistical differences. (**$p \leq 0.01$, ***$p \leq 0.001$, ****$p \leq 0.0001$).
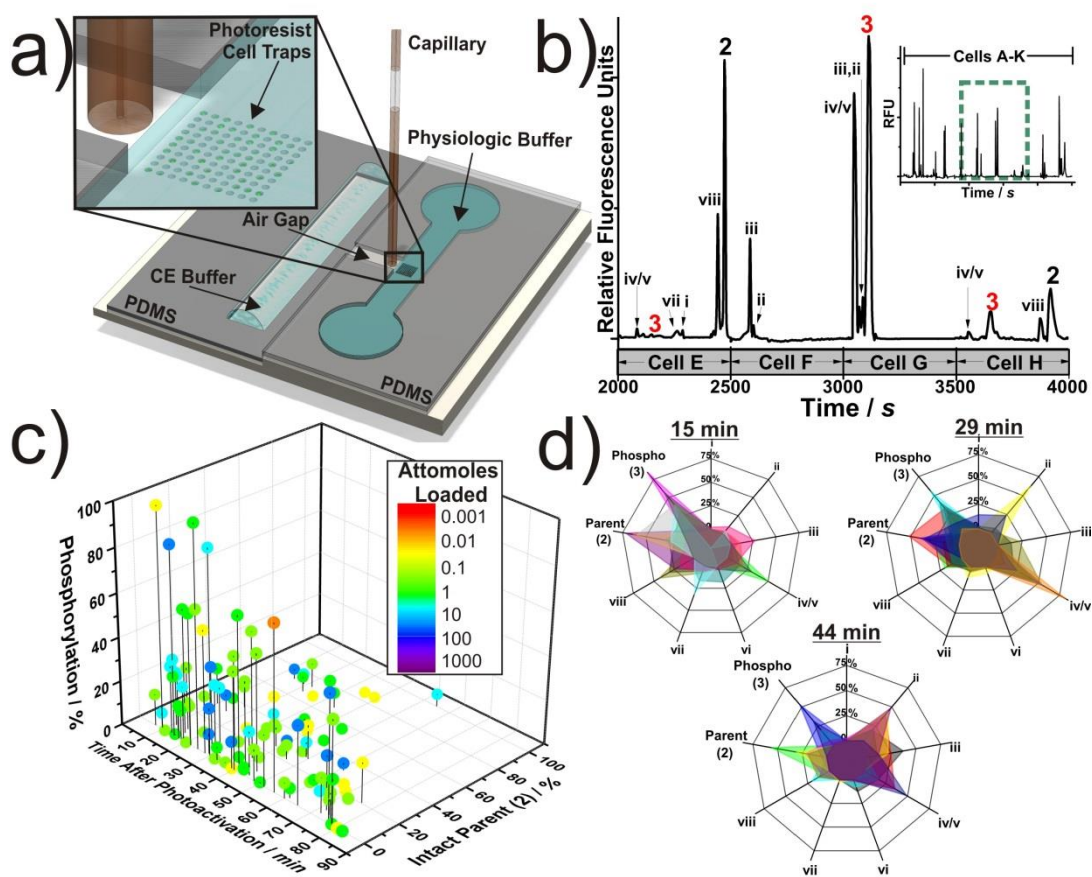
Figure 3.14 Automated single cell analysis. a) Schematic of the microfabricated system used for automated CE analysis. Cell traps (45 µM deep, inset) were loaded with PANC-1 cells and the peptide within the cell was photoactivated. The cells were then assayed by automated single-cell CE. b) Separation of intracellular contents from consecutively analyzed cells. The inset depicts 11 cells (A-K), and the expanded region shows cells E-H. c) Caged reporter loading and metabolism in PANC-1 cells. Each colored data point represents a single cell with the color denoting the moles loaded into the cell. d) Reporter metabolism at various time points after photoactivation. Each overlay (color) represents the metabolism from a single cell.
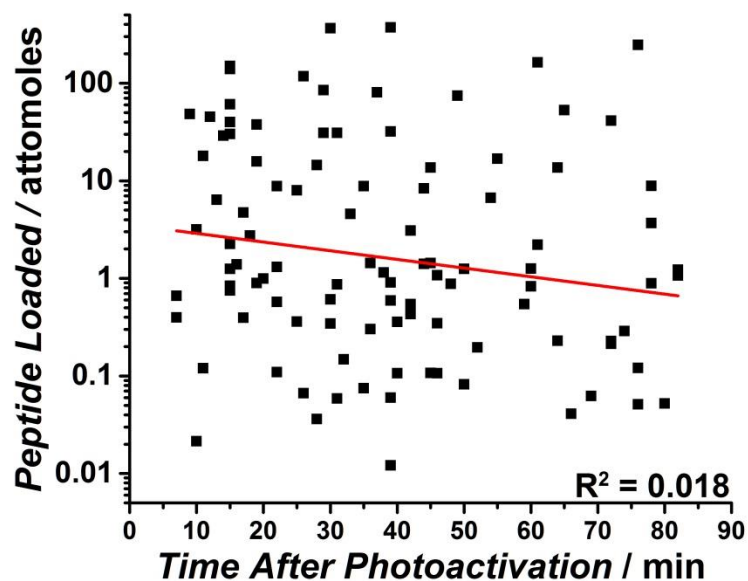
Figure 3.15 Moles of Peptide Detected ($n_{total} = n_{caged} + n_{photoactivated} + n_{phosphorylated} + n_{degraded}$) **From Single Cells at Various Times After Photoactivation.** The red line inidicates a linear fit of the data, suggesting there is minimal correlation between the peptide detected from the individual cells and the time after photoactivation.

Table 3.1 Proteolytic Fragments of Reporter 2

Name	Proteolytic Fragment
i	6FAM-G-OH
ii	6FAM-GR-OH
iii	6FAM-GRP-OH
iv	6FAM-GRP-*R*-OH
v	6FAM-GRP-*R*-A-OH
vi	6FAM-GRP-*R*-AF-OH
vii	6FAM-GRP-*R*-AFT-OH
viii	6FAM-GRP-*R*-AFTF-OH

Table 3.2 Process Parameters for Photolithography of Cell Traps

Parameter	Value
Desired Depth	45 µm
Spin Coating (1)	500 rpm ; 10 s
Spin Coating (2)	2200 rpm; 30 s
Softbake (95°C)	55 min
UV Exposure (mJ/cm^2)	650
Develop	3 min
Hardbake (1) 95°C	30 min
Hardbake (2) 120 °C	15 min
Hardbake (3) 150 °C	6 h

REFERENCES

1. Mortenson, M.; Galante, J. M.; Schlieman, M.; Bold, R. J. AKT: A novel target in pancreatic cancer therapy. *Cancer Therapy* **2004***, 2*, 227.

2. Eyler, C. E.; Foo, W. C.; LaFiura, F. M. Brain cancer stem cells display preferential sensitivity to Akt inhibition. *Stem Cells* **2008***, 26*, 3027.

3. Damayanti, N. P.; Parker, L. L.; Irudayaraj, J. M. K. Fluorescence Lifetime Imaging of Biosensor Peptide Phosphorylation in Single Live Cells. *Angewandte Chemie International Edition* **2013***, 52*, 3931–3934.

4. Ovcharenko, D.; Jarvis, R.; Hunicke-Smith, S.; Kelnar, K.; Brown, D. High-throughput RNAi screening in vitro: From cell lines to primary cells. *RNA* **2005***, 11*, 985-993.

5. Mainz, E. R.; Dobes, N. C.; Allbritton, N. L. Pronase E-Based Generation of Fluorescent Peptide Fragments: Tracking Intracellular Peptide Fate in Single Cells. *Anal. Chem.* **2015***, 87*, 7987-7995.

6. Veldhuyzen; Nguyen; McMaster; Lawrence A Light-Activated Probe of Intracellular Protein Kinase Activity. *Journal of the American Chemical Society* **2003***, 125*, 13358-13359.

7. Wojnar, J. M.; Evans, C. W.; DeVries, A. L.; Brimble, M. A. Synthesis of an Isotopically-labelled Antarctic Fish Antifreeze Glycoprotein Probe. *Aust. J. Chem.* **2011***, 64*, 723-731.

8. Muehlebach, M.; Cederbaum, F.; Cornes, D.; Friedmann, A. A.; Glock, J.; Hall, G.; Indolese, A. F.; Kloer, D. P.; Le Goupil, G.; Maetzke, T.; Meier, H.; Schneider, R.; Stoller, A.; Szczepanski, H.; Wendeborn, S.; Widmer, H. Aryldiones incorporating a [1,4,5]oxadiazepane ring. Part 2: chemistry and biology of the cereal herbicide pinoxaden. *Pest Manag. Sci.* **2011***, 67*, 1499-1521.

9. Schindelin, J.; Rueden, C. T.; Hiner, M. C.; Eliceiri, K. W. The ImageJ ecosystem: An open platform for biomedical image analysis. *Mol. Reprod. Dev.* **2015***, 82*, 518-529.

10. Berridge, M. V.; Herst, P. M.; Tan, A. S. Tetrazolium dyes as tools in cell biology: New insights into their cellular reduction. In ; Review, BT - Biotechnology Annual, Ed.; Elsevier: 2005; Vol. 11, pp 127-152.

11. Sinha, R. P.; Häder, D. P. UV-induced DNA damage and repair: a review. *Photochem. Photobiol. Sci.* **2002***, 1*, 225-236.

12. Pai; Wang; Salazar; Sims; Bachman; Li; Allbritton Photoresist with Low Fluorescence for Bioanalytical Applications. *Analytical Chemistry* **2007***, 79*, 8774-8780.

13. Dickinson, A. J.; Meyer, M.; Pawlak, E. A.; Gomez, S.; Jaspers, I.; Allbritton, N. L. Analysis of sphingosine kinase activity in single natural killer cells from peripheral blood. *Integr Biol (Camb)* **2015***, 7*, 392-401.

14. Proctor, A.; Wang, Q.; Lawrence, D.; Allbritton, N. Development of a Peptidase-Resistant Substrate for Single-Cell Measurement of Protein Kinase B Activation. **2012***, 84*, 7195.

15. Proctor, A.; Herrera-Loeza, G.; Wang, Q.; Lawrence, D. S.; Yeh, J.; Allbritton, N. L. Measurement of Protein Kinase B Activity in Single Primary Human Pancreatic Cancer Cells. *Analytical Chemistry* **2014***, 86*, 4573-4580.

16. Chauhan, A.; Tikoo, A.; Kapur, A. K.; Singh, M. The taming of the cell penetrating domain of the HIV Tat: Myths and realities. *Journal of Controlled Release* **2007***, 117*, 148.

17. Ciechanover, A. Proteolysis: from the lysosome to ubiquitin and the proteasome. *Nature Reviews: Molecular Cell Biology* **2005***, 6*, 79.

18. Jones, A. T.; Sayers, E. J. Cell entry of cell penetrating peptides: tales of tails wagging dogs. *Journal of Controlled Release* **2012***, 161*, 582.

19. Räägel, H.; Säälik, P.; Pooga, M. Peptide-mediated protein delivery—Which pathways are penetrable? *Biochimica et Biophysica Acta (BBA) - Biomembranes* **2010***, 1798*, 2240-2248.

20. Montrose, K.; Yang, Y.; Sun, X.; Wiles, S.; Krissansen, G. W. Xentry, a new class of cell-penetrating peptide uniquely equipped for delivery of drugs. *Sci Rep* **2013***, 3*, 1661.

21. Tadevosyan, A.; Létourneau, M.; Folch, B.; Doucet, N.; Villeneuve, L. R.; Mamarbachi, A. M.; Pétrin, D.; Hébert, T. E.; Fournier, A.; Chatenet, D.; Allen, B. G.; Nattel, S. Photoreleasable ligands to study intracrine angiotensin II signalling. *J Physiol* **2015***, 593*, 521-539.

22. Lindhurst, M. J.; Sapp, J. C.; Teer, J. K.; Johnston, J. J.; Finn, E. M.; Peters, K.; Turner, J.; Cannons, J. L.; Bick, D.; Blakemore, L.; Blumhorst, C.; Brockmann, K.; Calder, P.; Cherman, N.; Deardorff, M. A.; Everman, D. B.; Golas, G.; Greenstein, R. M.; Kato, B. M.; Keppler-Noreuil, K. M.; Kuznetsov, S. A.; Miyamoto, R. T.; Newman, K.; Ng, D.; O'Brien, K.; Rothenberg, S.; Schwartzentruber, D. J.; Singhal, V.; Tirabosco, R.; Upton, J.; Wientroub, S.; Zackai, E. H.; Hoag, K.; Whitewood-Neal, T.; Robey, P. G.; Schwartzberg, P. L.; Darling, T. N.; Tosi, L. L.; Mullikin, J. C.; Biesecker, L. G. A Mosaic Activating Mutation in AKT1 Associated with the Proteus Syndrome. *New England Journal of Medicine* **2011***, 365*, 611-619.

23. Lindhurst, M. J.; Parker, V. E. R.; Payne, F.; Sapp, J. C.; Rudge, S.; Harris, J.; Witkowski, A. M.; Zhang, Q.; Groeneveld, M. P.; Scott, C. E.; Daly, A.; Huson, S. M.;

Tosi, L. L.; Cunningham, M. L.; Darling, T. N.; Geer, J.; Gucev, Z.; Sutton, V. R.; Tziotzios, C.; Dixon, A. K.; Helliwell, T.; O'Rahilly, S.; Savage, D. B.; Wakelam, M. J. O.; Barroso, I.; Biesecker, L. G.; Semple, R. K. Mosaic overgrowth with fibroadipose hyperplasia is caused by somatic activating mutations in PIK3CA. *Nat Genet* **2012***, 44*, 928-933.

24. Hevner, R. F. Brain overgrowth in disorders of RTK-PI3K-AKT signaling: a mosaic of malformations. *Semin. Perinatol.* **2015***, 39*, 36-43.

25. Dickinson, A. J.; Armistead, P. M.; Allbritton, N. L. Automated Capillary Electrophoresis System for Fast Single-Cell Analysis. *2013* , 4797.

26. Van, T. N. N.; Morris, M. C. *Fluorescent Sensors of Protein Kinases: From Basics to Biomedical Applications;* Fluorescence-Based Biosensors: From Concepts to Applications; Academic Press: Waltham, MA, 2013.

Chapter 4: Iterative Redesign of the Akt Kinase Substrate Reporter for Improved Proteolytic Resistance

4.1. Peptide Stabilization Strategies

Owing to their straightforward synthesis, shelf stability, and customizable properties, short peptides have found diverse employment in biomedical research, including their integration within *in vitro* assays. Peptide substrates are commonly incubated with purified kinases in library screens to assess the therapeutic promise of targeted inhibitors, identify substrate consensus sequences, or for development of peptides that are themselves inhibitors.[1-3] However, these highly simplified environments often fail to recapitulate the complex intracellular interactions they were designed to model, which has resulted in the popularization of lysate and in-cell assays. These more accurately approximate the *in vivo* response, but many short peptides undergo rapid degradation at one or more sites once exposed to the cellular milieu, severely limiting their utility.[4-7] Multiple strategies, described below, have been enacted to prevent proteolytic fragmentation and improve the lifetime of peptide sensors in lysates and individual cells.

Modifications at either terminus are among the simplest to protect short sequences from peptidases and proteases which can sequentially remove residues or cleave at internal sites. N-terminal acetylation and C-terminal amidation or polyethylene-glycol modification (PEGylation) have met with success, but in many lysates or cells these peptides still have

116

half-lives on the order of minutes, precluding their use in time resolved studies.[8,9] More sophisticated approaches involve introducing secondary structure to peptides which reduce degradation by preventing entry into the tunnel-like catalytic site of cytosolic proteases. For example, the addition of β-turn sequences to the N-terminus of peptides improved their half-life by 40-fold in cytosolic lysates.[10] Similarly, peptide stapling aims to reduce proteolysis by introducing one or more hydrocarbon braces near sites of degradation, constraining peptide conformation.[11] Complete cyclization of sequences is another popular route to prevent peptide degradation by generating secondary structure, although a shared drawback of these techniques is the decreased substrate recognition that often occurs after inducing these structural changes.[12,13] Furthermore, these syntheses are rarely straightforward and may require significant chromatographic purification.[10]

An intermediate tactic to stabilize peptides against proteolysis is the introduction of amino acids which are less frequently recognized by intracellular proteases, including non-native and D-enantiomer residues. The inclusion of non-native N-methylated amino acids into several peptides have significantly protected them from proteolytic degradation.[14] Energy calculations showed that N-methylated peptides were also more likely to deviate from planar configurations than their native counterparts, hinting that subtle conformation differences imparted by such residues can have broad consequences on biological activity.[15,16] Standard solid phase peptide synthesis techniques can be utilized to introduce such amino acids into sequences, representing an effective manner of improving peptide lifetimes in cell-based assays with a relatively low expertise barrier. This chapter describes the development of a strategy to stabilize the peptide substrate reporter VI-B at key cleavage locations through the introduction of non-native amino acids.

4.2 Iterative Redesign of the Akt Kinase Substrate VI-B

As discussed in Chapters 2 and 3 of this dissertation, the peptide VI-B (6FAM-GRP-MeArg-AFTF-MeAla) acts as an Akt substrate within single cells, but is also degraded into several fluorescent fragments as a result of proteolysis. The primary cleavage site of VI-B is cell-line dependent, but a major fragment observed in individual cells from xenograft mice possessing human PDAC tumors occurred between phenylalanine and N-methyl alanine (MeAla), resulting in an eight amino acid fragment.[17] In this chapter, a degradation-resistant peptide substrate reporter, 76D (6FAM-GRP-MeArg-AFTF-Aib), was developed through modification of VI-B at this cleavage site.

In previous studies, a starting peptide based on the consensus sequence of Akt underwent iterative non-native amino acid replacement at identified cleavage sites, which resulted in VI-B.[18] This reporter featured improved phosphorylation efficiency and 4.5-fold improvement of peptide half-life in a lysate compared to the initial peptide, and was utilized for single cell studies described in this thesis. When incubated in single PANC-1 cells (a cell line derived from human pancreatic adenocarcinoma), the major cleavage site of VI-B (38 ± 10% of total peptide) was between phenylalanine and N-methyl alanine (MeAla). The peptide library described in this chapter evaluates peptides with modified amino acids in these two locations. Multiple non-native amino acids were included in the library at these amino acid locations to increase peptide stability. Library members were screened for time to 50% phosphorylation ($t_{50\%P}$) and half-life in a lysate ($t_{1/2}$). The lead peptide from the library was then microinjected into single cells with no measureable degradation of the reporter, although minimal phosphorylation was observed. Microinjection of the lead peptide's phosphorylated analogue revealed rapid dephosphorylation, suggesting that measurement of

Akt activity with an improved degradation-resistant reporter will require reporter modification or more complete inhibition of protein serine/threonine phosphatases (PSPs).

4.3 Experimental Section

4.3.1 Materials

9-fluoroenylmethoxycarbonyl (Fmoc) amino acids, resins, 2-(6-chloro-1*H*-benzotriazole-1-yl)-1,1,3,3-tetramethylaminium hexafluorophosphate (HCTU), 1-(mesitylene-2-sulfonyl)-3-nitro-1,2,4-trizaole (MSNT) were procured from Novabiochem or ChemPep. AnaSpec supplied 6-carboxyfluorescein (6FAM), N-Hydroxybenzotrizaole (HOBt), and Fmoc-Nα-Me-Arg(Mtr)-OH. Fmoc-α-MeAla-OH was purchased from Advanced ChemTech. Recombinant active human Aktα was purchased from Millipore. Dulbecco's Modified Eagle Medium (DMEM), was procured from Cellgro; 0.25% trypsin and penicillin/streptomycin were obtained from Gibco; fetal bovine serum (FBS) was purchased from Atlanta Biologicals. Bovine serum albumin (BSA) was procured from Calbiochem. All other reagents were described in previous chapters or were purchased from Fisher or Sigma-Aldrich.

4.3.2 Peptide Synthesis and Characterization

Peptides described in this chapter were synthesized by Dr. Qunzhao Wang in the laboratory of Dr. David Lawrence at UNC-CH. The purity of peptide products was assessed with high performance liquid chromatography – mass spectrometry (HPLC-MS) and further purified with HPLC if necessary. Peptides were lyophilized, resuspended in Tris buffer (pH 7.5), aliquoted, and stored at -80 °C.

4.3.2.1 Synthesis of Full Length Peptides

Automated Fmoc peptide synthesis methodologies (Prelude Peptide Synthesizer, Protein Technologies, Tucson,AZ) were employed to prepare full length substrate peptides containing an amidated C-terminus. Couplings were performed during two 5-min incubations in dimethylformamide (DMF) with 5 equivalents (eq) Fmoc amino acid, 5 eq HCTU, and 10 eq N,N-Diisopropylethylamine (DIPEA). Couplings of amino acids adjacent to N-methylated residues were performed with three 60-min incubations in N-Methyl-2-prrolidone (NMP) prior to capping with acetic anhydride. In some cases, coupling of amino acids required treatment with 5 eq of Fmoc amino acid, 5 eq HCTU, and 10 eq DIPEA in N-methyl-2-pyrrolidone (NMP) for 3 h, repeated for a total of three iterations. Fmoc deprotection was conducted with two 2.5-min incubations with 20% piperidine in DMF. Fluorescent labeling was achieved at the N-terminus of all peptides by reacting 5 eq of 6FAM, 5 eq diisopropylcarbodiimide (DIC), and 5 eq HOBt in DMF overnight, with subsequent treatment with 30% piperidine in DMF for 30 min. Peptides were cleaved from the resin overnight in a solution of trifluoroacetic acid (TFA): Phenol : H_2O : TIS in a ratio of 88:5: 5:2. In all cases, cleaved peptides were precipitated with ether and dried under air. Purity was determined with HPLC-MS and further purified with HPLC if necessary.

4.3.2.2 Synthesis of Peptide Fragments Possessing a Free Acid

Peptide fragment standards possessing a free carboxylic acid on the C-terminus were synthesized using either a 2-chlorotrityl or Wang resin. With the 2-chlorotrityl resin, 1 eq of the first Fmoc amino acid and 4 eq of DIPEA in dry CH_2Cl_2 was reacted with the resin for 2 h in a dry glass vial on a shaker. When using the Wang resin, 10 eq of the first Fmoc amino acid in CH_2Cl_2 was incubated with 7.5 eq 1-methyl-imidzaole and 10 eq MSNT for 15 min in

a dry glass vial on a shaker. The subsequent amino acids were coupled as described above for the full-length, amidated peptides and each peptide was fluorescently labeled with 6FAM on the N-terminus as described above.

4.3.2.3 Synthesis of a Myristoylated Peptide Reporter

Synthesis of a cell-penetrating 76D peptide reporter, termed Myr76D, involved the coupling of a carboxyfluorescein diacetate-linked 14-carbon fatty acid to the N-terminus of 76D. After coupling the fluorophore to the peptide, it was treated with 30% piperidine and washed. Peptide was then incubated with 10 eq myristic acid, HCTU, Oxyma, and 20 eq of DIPEA for 3 h.

4.3.3 *In vitro* Kinase Assays

Peptide phosphorylation assays were performed with 6 nM recombinant, purified human Aktα at 30 °C in assay buffer [8 mM MOPS (3-(N-morpholino)propanesulfonic acid), pH 7.0, 0.2 mM EDTA, 4 mM $MgCl_2$, 1 mM ATP] with 25 µM peptide substrate. Aliquots were removed over time from the reaction mixture and quenched by incubation at 90 °C for 4 min. Samples were then subjected to capillary electrophoresis with laser induced fluorescence detection (CE-LIF), and the amount of peptide phosphorylation was determined by dividing the peak area of phosphorylated peptide versus all other peaks in the electropherogram.

4.3.4 Measurement of Kinetic Parameters by Fluorescence Anisotropy

Kinase assays were performed as described above, except that the substrate concentration was varied from 0-200 µM. Initial estimates of assay timepoints required to generate small amounts (<10%) of phosphorylated peptide were performed by separating

samples with CE-LIF. Once timepoints were optimized, the immobilized metal ion affinity-based fluorescent polarization (IMAP) assay (Molecular Devices Corp., Sunnyvale, CA) was employed to detect phosphorylated peptide in each reaction mixture. Briefly, this assay employs the high-affinity interaction of trivalent metal nanoparticles with phosphoryl groups to detect phosphorylated peptides. A calibration curve was generated by measuring the fluorescence anisotropy of standard mixtures of containing native and phosphorylated sequences. Recombinant Aktα was reacted with peptides to generate a sample of 100% phosphorylated peptide, and was confirmed by CE-LIF and Matrix Assisted Laser Desorption Ionization Mass Spectrometry (MALDI-MS). A florescence plate reader (SpectraMax M5, Molecular Devices, Sunnyvale, CA) with an excitation of 485 nm (9 nm bandwidth) and emission of 525 nm (15 nm bandwidth) was employed to measure anisotropy. Assay samples were diluted to 100 nM for anisotropy measurements.

4.3.5 Cell Culture

PANC-1 cells, originating from a 56 year old male with Pancreatic Ductal Adenocarcinoma (PDAC) with metastases in the lymph node, were obtained from the American Type Culture Collection (Manassas, Virginia). This adherent cell line was cultured in DMEM medium supplemented with 10% FBS, streptomycin (100 µg/mL), and penicillin (100 units/mL) and was maintained in a humidified atmosphere at 37 °C with 5% CO_2. Cells were cultured to a maximum density of 80% confluency and were disadhered from the growth surface into fresh media by treatment with 0.25% trypsin for 5 min.

4.3.6 Peptide Degradation in Cell Lysates

PANC-1 cells were released from the growth surface with 0.25% trypsin treatment, pelleted via centrifugation, and washed 3X with Phosphate Buffered Saline (PBS; 137 mM

NaCl, 10 mM Na_2HPO_4, 27 mM KCl, 1.75 mM KH_2PO_4, pH 7.4) to remove excess growth

media. Cell pellets were submerged in liquid nitrogen for 1 minute intervals with full

thawing between each cycle at 37 °C, for a total of 3 cycles. The solution was then

centrifuged at 14,000 x g for 15 min at 4 °C. The supernatant was collected and transferred to

a sterile container where it was sustained at 4 °C until the point of the assay. The total protein

content within the supernatant was determined with fluorescamine.[19] A standard curve was

generated by reacting various amounts of BSA ($0 - 100$ μg mL^{-1}) with fluorescamine.

Briefly, 30 μL of cell lysate was mixed with 10 μL fluorescamine (3 mg/mL in acetone) and

incubated for 5 min at 25 °C in darkness. A fluorescence plate reader (SpectraMax M5,

Molecular Devices, Sunnyvale, CA) with an excitation of 390 ± 4.5 nm and emission of 475

nm (bandwidth 15 nm) was employed to measure the resulting fluorescence. Lysates were

prepared to 3 mg mL^{-1} total protein in PBS immediately prior to use in degradation assays.

Peptide lifetimes within cytosolic cell lysates were evaluated by mixing peptide substrate (1

μM) with the prepared lysate and incubating the solution at 37 °C. Aliquots were removed

over time and quenched by the addition of HCl to a final concentration of 100 mM. To obtain

a 0 min timepoint, the lysate was pre-quenched with acid prior to the addition of peptide.

Samples from these reactions were separated and detected with CE-LIF. Peptide fragments

were identified by the addition of fragment standards (200 nM) to the acid-terminated

aliquots, and comparing the electropherograms before and after the addition of the standard.

Positive identification of a fragment was defined by a 50% increase (at minimum) of

corrected peak area of the comigrating peak appearing in the degradation assay. Peptide

lifetime, or the total amount of full-length peptide remaining in assay samples, was

calculated by dividing the peak area of the parent peptide by the total area of peaks in the electropherogram.

4.3.7 Capillary Electrophoresis

Separation of peptide samples were performed on a commercial CE-LIF instrument (ProteomeLab PA 800) in 50 μM inner diameter fused silica capillaries (30 cm length, 20 cm effective length). Sample injection was initiated by applying 0.5 psi for 5 s to the inlet of the capillary. Electrophoresis was performed at 333 V/cm in buffer. 100 mM borate, pH 7.7 was employed for CE separations of native and phosphorylated 59C. 100 mM Borate, 7 mM SDS at pH 9.5 was used in separations for all remaining peptide samples. Analytes were detected with an argon-ion laser (emission at 488 nm, detection at 520 nm). The capillary was rinsed for 2 minutes at 20 psi with 1 M NaOH, H_2O, and sample buffer prior to each separation. Phosphorylation (%) or intact peptide (%) was measured as a ratio of integrated peak areas between modified and total reporter.

4.3.8 Single Cell Capillary Electrophoresis

Single PANC-1 cells were analyzed by single cell CE-LIF as described in previous chapters, except that cells were either microinjected with VI-B, 76D, or phosphorylated 76D, and separations occurred in 400 mM Borate, pH 9.5.

4.4 Results and Discussion

4.4.1 Characterization of Peptides Following Replacement of C-terminal Phenylalanine

Starting with the C-terminal phenylalanine, amino acids on both the N- and C-terminal side of the primary proteolysis clip site of VI-B were replaced with non-native residue analogs to determine if greater peptide stability could be gleaned. D-phenylalanine

and N-methyl phenylalanine (Figure 4.1A) were included in the sequence, both of which have been shown to impart stability to peptides.[20,21] Peptides 59D and 59F (Table 4.1) were synthesized, purified, and incubated in a PANC-1 cytosolic lysate. Samples removed over time were separated by CE-LIF and the amount and number of fluorescent fragments determined. The peptides showed disparate resistance to degradation: 59D and 59F degraded into 5 and 3 fragments, respectively. To compare the two peptides, the percentage of intact peptide was plotted as a function of time, and the peptide half-life ($t_{1/2}$) calculated. Peptide 59D possessing N-methyl phenylalanine had a half-life of 43 ± 7.8 min, an approximately 2-fold slower rate of degradation than the starting peptide. Conversely, peptide 59F containing D-Phenylalanine had a half-life of 142 ± 8.4 min, a 7.5-fold improvement in degradation resistance.

To assess whether these modified peptides, both of which possessed improved degradation resistance, retained their ability to act as substrates for Akt, each was incubated with recombinant, purified Akt *in vitro*, and phosphorylation over time was assessed by CE-LIF. 59D failed to be phosphorylated by Akt after 120 min incubation, while 59F possessed a time to 50% phosphorylation ($t_{50\%P}$) of 126 ± 5.7 min, a rate over two-fold slower than the starting peptide (Figure 4.3). The inadequate phosphorylation of these peptides led to assessment of other non-native amino acid-based modifications.

4.4.2 Characterization of Peptides Following Substitution of C-terminal N-Methyl Alanine

After determining that modifications at the 7th residue of VI-B resulted in improved degradation resistance, but at the sacrifice of phosphorylation efficiency, substitutions on the C-terminal side of the susceptible bond were explored. Peptides 76D, 59A, and 59C (Table

4.1) were synthesized with α-aminoisobutyric acid, N-methyl- α-aminoisobutyric acid, and N-benzyl alanine (Figure 4.1B), respectively. Peptides were then individually incubated in cytosolic PANC-1 lysates and degradation patterns monitored with CE-LIF. VI-B, 59A, and 59C were metabolized into four fluorescent fragments, while 76D resulted in two fragmentation products (Figure 4.3). When each modified peptide was compared to the starting peptide, it was apparent that 76D was highly degradation resistant, with $92 \pm 3.8\%$ parent peptide remaining intact after 60 min. The half-life of this peptide in a lysate was 352 ± 5.2 min, an 18.5-fold improvement in degradation resistance over VI-B. Comparatively, peptides 59A and 59C possessed half-lives of 48 ± 13.8 and 20 ± 12 min, respectively.

The ability of each substituted peptide to undergo phosphorylation by Akt kinase was assessed via an *in vitro* assay. Peptides were incubated with recombinant, active Akt and samples taken over time were separated by CE-LIF. Peptides 59A and 59C were minimally phosphorylated, with $t_{50\%P}$ values of 256 ± 7.2 and 167 ± 7.8 min, respectively. This result, combined with rapid peptide degradation in lysates, precluded further study of these peptides. However, peptide 76D possessed a $t_{50\%P}$ of 40 ± 10.3 min, a 1.4-fold improvement in phosphorylation rate from the starting peptide. Indeed, 76D both acted as an efficient substrate while resisting intracellular degradation to a high degree, and was determined to be the lead peptide from this library screen

In order to quantitatively assess the ability of Akt to phosphorylate the lead peptide, 76D, versus the starting peptide, VI-B, the kinetic parameters of K_M and k_{cat} were determined for each peptide. The amount of phosphorylated substrate was measured using the immobilized metal affinity fluorescence polarization (IMAP) assay, which employs the high-

affinity interaction of trivalent metal nanoparticles with phosphoryl groups. 76D demonstrated a 4-fold lower K_M than VI-B (15 µM versus 56 µM) as well as a 6.7-fold greater k_{cat} (400 s^{-1} versus 60 s^{-1}). The ratio k_{cat}/K_m, known as the specificity constant, is a useful index for comparing the relative rates of substrate phosphorylation by Akt. 76D demonstrated a 25-fold greater k_{cat}/K_m ratio than VI-B (2.7 x 10^7 M^{-1} s^{-1} versus 1.1 x 10^6 M^{-1} s^{-1}), confirming its improved suitability as a degradation-resistant Akt substrate.

4.4.3 Separation and Identification of Peptide Fragments

Although it was shown that the lead peptide 76D was resistant to degradation within a cytosolic lysate, it has been shown that peptide fragmentation patterns and rates can differ within an intact intracellular environment. [18,22] In order to identify the exact cleavage sites of any fragments occurring within individual cells as well as unambiguously identify phosphorylated and parent peptide in separations, standards consisting of all fluorescent fragments of the lead peptide (76D) were synthesized and characterized by CE-LIF. Under optimized conditions (400 mM Borate pH 9.5), full length peptide and phosphorylated peptide migrated at discrete times as single peaks (Figure 6.5), and fragments were identifiable by migration time. Thus, any fragments formed during single-cell incubations could be easily identified.

4.4.4 Myr76D as a Cell Permeable Akt Reporter

Studies of single intact cells with peptides such as 76D require loading of cells. This poses a large obstacle due to the selective permeability of cell membranes. Hydrophobic molecules such as steroids are lipid soluble and can diffuse through the phospholipid membrane, gaining entry into cells,[23] while peptides generally cannot permeate the membrane owing to their bulk and charge. There are multiple methods for introducing

127

macromolecules into living cells. Microinjection has the highest delivery to toxicity ratio but is low throughput. Pinocytic loading, electroporation, and optoporation have also been utilized to introduce peptides into cells.[24-27] While these methods are effectual for peptide loading, they are still capable of inducing significant cellular stress that may activate the Akt pathway, obscuring accurate measurements of normal versus aberrant enzyme activity. For this reason, a non-disruptive loading technique was attempted to translocate 76D into the cytosol. The addition of a C_{14} myristoyl chain to a peptide has been shown to promote passive entry of peptides into cells, with minimal endosomal uptake.[26] However, in order for the reporter to be liberated from the membrane and diffuse into the cytosol where active Akt is located, the myristate moiety must be freed from the fluorescent peptide. A novel approach is illustrated in Figure 4.5 with 6-FAM replaced by a 6-carboxyfluorescein diacetate (6-FAMDA) fluorophore, which is cleaved by intracellular esterases to its fluorescent anion.[28] The myristate group was coupled to one of the cleavable acetate groups, resulting in a detachable reporter.

PANC-1 cells were incubated with Myr76D and visualized with fluorescence microscopy. No visible increase in fluorescence was detected compared to untreated PANC-1 cells, suggesting minimal loading of the peptide, limited esterase cleavage, or possibly both. Loaded cells were subjected to single-cell lysis and separation by CE-LIF to assess the presence of any reporter phosphorylation, which would strongly suggest the reporter crossing the cell membrane and detaching from its hydrophobic tether. However, phosphorylation of Myr76D could not be confirmed due to extremely low signal from the cells. Notably, the same separation conditions were conducive to separation of myristoylated reporter as native peptide, and the myristoylated reporter possessed the same degradation resistant

characteristics as native 76D, with $93 \pm 3.9\%$ peptide remaining intact after 60 min in a PANC-1 lysate. Unfortunately, the limited loading of the reporter into cells precluded any future study with this peptide and this approach was ultimately abandoned. However, given the chemical innovations detailed in Chapter Three, it is possible that this peptide sequence could be rendered cell permeable through coupling with the hydrophobic caging group, DMNB.

4.4.5 Kinase Activity Measurement in Single PANC-1 Cells

Evaluation of kinase activity at the single cell level permits the observation of signaling behaviors within the intact context of the cellular environment, and maintains the ability to assess population heterogeneity. Initial attempts to quantify kinase activity involved microinjection of 76D into PANC-1 cells and subsequent analysis with CE-LIF. Cells were either grown in the presence of serum or starved of serum for 15-24 hrs. In the latter case, cells were analyzed after 30 min stimulation with serum (Figure 4.6B). In untreated cells (n=11), one cell returned a miniscule amount of 76D phosphorylation (2%), whereas the starting peptide, VI-B, underwent phosphorylation ranging between 0-25% (Figure 4.6C). The starting peptide also possessed more favorable phosphorylation rates in stimulated cells than 76D. The phosphorylated analogue of 76D was injected to determine if the lack of reporter phosphorylation was due to dephosphorylation by intracellular protein serine/threonine phosphatases (PSPs). This phenomenon was confirmed by the rapid dephosphorylation of the reporter within single PANC-1 cells (Figure 4.7). Seeing as 76D possesses more favorable phosphorylation kinetics than VI-B, it stands to reason that with PSP inhibition prior to microinjection, 76D dephosphorylation could be slowed to the point where Akt activity, in the form of 76D phosphorylation, could be observed. Alternatively, the

peptide sequence can be modified to limit its recognition by intracellular phosphatases.[29] It is of note that under all conditions tested, 76D completely resisted proteolytic degradation in single cells, demonstrating that the systematic replacement of proteolysis-prone amino acids in a sequence is a viable strategy to generate stable peptides.

4.5 Conclusions

An iterative screening process was employed to stabilize locations susceptible to proteolysis in the starting peptide reporter VI-B. Locations at the 7th and 8th amino acid locations were targeted for modification based on the proteolysis sites observed in PANC-1 lysates and single cells. Sequential modification at each of these sites followed by characterization of stability in lysates as well as suitability as a Akt substrate was evaluated. This strategy was successful in generating a substrate more resistant to proteolysis; however the rapid dephosphorylation by phosphatases of 76D in individual cells precluded its use as a reporter for Akt activity in individual cells. Additional studies will be required to assess if this peptide could potentially be utilized as a phosphatase reporter or if PSPs can be inhibited to the degree where Akt activity as measured by peptide phosphorylation can be observed. Future studies for all peptides described in this work also includes modifications to render reporters cell-permeable as well as performing higher-throughput analysis with capillary electrophoresis systems.
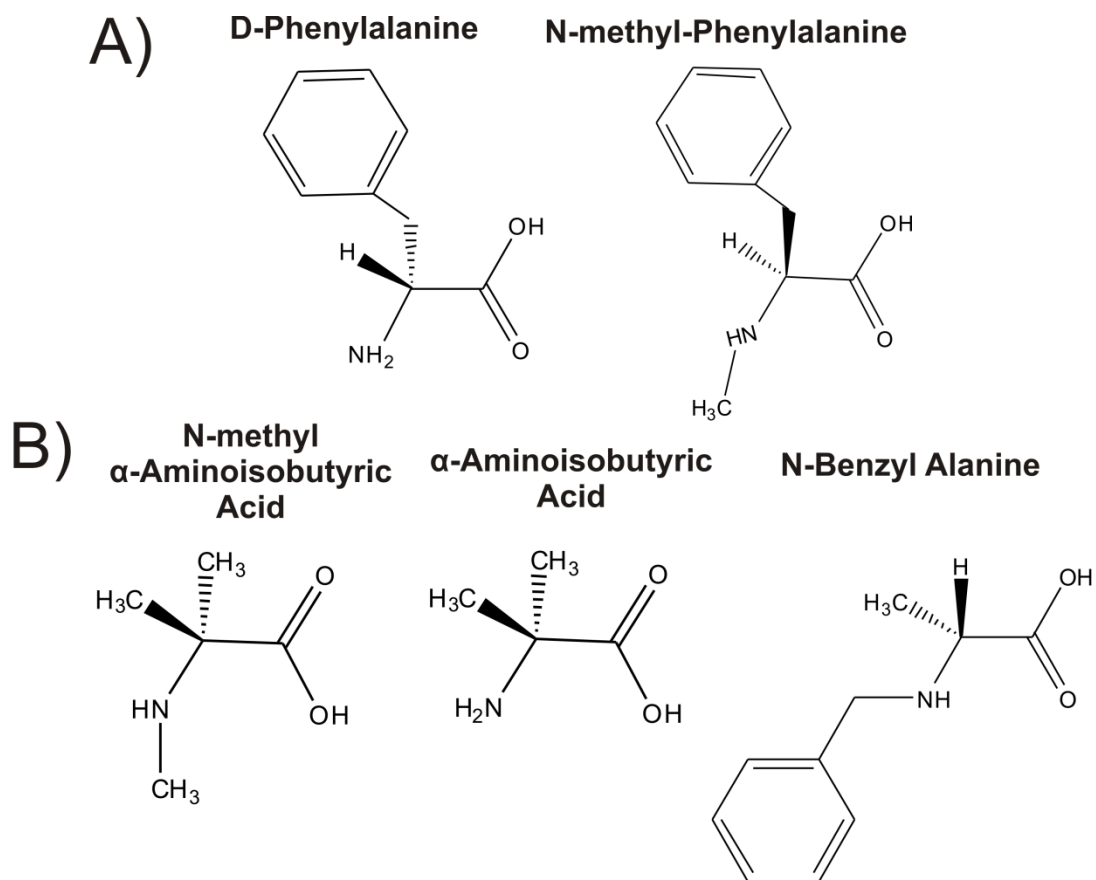
Figure 4.1 Line Bond Structures of Non-native Amino Acids Incorporated in the Synthesis of Library Peptides. A) L-phenylalanine derivatives for replacement of amino acids at the 8th amino acid cleavage site B) L-alanine derivatives for replacement at the 9th amino acid residue
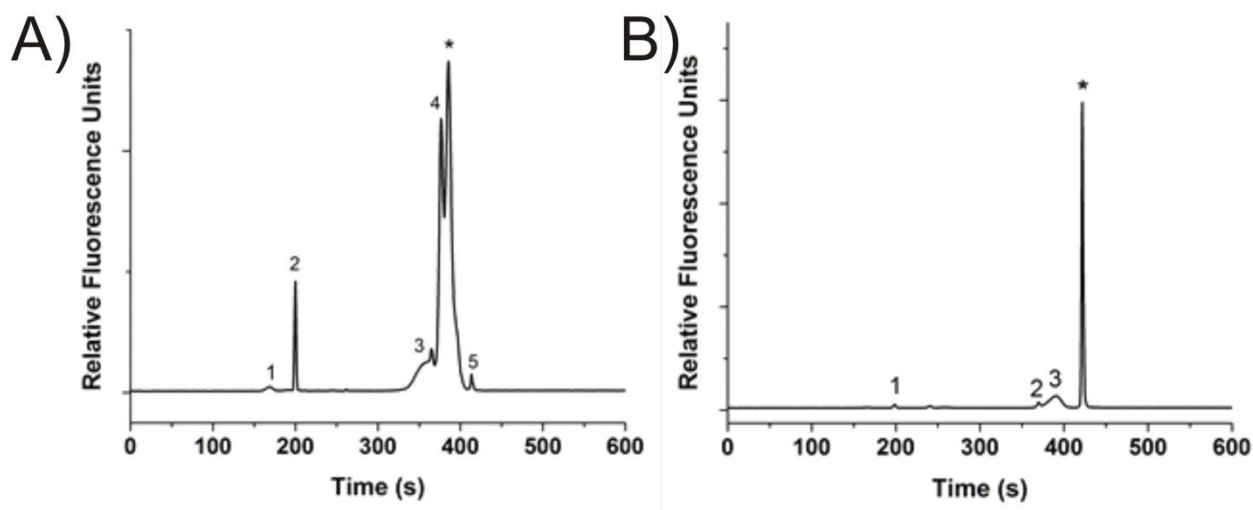
Figure 4.2 Electropherograms of Peptide 59D (A) and 59F (B) 60 min After Incubation in a PANC-1 Lysate. The asterisk (*) labeled peak in each electropherogram represents the peak comigrating with intact, full length peptide. The numbered peaks correspond to fluorescent fragments generated by proteolysis.

Figure 4.3 Electropherograms of Peptide VI-B (A), 76D (B), 59A (C), 59C (D) 60 min After Incubation in a PANC-1 Lysate. The asterisk (*) labeled peak represents the peak comigrating with intact, full length peptide. The numbered peaks correspond to fluorescent fragments generated by proteolysis.
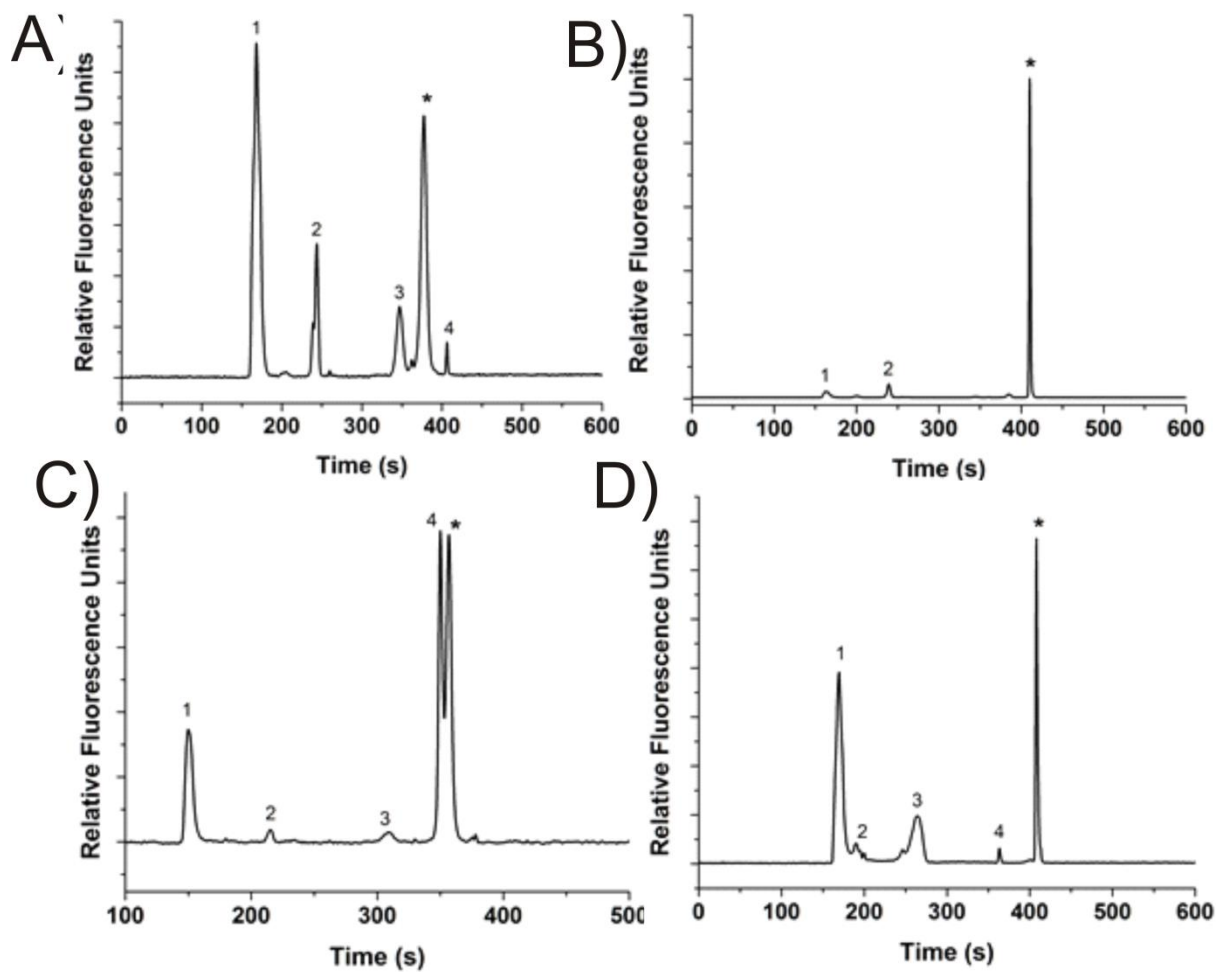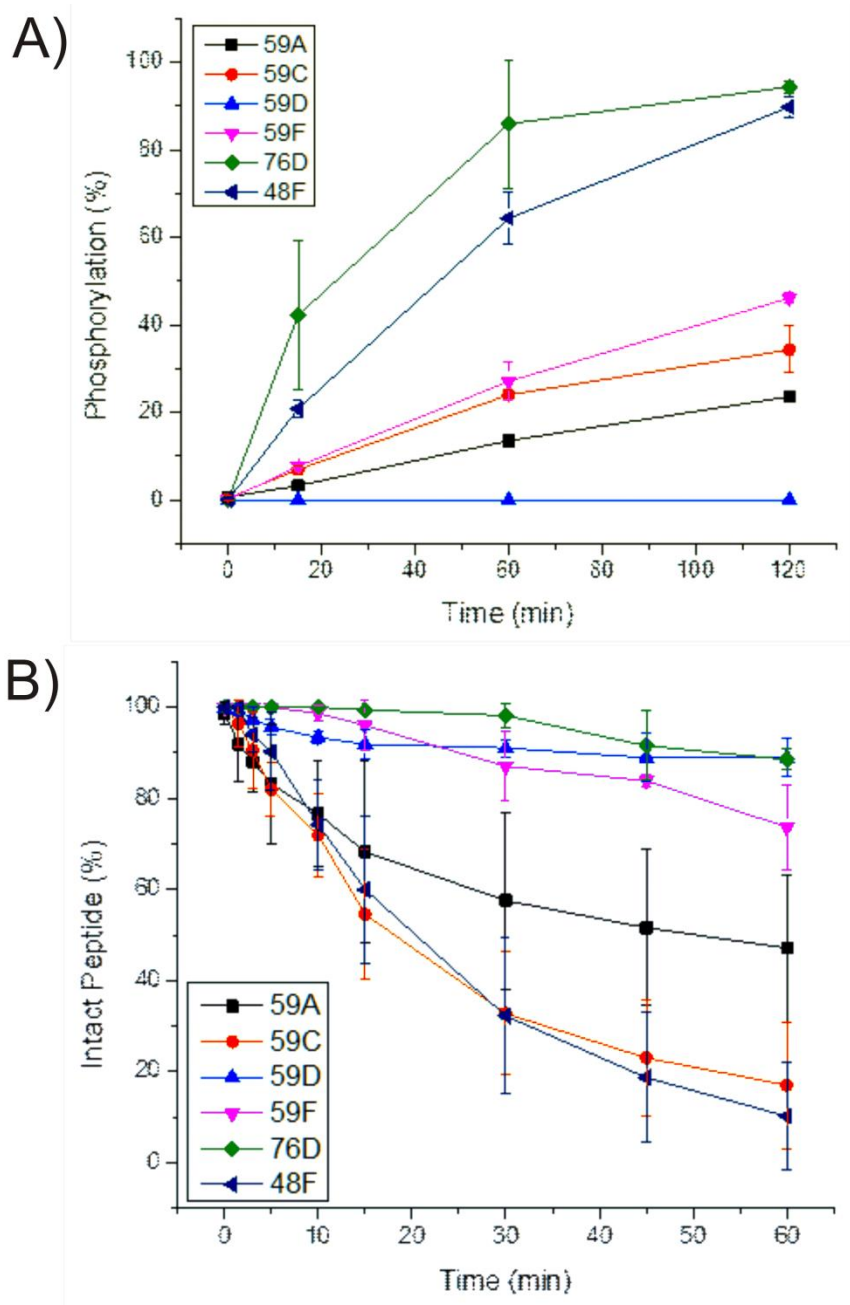
Figure 4.4 Characterization of Peptide Library. A) In-vitro phosphorylation of peptide library by Aktα in the presence of ATP. Phosphorylation (%) was measured as a ratio of peak areas between phosphorylated and total reporter in CE electropherograms. B) Degradation of peptide library in PANC-1 cytosolic lysates. Intact peptide (%) was measured as a ratio of integrated peak areas between intact peptide and fragment peaks in CE electropherograms.
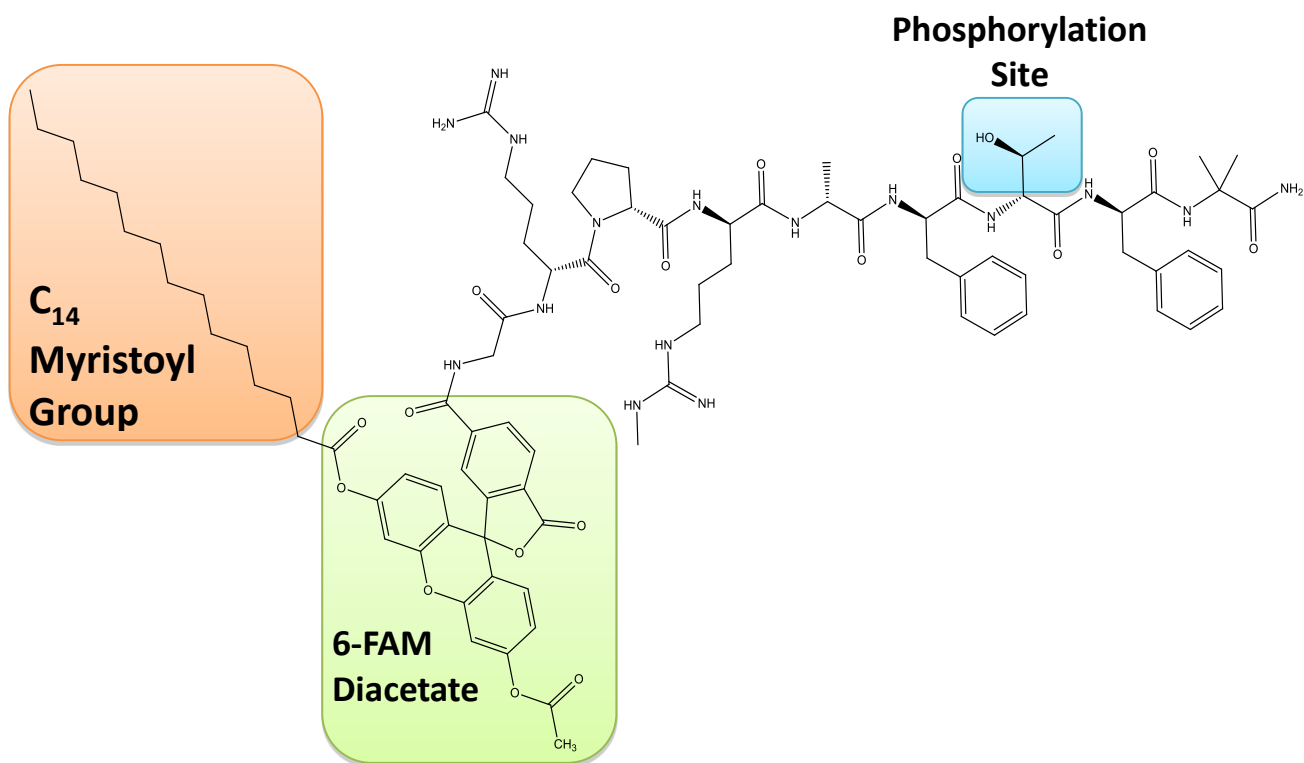
Figure 4.5 Structure of Myristoylated FAMDA-76D Peptide (Myr76D).
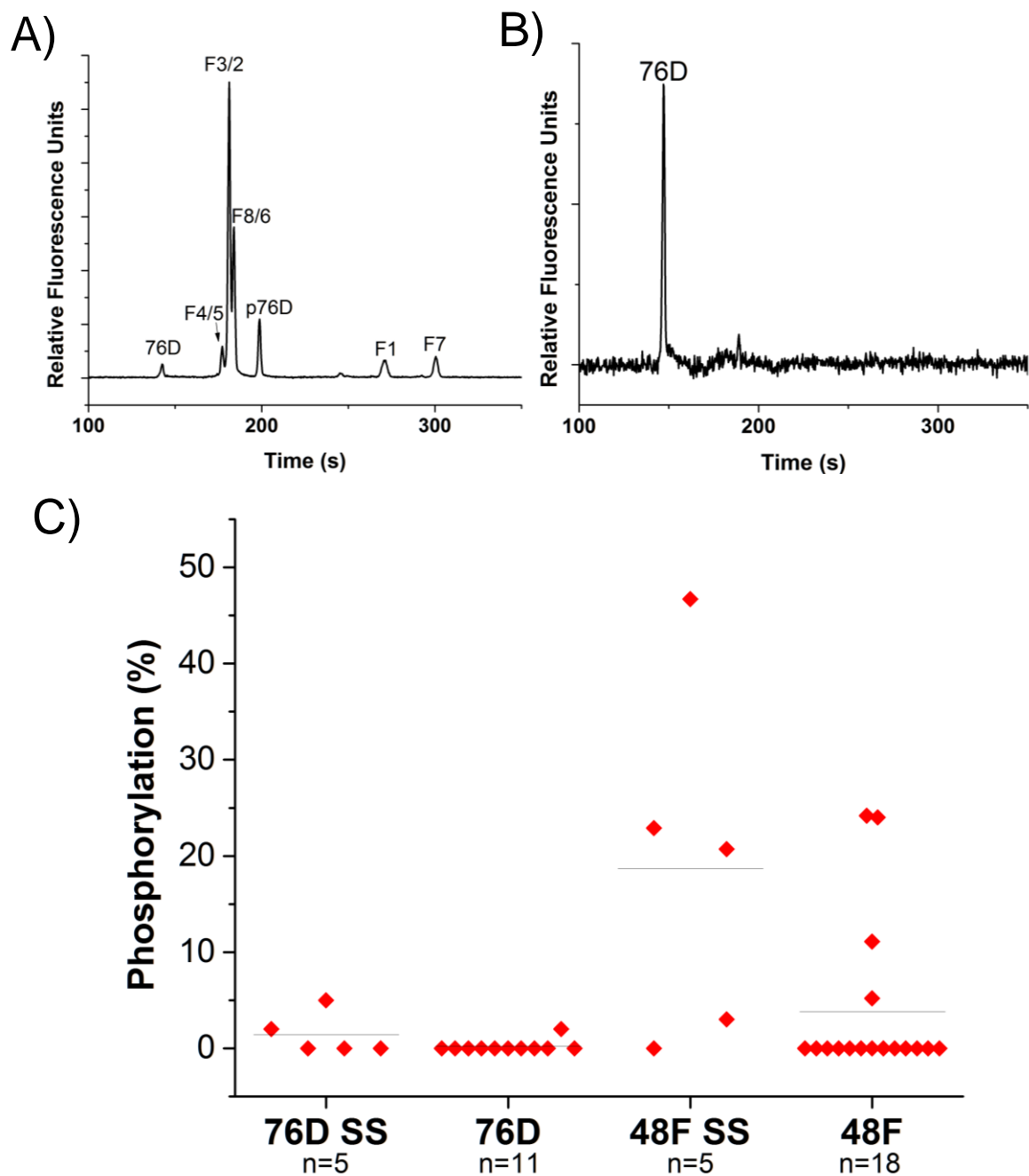
Figure 4.6 Microinjection of Peptides Into PANC-1 Cells. A) Standards of 76D, phosphorylated 76D (p76D) and all possible fluorescent fragments. F1 corresponds to the one-amino acid fragment, and each subsequent number corresponds to a fragment with one additional residue at the C terminus B) Electropherogram of PANC-1 cell 2.5 min after microinjection with fully intact parent peptide 76D. C) Summary of reporter phosphorylation in cells microinjected with 76D and VI-B, and cells with serum stimulation (SS). The bars represent the median for each measurement.

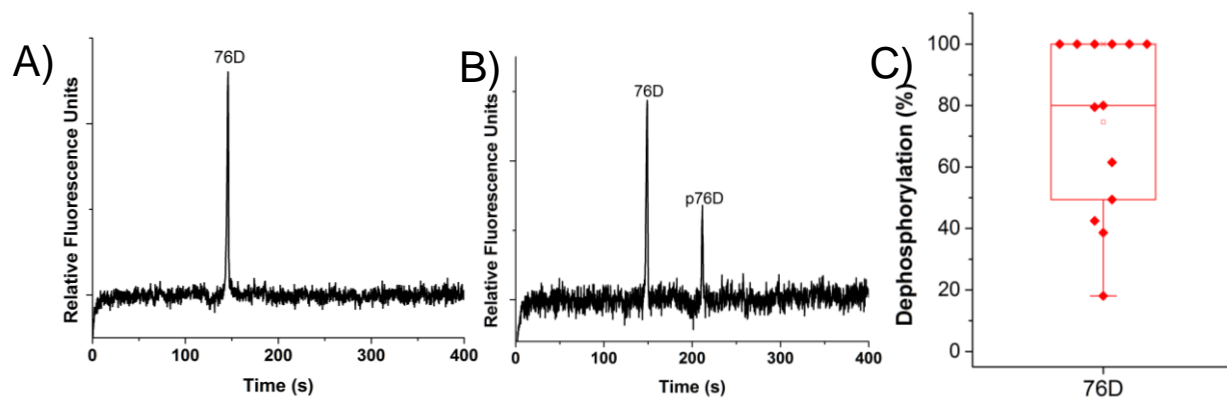**Figure 4.7 Dephosphorylation of p76D in PANC-1 Cells.** Phosphorylated 76D was microinjected into single PANC-1 cells. Dephosphorylation observed at (A) 5 min or B) 2.5 min timepoints after injection. C) Summary of dephosphorylation 2.5 min after incubation in PANC-1 cells, where each data point represents a single PANC-1 cell.

.

Table 4.1 Properties of the Modified Peptides Derived From Starting Peptide VI-B.

Peptide	Peptide Sequence	$t_{50\%P}$ (min)	$t_{1/2}$ (min)
VI-B*	6FAM-GRP-MeArg-AFTF-MeAla	57 ± 6.8	19 ± 12.1
76D	6FAM-GRP-MeArg-AFTF-**Aib**-NH$_2$	40 ± 10.3	352 ± 5.2
59A	6FAM-GRP-MeArg-AFTF-**MeAib**-NH$_2$	256 ±7.2	48 ± 13.8
59C	6FAM-GRP-MeArg-AFTF-**BnAla**-NH$_2$	167 ± 7.8	20 ± 12.2
59D	6FAM-GRP-MeArg-AFT-**MePhe**-MeAla-NH$_2$	ND	43± 7.8
59F	6FAM-GRP-MeArg-AFT-**D-Phe**-MeAla-NH$_2$	126 ± 5.7	142 ± 8.4

* Indicates starting peptide. Modified residues from VI-B are shown in bold. ND= Not determined. Non-native amino acid abbreviations: MeAib : α-(methylamino)isobutyric acid; Aib: α-aminoisobutryic acid; BnAla: Benzylalanine; MePhe: N-methyphenylalanine; MeAla: N-methylalanine D-Phe: D-Phenylalanine

REFERENCES

1. Nishikawa, K.; Sawasdikosol, S.; Fruman, D. A.; Lai, J.; Songyang, Z.; Burakoff, S. J.; Yaffe, M. B.; Cantley, L. C. A Peptide Library Approach Identifies a Specific Inhibitor for the ZAP-70 Protein Tyrosine Kinase. *Molecular Cell* 2000*, 6*, 969-974.

2. McBride, J. D.; Freeman, N.; Domingo, G. J.; Leatherbarrow, R. J. Selection of Chymotrypsin Inhibitors from a Conformationally-constrained Combinatorial Peptide Library. *Journal of Molecular Biology* 1996*, 259*, 819.

3. Songyang, Z.; Blechner, S.; Hoagland, N.; Hoeskstra, M. F.; Piwnica-Worms, H.; Cantley, L. C. Use of an oriented peptide library to determine the optimal substrates of protein kinases. *Current Biology* 1994*, 11*, 973.

4. Bohley, P.; Seglen, P. O. Proteases and proteolysis in the lysosome. *Experientia* 1992*, 48*, 151.

5. Tholey; Zabet-Moghaddam; Heinzle Quantification of Peptides for the Monitoring of Protease-Catalyzed Reactions by Matrix-Assisted Laser Desorption/Ionization Mass Spectrometry Using Ionic Liquid Matrixes. *Analytical Chemistry* 2006*, 78*, 291-297.

6. Brown, R. B.; Hewel, J. A.; Emili, A.; Audet, J. Single amino acid resolution of proteolytic fragments generated in individual cells. *Cytometry Part A* 2010*, 77A*, 347–355.

7. Li, H.; Sims, C. E.; Stanbridge, E. J.; Allbritton, N. L. Quantitative Single-Cell Assay for Protein Kinase B Reveals Important Insights into the Biochemical Behavior of an Intracellular Substrate Peptide. *Biochemistry* 2004*, 43*, 1599.

8. Brinckerhoff, L. H.; Kalashnikov, V. V.; Thompson, L. W.; Yamshchikov, G. V.; Pierce, R. A.; Galavotti, H. S.; Engelhard, V. H.; Slingluff, C. L. Terminal modifications inhibit proteolytic degradation of an immunogenic mart-127–35 peptide: Implications for peptide vaccines. *International Journal of Cancer* 1999*, 83*, 326–334.

9. Proctor, A.; Wang, Q.; Lawrence, D. S.; Allbritton, N. L. Metabolism of peptide reporters in cell lysates and single cells. *Analyst* 2012*, 137*, 3028.

10. Yang, S.; Proctor, A.; Cline, E.; Houston, K.; Waters, M.; Allbritton, N. L. β-Turn sequences promote stability of peptide substrates for kinases within the cytosolic environment. *The Analyst* 2013*, 138*.

11. Bird; Madani; Perry; Princiotto; Supko; He; Gavathiotis; Sodroski; Walensky Hydrocarbon double-stapling remedies the proteolytic instability of a lengthy peptide therapeutic. *Proceedings of the National Academy of Sciences* 2010*, 107*, 14093-14098.

12. Roxin; Zheng Flexible or fixed: a comparative review of linear and cyclic cancer-targeting peptides. *Future Medicinal Chemistry* 2012*, 4*, 1601-1618.

13. Tal-Gan; Hurevich; Klein; Ben-Shimon; Rosenthal; Hazan; Shalev; Niv; Levitzki; Gilon Backbone Cyclic Peptide Inhibitors of Protein Kinase B (PKB/Akt). *Journal of Medicinal Chemistry* 2011*, 54*, 5154-5164.

14. Bruehlmeier, M.; Garayoa, E. G.; Blanc, A.; Holzer, B.; Gergely, S.; Tourwé, D.; Schubiger, P. A.; Bläuenstein, P. Stabilization of neurotensin analogues: effect on peptide catabolism, biodistribution and tumor binding. *Nuclear Medicine and Biology* 2002*, 29*, 321-327.

15. Manavalan, P.; Momany, F. A. Conformational energy studies on N-methylated analogs of thyrotropin releasing hormone, enkephalin, and luteinizing hormone-releasing hormone. *Biopolymers* 1980*, 19*, 1943–1973.

16. Conti, F.; De Santis, P. On the conformations of poly-N-methyl-L-alanine (PNMA) in solution. *Biopolymers* 1971*, 10*, 2581–2590.

17. Proctor, A.; Herrera-Loeza, G.; Wang, Q.; Lawrence, D. S.; Yeh, J.; Allbritton, N. L. Measurement of Protein Kinase B Activity in Single Primary Human Pancreatic Cancer Cells. *Analytical Chemistry* 2014*, 86*, 4573-4580.

18. Proctor, A.; Wang, Q.; Lawrence, D.; Allbritton, N. Development of a Peptidase-Resistant Substrate for Single-Cell Measurement of Protein Kinase B Activation. 2012*, 84*, 7195.

19. Udenfriend; Stein; Bohlen; Dairman; Leimgruber; Weigele Fluorescamine: A Reagent for Assay of Amino Acids, Peptides, Proteins, and Primary Amines in the Picomole Range. *Science* 1972*, 178*, 871-872.

20. Hong, S. Y.; Oh, J. E.; Lee, K. Effect of d-amino acid substitution on the stability, the secondary structure, and the activity of membrane-active peptide. *Biochemical Pharmacology* 1999*, 58*, 1775-1780.

21. Gentilucci; De Marco; Cerisoli Chemical Modifications Designed to Improve Peptide Stability: Incorporation of Non-Natural Amino Acids, Pseudo-Peptide Bonds, and Cyclization. *Current Pharmaceutical Design* 2010*, 16*, 3185-3203.

22. Proctor, A.; Wang, Q.; Lawrence, D. S.; Allbritton, N. L. Metabolism of peptide reporters in cell lysates and single cells. *The Analyst* 2012*, 137*.

23. Hammes, A.; Andreassen, T. K.; Spoelgen, R.; Raila, J.; Hubner, N. Role of endocytosis in cellular uptake of sex steroids. *Cell* 2005*, 122*, 751.

24. Okada, C. Y.; Rechsteiner, M. Introduction of macromolecules into cultured mammalian cells by osmotic lysis of pinocytic vesicles. *Cell* 1982*, 29*, 33.

25. Tsong, T. Electroporation of cell membranes. *Biophysical Journal* 1991*, 60*, 297.

26. Nelson, A.; Borland, L.; Allbritton, N.; Sims, C. Myristoyl-Based Transport of Peptides into Living Cells. *Biochemistry* 2007*, 46*, 14771.

27. Madani, F.; Lindberg, S.; Langel, U.; Futaki, S.; Graslund, A. Mechanism of Cellular Uptake of Cell-Penetrating Peptides. *Journal of Biophysics* 2011*, 2011*.

28. Thomas, J.; Buchsbaum, R. N.; Zimniak, A.; Racker, E. Intracellular pH Measurements in Ehrlich Ascites Tumor Cells Utilizing Spectroscopic Probes Generated in Situ. *Biochemistry* 1979*, 18*, 2210.

29. Donella-Deana, A.; Ruzza, P.; Cesaro, L.; Brunati, A. M.; Calderan, A.; Borin, G.; Pinna, L. A. Specific monitoring of Syk protein kinase activity by peptide substrates including constrained analogs of tyrosine. *FEBS Letters* 2002*, 523*, 48-52.

Chapter 5: Pronase E-Based Generation of Fluorescent Peptide Fragments: Tracking Intracellular Peptide Fate in Single Cells

5.1 Overview

The ability to track intracellular peptide proteolysis at the single cell level is of growing interest, particularly as short peptide sequences continue to play important roles as biosensors, therapeutics, and endogenous participants in antigen processing and intracellular signaling. We describe a rapid and inexpensive methodology to generate fluorescent peptide fragments from a parent sequence with diverse chemical properties, including aliphatic, nonpolar, basic, acidic, and non-native amino acids. Four peptide sequences with existing biochemical applications were fragmented using incubation with Pronase E and/or formic acid and in each case a complete set of fluorescent fragments was generated for use as proteolysis standards in chemical cytometry. Fragment formation and identity was monitored with capillary electrophoresis with laser-induced fluorescence detection (CE-LIF) and matrix assisted laser desorption ionization-time of flight mass spectrometry (MALDI-MS) to confirm the presence of all sequences and yield fragmentation profiles across Pronase E concentrations which can readily be used by others. As a pilot study, Pronase E-generated standards from an Abl kinase sensor and an ovalbumin antigenic peptide were then employed to identify proteolysis products arising from the metabolism of these sequences in single cells. The Abl kinase sensor fragmented at 4.2 ± 4.8 zmol μM^{-1} s^{-1} and the majority of cells possessed similar fragment identities. In contrast, an ovalbumin epitope peptide was degraded at 8.9 ± 0.1 zmol μM^{-1} s^{-1} but with differential fragment formation between

142

individual cells. Overall, Pronase E-generated peptide standards were a rapid and efficient method to identify proteolysis products from cells.

5.2 Introduction

Intracellular proteolytic processing of short peptides is an important biological phenomenon, with demonstrated functions in antigen presentation,[1] pheromone secretion,[2] gene regulation[3] and modulation of signal transduction.[4] Proteins and peptides are metabolized by complex multi-protein systems such as the proteasome, producing oligopeptides subsequently transported in the cytoplasm, secretory granules, or nucleus.[5,6] These short sequences can then continue on to one of many fates, for example, reduction to their component amino acids for use as synthetic building blocks, aggregation into disease-inducing amyloid plaques[7], or transportation to the extracellular membrane to act as antigens. Additionally, exogenous loading of peptidic sequences into cells has been used to study peptide processing[8] and intracellular signaling[9-12] as well as to deliver drugs and to enhance imaging contrast.[13] The ability to assess cells individually for specific peptidolytic phenotypes is also increasingly desirable such as for the development of engineered T-cell therapies or the assay of peptidase heterogeneity for targeted tumor therapeutics. These recent advances for the design and delivery of peptide-based therapeutics further fuel the growing interest in tracking intracellular peptide stability and fate, particularly at the single-cell level. Thus tools to enhance the ability to directly monitor peptide reactions within cells will have tremendous value in a wide range of areas from sensor development to therapeutics and basic physiology.

Regardless if sequences are designed to undergo systematic degradation as sensors of protease activity, are delivered as a vaccine,[14] or used for other purposes, the ability to study peptide fragmentation patterns is critical to tracking peptide fate. Measurements of intracellular peptide metabolism particularly that incorporate a separation step such as chemical cytometry also require a set of fragment standards to unambiguously detect peptide fragments.[15,16] Facile generation of a full fragment set would enable rigorous characterization of the intracellular fate of peptides used as reporters for kinases, phosphatases and other enzymes in chemical cytometry as well as applications in mass spectrometry-based proteomics and peptide sequencing. Rapid generation of peptide fragments may also accelerate the determination of biologically active sequences from larger peptides or proteins, such as in the delineation of specific peptide binding motifs for the prediction of T-cell epitopes. Currently, this process involves screening all potentially active sequences from a parent peptide, requiring the laborious synthesis of all fragments.[17]

Methods to generate fragments from a peptide sequence center around three main approaches: solid phase peptide synthesis (SPPS), chemical fragmentation, and enzymatic digestions. While SPPS is unparalleled at guaranteeing the presence of all desired sequences, the synthesis of fragment mixtures from complex cyclized, cross-linked or stapled peptides may be highly difficult and can require lengthy chromatographic purification.[18] Chemical cleavage of peptides has been performed with a variety of reagents such as cyanogen bromide, 3-Bromo-3-methyl-2-(2-nitrophenylthio)-3H-indole, formic acid and hydroxylamine, which clip C-terminally of methionine, tryptophan, aspartic acid and asparagine, respectively.[19] However, the nature of chemoselective fragmentation in combination with the relatively low abundance of the specified amino acid loci often result in

the generation of long peptides. Thus, for the generation of all sequences from a peptide, concatenated cleavage steps with multiple reagents may be required and do not guarantee the presence of all fragments.

A popular route to generating peptide fragment ladders is directed enzymatic cleavage, a technique borrowed from bottom-up mass spectrometry-based proteomics in which proteins are digested with trypsin or chymotrypsin to generate short peptide sequences.[20] However, these two enzymes have well-defined specificity and only yield peptide fragments by hydrolysis at five of the twenty amino acids. In cases where nonspecific peptide cleavage is desired, proteases such as Pepsin A and Proteinase K which cleave peptides with limited substrate specificity are often employed, although sequence coverage with these two enzymes is not 100%.[21] Pronase E from the extracellular fluid of *Streptomyces gresius* is a commercially available, broad-specificity mixture of at least ten enzymatic components, including five serine-type proteases, two Zn^{2+}-endopeptidases, two Zn^{2+}-leucine aminopeptidases and a Zn^{2+} carboxypeptidase.[22,23] The reported ability of Pronase E to hydrolyze peptide bonds internal to a sequence as well as sequentially remove amino acids from both the N and C terminus make this enzyme mixture an attractive alternative to enzymatic digestion with trypsin or chymotrypsin, whose regulated activity would deliver only specific fragments.[24]

It was hypothesized that the broad range of proteolytic activities afforded by Pronase E would affect cleavage at each peptide bond, resulting in a standard mixture of all possible fluorescent fragments of a full-length peptide. Herein, we demonstrate the utility of Pronase E as a nonspecific, rapid, and inexpensive method to generate fluorescent peptide fragment

ladders. We also introduce the use of secondary formic acid digestion as a post-enzymatic step to promote the formation of acidic fragments. Fragment formation and identity were synergistically monitored with CE-LIF and MALDI-MS in parallel. Finally, peptide fragment standards generated by Pronase E were then applied to identification of degradation products from peptide-based probes in single cell assays. Peptide ladders generated by Pronase E should have wide applicability in the identification of degradation products in single cell assays, for peptide sequencing purposes, and for the generation of biologically active sequences when identifying immunogenic epitopes.

5.3 Experimental Section

5.3.1 Chemicals

Aside from the following reagents, chemicals were purchased from Sigma Aldrich or Fisher Scientific. For cell culture, Dulbucco's Modified Eagle's Medium (DMEM) was acquired from Cellgro; Penicillin/streptomycin was obtained from Gibco, and fetal bovine serum (FBS) was purchased from Atlanta Biologicals.

5.3.2 Peptide Synthesis

The full length peptides I-III (Figure 5.1A) were synthesized using standard SPPS methodology on TGR resin, while peptide acid fragments were synthesized on 2-chlorotritylchloride resin, both using an automated peptide synthesizer (PS3, Protein Technologies, Tuscon, AZ). Each was fluorescently labeled at the N-terminus with either 5 or 6FAM. Fmoc-Asp(OMpe)-OH was used in the synthesis of Peptide III to prevent racemization through aspartimide formation. Synthesis of Peptide IV was performed at the High-Throughput Peptide Synthesis and Arrays (HTPSA) Core Facility at the University of North Carolina at Chapel Hill.

146

5.3.3 Cell Culture

PANC-1 cells were obtained from the American Type Culture Collection and maintained in a humidified atmosphere of 37°C in 5% CO_2. Cells were cultured in DMEM supplemented with 10% FBS, penicillin (100 units/mL) and streptomycin (100 µg/mL) and were passaged at 60-80% confluence with 0.25% trypsin solution. Cells were plated for single-cell analysis the day prior to analysis by adding a dilute cell solution to 400 microliters of DMEM media in cell chambers.

5.3.4 Pronase E Peptide Digestions

Pronase E from *Streptomycies gresius* was prepared in phosphate buffered saline (PBS; 137 mM NaCl, 10 mM Na_2HPO_4, 2.7 mM HCl, 1.75 mM KH_2PO_4, pH 7.4) to 2 mg/mL. Assessment of peptide degradation was performed in triplicate by combining peptide (10 µM) with various concentrations of Pronase E (0.001 µg/mL-1000 µg/mL) and incubating at 37°C. Aliquots were removed at time points and inactivated at 90°C for 4 min. Negative controls without peptide were concurrently sampled and heat-inactivated. Samples were diluted 100X in electrophoretic buffer prior to separation and detection with CE-LIF.

5.3.5 Supplemental Formic Acid Assisted Digestion

Additional fragments of Peptide III were generated by incubating partially digested samples from Pronase E assays in 1-5% formic acid solution at 37°C. Aliquots were neutralized with an equal volume of 200 mM NaOH to bring the pH to 6.5-7.5.

5.3.6 Capillary Electrophoresis

For separations not involving single cells, CE-LIF (488 nm) was performed using a Proteome-Lab PA 800 (Beckman Coulter, Fullerton, CA) equipped with 30 cm fused silica

capillaries of 30 or 50 µM inner diameter, 360 µM outer diameter (Polymicro Technologies, Phoenix, AZ). Electrophoretic buffers for Peptides I, II, III, and IV were 100 mM tris, 100 mM tricine, pH 8.1; 140 mM borate, 70 mM sodium dodecyl sulfate (SDS), pH 9.5; 300 mM borate, pH 7.5; and 100 mM tris, 100 mM tricine, 5 mM sodium cholate, pH 8.1, respectively. Electropherograms were integrated using customized software[20] constructed using MATLAB (Natick, MA).

5.3.7 MALDI-MS Analysis

MALDI-MS analyses were performed in high-resolution reflectron mode with an AB SCIEX 4800 Plus instrument equipped with a 337 nm laser. Peptide standards and assay samples were diluted in deionized water to 3 µM. Samples were prepared by spotting a 500 nL sample volume onto a 364-spot MALDI sample plate immediately followed by 500 nL of saturated α-cyano-4-hydroxycinnamic acid matrix solution. Spots were air-dried under laminar flow. The laser intensity was set to 4200 mW and 50 shots were averaged for the peptide spectra.

5.3.8 Single Cell Capillary Electrophoresis

Custom glass chambers for housing cells were placed on the stage of a customized single-cell CE system with LIF detection (488 nm).[25] Cells were microinjected with 100 µM peptide (I or IV) using a Transjector 5246 microinjection system (Eppendorf AG, Hamburg, Germany). Cells were maintained at 37°C with a constant flow of warmed extracellular buffer (ECB; 10 mM HEPES, 135 mM NaCl, 5 mM KCl, 1 mM $CaCl_2$, 1 mM $MgCl_2$, pH 7.4) throughout incubation and analysis. At 2 min post microinjection, the cell was lysed with a focused Nd:YAG laser pulse as previously described[26] and the contents injected into the capillary by applying a negative potential to the capillary outlet reservoir (5 s at 79

V/cm). For separations of single cells microinjected with Peptides I or IV, electrophoresis was performed in respective buffers at -171 and -263 V/cm, respectively.

5.4 Results and Discussion

5.4.1 Experimental Overview

The goal of this work was to develop a simple strategy to generate fluorescent peptide fragments regardless of their sequence or structure. To that end, a small collection of chemically diverse peptides with existing biochemical applications was selected (Figure 5.1A), and the efficacy of Pronase E in generating fragments as a function of substrate chemistry and enzyme concentration was examined. Each peptide under investigation was incubated with Pronase E at varying concentrations for up to 60 min (Figure 5.1B,C). Samples were then divided into two equivalent fractions and subjected to parallel analysis by CE-LIF and MALDI-MS in order to determine how many fluorescent fragments were generated (Figure 5.1D). The number of fragments formed and the rate of peptide degradation was determined from the number and area of peaks appearing in electropherograms (see Figure 5.1A for fragment nomenclature for Peptides I-III, Table 5.1 for Peptide IV). MALDI-MS identified which fragments formed under the different conditions. To validate the identity of fragments in electropherograms, all fluorescent fragments of Peptides I-III were synthesized using SPPS to identify unique electrophoretic and mass footprints. We then applied the assay to the formation and identification of fragments from Peptide IV, an ovalbumin epitope sequence without synthesized standards. Pronase E-generated standards were then employed to identify peptides formed due to protease activity in single cells.

5.4.2 Identification of fragments formed in Pronase E assays

For peptides I-III, standards of all possible fluorescent peptide fragments were synthesized, purified, and characterized by CE-LIF. Separation methods were developed for each peptide under which all N-terminal fragments were resolved from the parent peptide and from all other species. This allowed facile identification of Pronase E cleavage sites for each peptide. Full length peptides were incubated with Pronase E, and after stopping the reaction each of the possible fluorescent peptide standards was sequentially added into the reaction mixture to identify peptide fragments by CE-LIF. Each peak present in the CE analysis of the assay sample was attributable to a standard fragment, permitting unambiguous identification of each fragment formed. Intact full length peptide was identified by adding standard peptide to the heat-inactivated aliquots. Peaks appearing at migration times differing from the full length peptide were identified as fragments by the addition of synthesized fragment standards and/or by confirming the presence of fragment masses by MALDI-MS. The percentage of intact parent peptide was calculated by the ratio of the peak area of intact peptide to that of all peaks in the electropherogram.

To identify fragments of Peptide IV, a combination of CE-LIF and MALDI-MS were utilized. As proof of principle, fragments were identified without the use of synthesized standards. Because it is labeled on an internal lysine sidechain, fluorescent fragments of Peptide IV may be formed by removal of amino acids from both the N and C terminus; therefore fragment nomenclature was based on mass (Table 5.1). Samples resulting from digestions at various Pronase E concentrations were subjected to MALDI–MS until a condition was identified that generated all possible fragments. When the mass for at least one

member of an identical mass pair for peptide IV was identified by MALDI-MS, 50% of that detected was arbitrarily assigned to each fragment in the pair.

5.4.3 Enzymatic Generation of Peptide I Standards

Peptide I (5FAM-GGAYAAPFKKKA-NH$_2$), a sequence employed as an Abl kinase sensor, contains primarily hydrophobic and basic residues and was well matched to the reported specificity of Pronase E.[22,23] All fragments of Peptide I were readily separated in an optimized[10] buffer system (Figure 5.2A) and efficiently detected by MALDI-MS (Figure 5.2B). Due to moderate salt levels in the sample matrix, Peptides I-k, I-g, I-f, and I-e often ionized as sodium or potassium adducts, which are denoted in mass spectra by asterisks (*). After verifying that all fragments possessed unique electrophoretic and mass footprints, Peptide I was incubated with Pronase E and the assays sampled over time by CE-LIF to assess the formation of fluorescent fragments. Complete degradation into all representative fragments was observed after incubation with 0.02 µg/mL enzyme for 15 min, represented by the appearance of 11 new peaks in electropherograms (Figure 5.2C) and the identification of each fragment mass by MALDI-MS (Figure 5.2D). Fragments I-j (23±4.2%) and I-l (30±5.6%), resulting from cleavage at Ala-Tyr and Gly-Gly bonds, respectively, were among the predominant fragments formed, although all 11 were detected by both CE-LIF and MALDI-MS. Taken with data from incubation of Peptide I with more concentrated solutions of Pronase E (Figure 5.3A), these results indicated that the enzyme mixture first hydrolyzes multiple peptide bonds within a sequence before reducing the peptide to the shortest peptide fragments. Overall, Pronase E was capable of generating all fluorescent fragments of Peptide I in as short as 15 min, which, at minimum, is 50 fold faster than by SPPS.

5.4.4 Enzymatic Generation of Fragments for Peptide II

After verifying that Pronase E could be used to generate fragments of a peptide containing residues similar to its reported preference, a longer and more charge diverse sequence was evaluated. Peptide II (6FAM-RAHEEIYHFFFAKKK-NH_2) is a substrate of epidermal growth factor receptor (EGFR) tyrosine kinase and has found widespread utility for *in vitro* enzymatic characterization of EGFR.[27,28]Containing aromatic, aliphatic, acidic, and basic residues, Peptide II represents a chemically-diverse testing ground for the formation of fragments by this enzyme mixture. Peptide II was incubated with various concentrations of Pronase E, and aliquots were removed over time and heat inactivated. Samples were separated with CE-LIF to detect the formation of fluorescent fragments. As with Peptide I, preparations of Pronase E below 0.001 µg/mL were insufficient to produce any detectable proteolysis within 60 min. However, after increasing the Pronase E concentration to 0.01 µg/mL for 15 min, only 13.5±4.5% of the full length peptide remained, and 9 of 15 fragments were formed and separated by CE-LIF (Figure 5.3B). The primary products were II-d (22.3±3.4%) and II-g (15.8±2.6%), resulting from cleavage at Ala-Arg and Phe-Phe bonds, respectively. After treatment with up to 0.01 µg/mL Pronase E, the shortest fluorescent fragment detected was 7 amino acids (II-i; 11.6±2.1%), which, taken with results from Peptide I, suggests that at these and lower concentrations of lower E possesses greater activity towards charged and hydrophobic residues. No fragments resulting from cleavage at sites upstream of position 7 (II-i) were detected, despite reports of an acidic amino acid-specific endopeptidase purified from Pronase E which preferentially cleaves at such sites.

0.1 µg/mL Pronase E was required to form all 15 fragments within 15 min (Figure 5.3B, Figure 5.4B). Although fragments II-l and II-m formed less than 2% of the total fragments detected by CE-LIF, these were readily identified with CE-LIF and also with MALDI-MS (Figure 5.5). With further increased enzyme concentration (5 µg/mL), the majority of fragments furnished from digestion were low mass short fragments, namely II-n and II-o. While a moderate concentration of Pronase E was sufficient to generate all fragments, it should be noted that pooling samples from differing concentrations which contain overlapping sequence coverage is a method in which the desired fragments can be obtained.

5.4.5 Pronase E digestion of degradation resistant Peptide III

In order to assess limitations of Pronase E to generate all fluorescent fragments of a peptide, a degradation resistant sequence was identified and synthesized, along with its corresponding fluorescent fragments. Peptide III (6FAM-LEDDYEDDNle-NH$_2$, where Nle is Norleucine) was adapted from a substrate of protein tyrosine phosphatases (PTPs).[9] In single cells, the median half-life of the peptide was 35 min; 70-fold longer than that of Peptide I.[11,29] Though truncated from its original 13 amino acid sequence, Peptide III possesses 80% of the glutamic and aspartic acid residues to which its degradation resistance was attributed. This peptide also contains a non-native amino acid, which confers resistance to degradation, presumably due to the limited ability of peptidases to recognize non-coding amino acids.[30,31]

Peptide III was resistant to enzymatic degradation 60 min after incubation with 50 µg/mL Pronase E, a 500-fold more concentrated solution than that required to generate all

fluorescent fragments of Peptide II in 15 min. However, by incubating the peptide with 500 µg/mL Pronase E for 15 min all fluorescent fragments were generated and detected with CE-LIF (Figure 5.6A). As expected, the majority of fragments formed during digestion were the result of cleavage between native amino acids. The three fragments forming in the smallest percentages were all generated by cleavage between two acidic residues (III-c, e, g), which falls in agreement with reports of the resistance of peptide bonds between anionic residues to hydrolysis.[29] Due to the highly sensitive nature of CE-LIF, several fragments formed in small quantities detectable by CE but were not identified through MALDI-MS analysis (Figure 5.6B). These included III-b, c and e, all fragments resulting from cleavage involving acidic or non-native amino acids, which were identified with fragment standards. Increasing the Pronase E concentration to 1000 µg/mL had the effect of generating a higher fraction of short (<5 residues) peptides and fragment III-b due to cleavage of Nle (Figure 5.3C), but fragments such as III-c, III-e and III-g were never formed in amounts greater than 3% of the total fragments detected in electropherograms, and were rarely detected with MALDI-MS.

5.4.6 Formic Acid-Assisted Degradation of Peptide III

We hypothesized that the acidic nature of Peptide III contributed to the limited formation of several fragments and our resultant inability to detect some fragments with MALDI-MS. Thus, we sought a method which could be used in combination with Pronase E to generate fragments in a more equivalent fashion. Given that conditions for the selective cleavage of peptides and proteins at the carboxyl side of acidic residues such as aspartic acid using formic acid had been reported,[32] we selected formic acid for digestions. Formic acid treatment alone was insufficient to generate all fragments (Figure 5.7). However, if Peptide III was first partially hydrolyzed with 500 µg/mL Pronase E for 15 min, heat-inactivated, and

then exposed to 2% formic acid for 15 min at 37°C, all 8 fragments were detected along with native peptide. The fraction of peptides produced due to cleavage at the C-terminal end of aspartic acid residues each improved to a minimum composition of 6%, and was easily detected with CE-LIF (Figure 5.6C). The use of formic acid also resulted in improved sensitivity and better representation of true peptide stoichiometries in MALDI-MS spectra (Figure 5.6D), presumably due to improved ionization garnered after protonation by formic acid.[33] Overall it was found that the combination of enzymatic and chemical peptide hydrolysis produced a simple, rapid, and novel method to nonspecifically generate fragments of an acidic, degradation-resistant peptide.

5.4.7 Degradation of an immunogenic peptide with an internal fluorophore

Intracellular peptide metabolism gives rise to many compounds of biological importance, including epitopes recognized by cytotoxic T-cells (CTL). Use of these antigens as immunotherapy is a promising new treatment for patients with advanced stage oncological malignancies, but antigen immunotherapy is limited by the paucity of suitable peptide antigens that are recognized by CTLs,[34] necessitating laborious epitope mapping screens in which full length peptides and all possible truncated active sequences must be synthesized. Thus, a mixture of all possible fragments from a potential epitope-containing peptide or protein could be useful, especially since it has been shown that pooling of peptide fragments does not cause masking of the active sequences in high-throughput screens.[35] Peptide IV (SIINFE(K-5FAM)L-OH) is the 256-264 residue class I (Kb)-restricted peptide of ovalbumin, a frequently modeled epitope in the context of the major histocompatibility complex (MHC) Class I allotype. It has been demonstrated that the peptide can be used to elicit strong CD8+ cytolytic T cell responses.[36] Although presentation of Peptide IV requires

no further proteolytic processing, this sequence acted as proof of principle for the enzymatic generation of all possible fluorescent fragments of an active epitope with Pronase E.

To establish whether all fragments of a peptide with an internal fluorophore could be generated without the use of synthesized standards, Peptide IV was incubated with varying amounts of Pronase E until the maximum number of fluorescent fragments (nomenclature; Table 5.1) were identified with MALDI-MS (Figure 5.8). Compared to Peptides I-III, an intermediate concentration of Pronase E (5 µg/mL) was required to generate all fluorescent fragments of this sequence (Figure 5.3D). Three pairs (IV-d/e, IV-f/g, and IV-h/i) of Peptide IV fragments possessed similar or identical masses (Table 5.1) and could not be unambiguously identified by MALDI-MS alone, making identification of these fragments a unique challenge. One species, fragment IV-n, could not be identified by MALDI-MS, potentially due to poor ionization under the conditions tested. To ensure that all fluorescent fragments were indeed formed, the same sample was subjected to separation with CE-LIF. 15 unique peaks were identified, each presumably representing a fragment. Since sequence-specific identities could not be assigned to peaks appearing in electropherograms, fragments of Peptide IV detected by CE-LIF were labeled with roman numerals according to migration time (Figure 5.9D). While the sequence of each fragment cannot be determined by migration time alone, the combination of MALDI-MS and CE-LIF data indicates that each fragment is present. Based on the MALDI-MS analysis, we can speculate that fragments formed in greater quantities, such as IV-a and IV-k, may correspond to species generating a large peak area in CE-LIF analysis, such as IV-xiii and IV-ii, respectively. Peptide IV was identified as IV-ix based on co-migration with the synthetic full length sequence. Interestingly, the contents of the slowest migrating peak in Figure 5.9D and Figure 5.10 co-migrated with the

free fluorophore (5FAM) which was not observed in Pronase E assays with Peptides I-III, which are fluorescently labeled on the N-terminus rather than an internal residue. Overall, Pronase E was a rapid and simple method to generate fluorescent fragments regardless of the fluorophore placement. Thus, this technique finds applications in comprehensive fragment profile generation with the exact sequence-specific peptides being unknown. However, in such cases where comprehensive fragment profiles are generated without the use of synthesized standards, a secondary method of peptide sequence generation or a combination of separation and mass spectrometry may be required if identification of sequence-specific fragments is desired.

5.4.8 Tracking proteolysis of peptides in single cells

Single-cell CE-LIF permits highly sensitive (10^{-20} mole)[9,25] enzyme activity measurements within individual cells. However in order to identify species arising from reporter or peptide degradation, it is necessary to generate a set of peptide standards which represent all possible degradation products for use as migration standards. This is especially true when the degradation products of peptides within individual cells are unknown and may co-migrate with other peptide modifications such as phosphorylation or acetylation. Although mass spectrometric methods have the capability to directly assign species identities, the combination of high-salt physiological buffers, limited sensitivity, variable analyte ionization, and small sample volumes have proven generally incompatible with mass spectrometry to directly identify products from single cells.[15,37-39] To demonstrate the utility of a simple and rapid method to generate all fluorescent fragments in tracking single-cell peptide metabolism, the intracellular fate of peptides was tracked in single-cells by CE-LIF.

157

Peptide I (38±9 amol, n=4 cells), or IV (46±15 amol, n=7 cells) was microinjected into individual PANC-1 cells, a pancreatic adenocarcinoma cell line. This cell line was chosen based our observations that PANC-1 cells possess robust proteolytic activity and would likely generate fragments of the selected peptides.[25] Peptide was incubated for 2 min before cells were lysed with a pulse from an Nd:YAG laser and the contents loaded into a capillary directly above the cell. Intracellular metabolism of the peptide was identified using standard fragment mixtures obtained from incubation with Pronase E. With the exception of a peak detected due to cell fluorescence (Figure 5.9D), each fragment formed in the cell co-migrated with a standard fragment suggesting that all cell-derived peaks were fragments formed by cleavage at peptide bonds and were not due to other metabolic processes such as phosphorylation or acetylation, which would likely shift the migration times observed in CE-LIF.

During a 2-min incubation, Peptide I, an Abl kinase sensor, underwent proteolysis within the cytosol of all intact cells analyzed, and all fragments were identified through the use of Pronase E-generated standards. The five-residue fragment I-h, a result of cleavage between the Ala-Ala residues (Figure 5.9A), was preferentially formed in all cases. Similar peptide cleavage sites were observed among the cells analyzed, with between 5-7 fragments formed within the 2 min incubation period, and the identities of fragments formed between cells varied only slightly (Figure 5.9E and 5.11). No fragments shorter than 3 amino acids were observed. The average rate of degradation of Peptide I within cells was 4.2±4.8 zmol μM^{-1} s^{-1}, and resulted in 24-78% intact Peptide I after 2 min. While one of the four cells tested did not exhibit significant amounts of peptide fragment generation, the peptides generated possessed similar profiles between cells (Figure 5.11). The variability in absolute

fragmentation rate observed in these studies combined with previous work displaying the rapid fragmentation of this peptide sensor in single cells[10] indicates that in numerous cases this sequence is quickly degraded and requires fragmentation monitoring within the intracellular environment, even in cases where peptide phosphorylation is the desired readout.

Peptide IV was also rapidly metabolized in cells, with an average of 8.8±5.3% intact remaining after 2 min (Figure 5.9B). The average rate of proteolysis was 8.9±0.1 zmol μM^{-1} s^{-1}. Although Peptide IV requires no additional proteolytic processing for antigen presentation, its limited intracellular lifetime suggests rapid peptidase activity towards this sequence. This is consistent with advancement of degraded peptides to one of multiple fates, including binding to MHC class I molecules to become immunologically relevant or acting as substrates for various cytosolic peptidases which hydrolyze peptides into their component amino acids.[6] The 7 individual cells produced between 3-11 unique fluorescent peptide sequences, with no two cells possessing the same profile of fragments (Figure 5.9F and 5.12). The constant incubation time combined with the negligible correlation between the number of fragments generated in individual cells and amount of Peptide IV delivered by microinjection (R^2 = 0.15, Figure 5.13) indicates that the cleavage site heterogeneity was not a function of the loading technique or duration. While additional single cell analyses will be required to provide further evidence of any subpopulations of cells with differential proteolysis phenotypes, these pilot studies show the ease and feasibility of tracking intracellular peptide fate with standards generated by Pronase E. The variation in fragments formed in single cells as identified by Pronase E standards may provide useful biological information even without certainty of peak assignments, particularly in cases where specific

peaks act as bioindicators. Variations in fragment number or degradation rate can be a simple indicator of the activation or inhibition of enzymes or particular pathways upon drug treatment, sample handling practices, or upregulation as a result of a disease state.[40,41]

5.5 Conclusions

Rapid digestion of peptide sequences with Pronase E and synergistic CE-LIF and MALDI-MS detection of fluorescent fragments was validated *in vitro* and implemented in the identification of fragments from single cells. A small but chemically diverse group of peptide sequences underwent proteolysis with Pronase E, and conditions for the hydrolysis of basic, polar, and nonpolar amino acids within a sequence were demonstrated. Synthesized fragments were employed to verify the identities of sequences in initial studies (Peptides I-III), and then all fragments from Peptide IV were generated and identified from assay mixtures alone. It was shown that limited hydrolytic capabilities of Pronase E towards acidic or non-native amino acids could be overcome by supplementing enzymatic degradation with formic acid-induced peptide cleavage. The formation of peptide fragments was tracked in single PANC-1 cells, and the simultaneous identification of degradation products as well as the rate of their formation was achieved with a combination of Pronase E-generated fragment standards and chemical cytometry. In cells incubated with Peptide IV, there was substantial variation in the identity of fragments formed between cells. This heterogeneity reflects the value of single cell analysis, as the unique fragment profiles formed in each cell would not be visible in population averages.

This approach for the generation of peptide fragments has several advantages over existing methodologies, primarily in its simplicity and flexibility. The relatively nonspecific

nature of Pronase E is well suited to the generation of fragments from a wide range of peptides, and by varying the concentration of enzyme mixture, even degradation resistant sequences can be fragmented. Based on our success with post-enzymatic chemical peptide cleavage, it stands to reason that directed chemical cleavage with other reagents in cases where Pronase E is insufficient is possible, and will be the focus of further studies. Overall, the use of Pronase E to rapidly generate fragments should see wide applicability in peptide sequencing, rapid generation of biologically active peptides from larger proteins, and in generation of fragment standards for chemical cytometry.

5.6 Figures and Tables
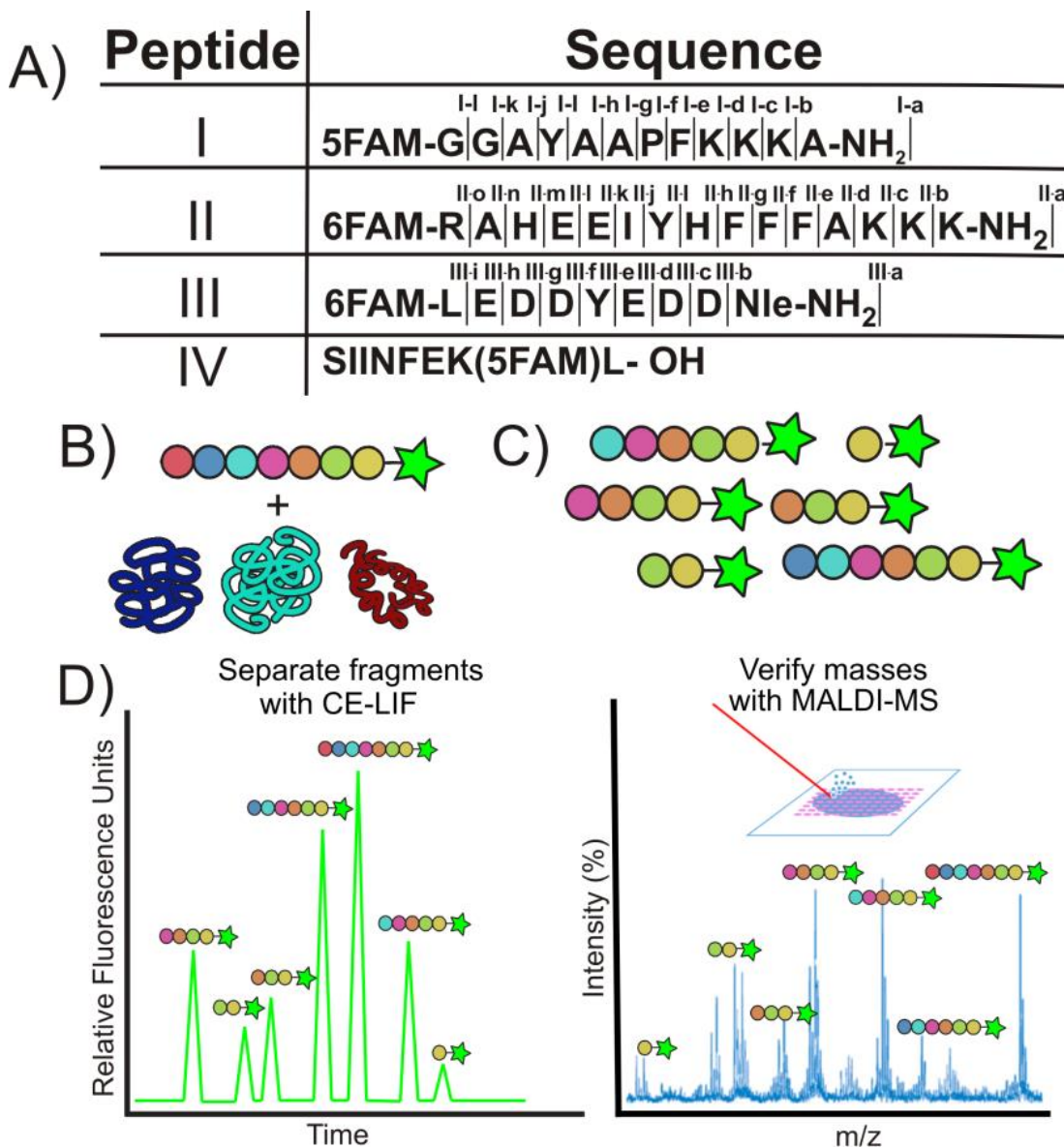
Figure 5.1 Schematic of a Pronase E Peptide Degradation Assay. A) Synthesized full length peptides for individual degradation by Pronase E. Uppercase letters represent single letter amino acid abbreviations, Nle is Norleucine, and NH_2 or OH represent amidated or carboxylated C-termini, respectively. Lowercase letters indicate cleavage locations that form the specified fluorescent peptide fragments. Fragment nomenclature for Peptide IV can be found in Table 5.1. B) Each peptide was incubated with active Pronase E. Colored circles represent the different amino acids present in each sequence, and stars represent fluorescein (FAM). C) The resulting mixture containing fluorescent fragments. D) Results of parallel CE-LIF and MALDI- MS analysis identifying fluorescent fragments.
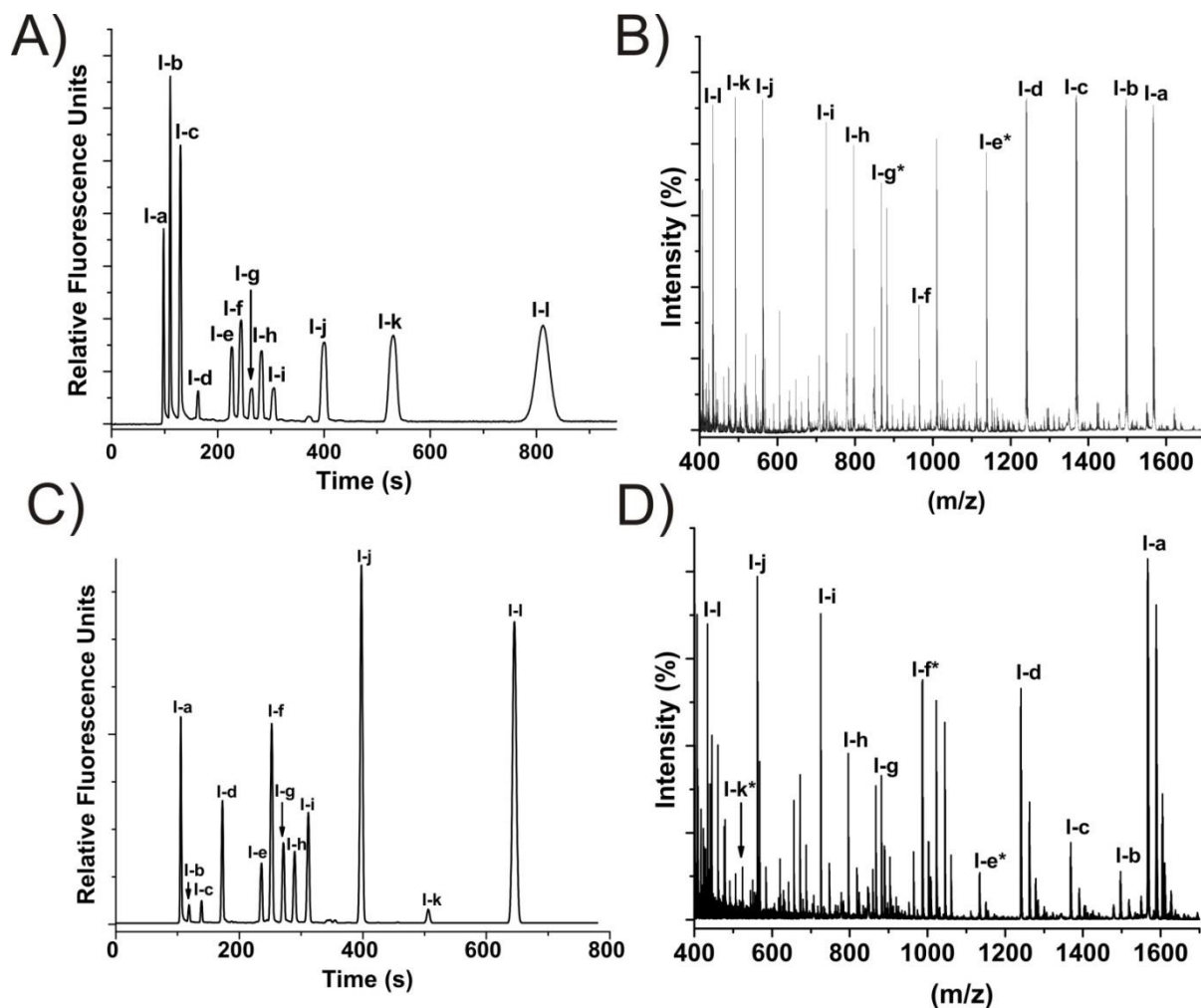
Figure 5.2 Separation and Detection of Peptide I Fragments. A) CE-LIF separation of peptide fragments prepared by SPPS. B) Positive-ion MALDI-MS spectra of synthesized Peptide I fragments. C) CE-LIF separation of fragments generated by incubation of Peptide I with 0.02 µg/mL Pronase E for 15 minutes. D) Positive-ion MALDI-MS spectra of Pronase E assay sample separated in (C).

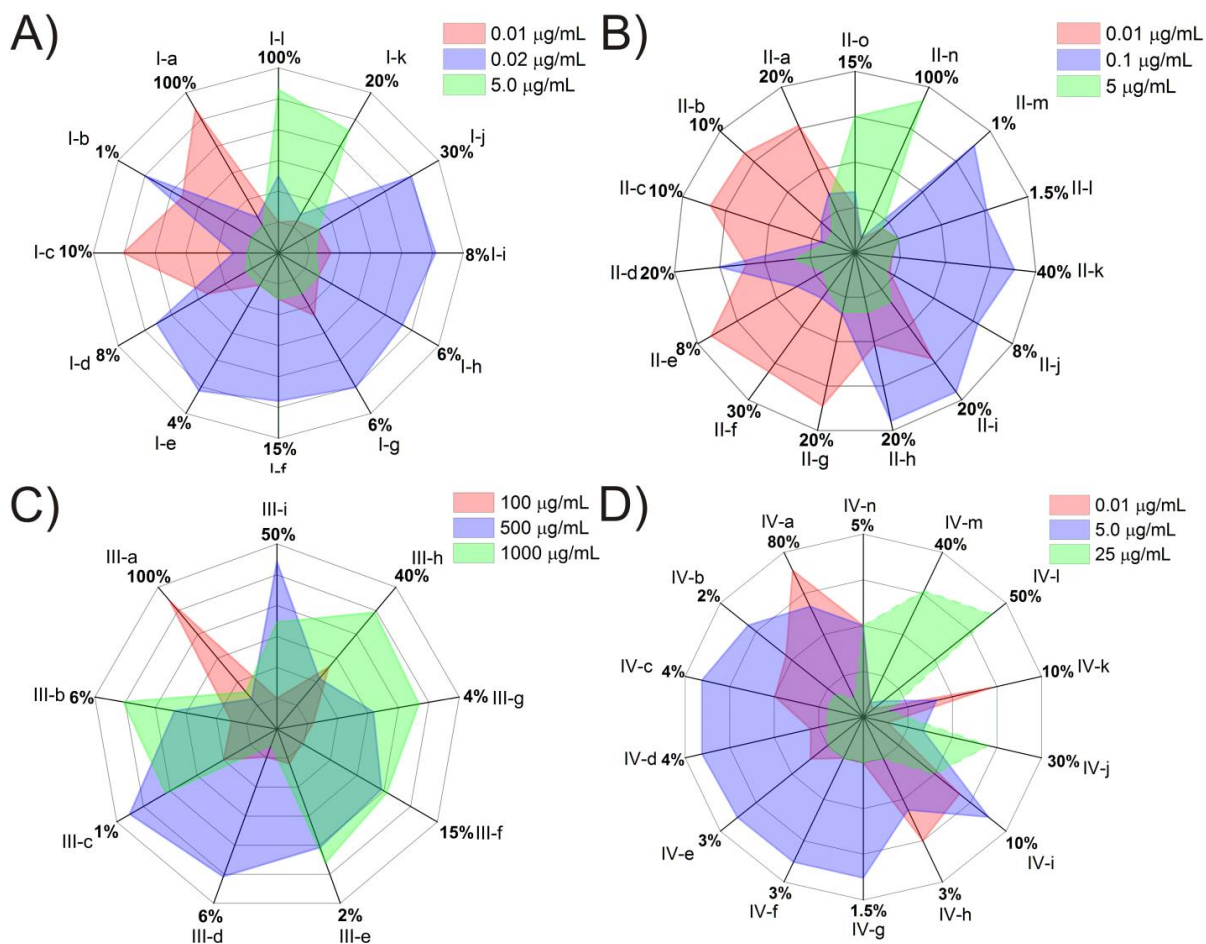**Figure 5.3 Summary of Pronase E Degradation Profiles for Peptide A) I B) II C) III D) IV.** Each plot represents the fragments formed during 15 minutes incubation with the indicated enzyme concentration (µg/mL). The blue layer signifies the Pronase E concentration that generated the most complete distribution of fragments. The percentage of fragment formation (0-100%) is scaled independently for each fragment. Fragment (I-IV)a in each plot indicates the full length peptide sequence. With the exception of Peptide IV (Fragment nomenclature in Supplemental Table S1) each subsequent letter represents the fragment resulting from removal of one residue from the C-terminus. The variation in fragment formation between replicates of each peptide's optimized Pronase E concentration (blue layer) is described in Figure 5.4.
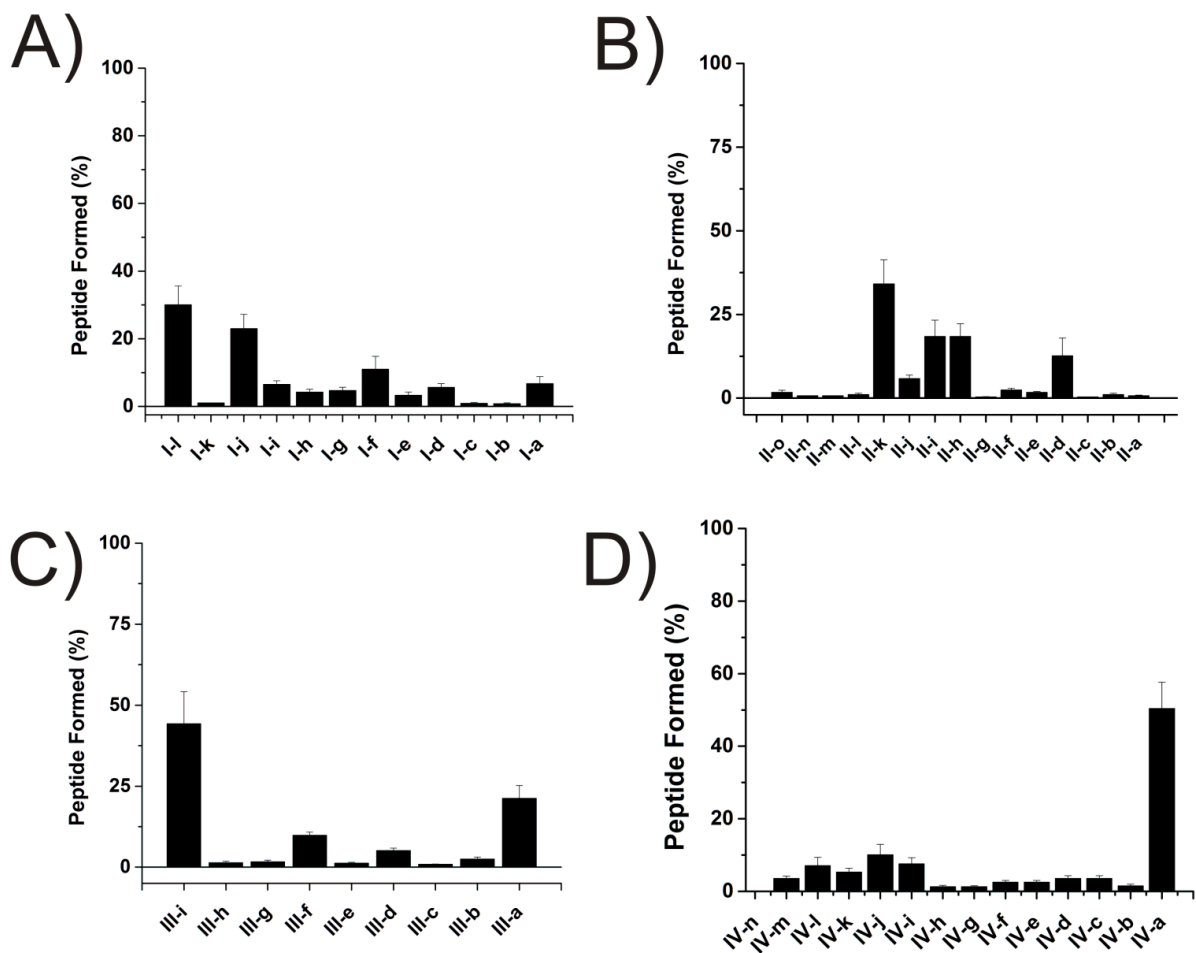
Figure 5.4 Fragment Formation Under Optimized Pronase E Conditions for Peptide A) I B) II C) III D) IV. The solid bars represent the percentage peptide formed in the reaction mixture while the error bars represent the standard deviation (n = 3).
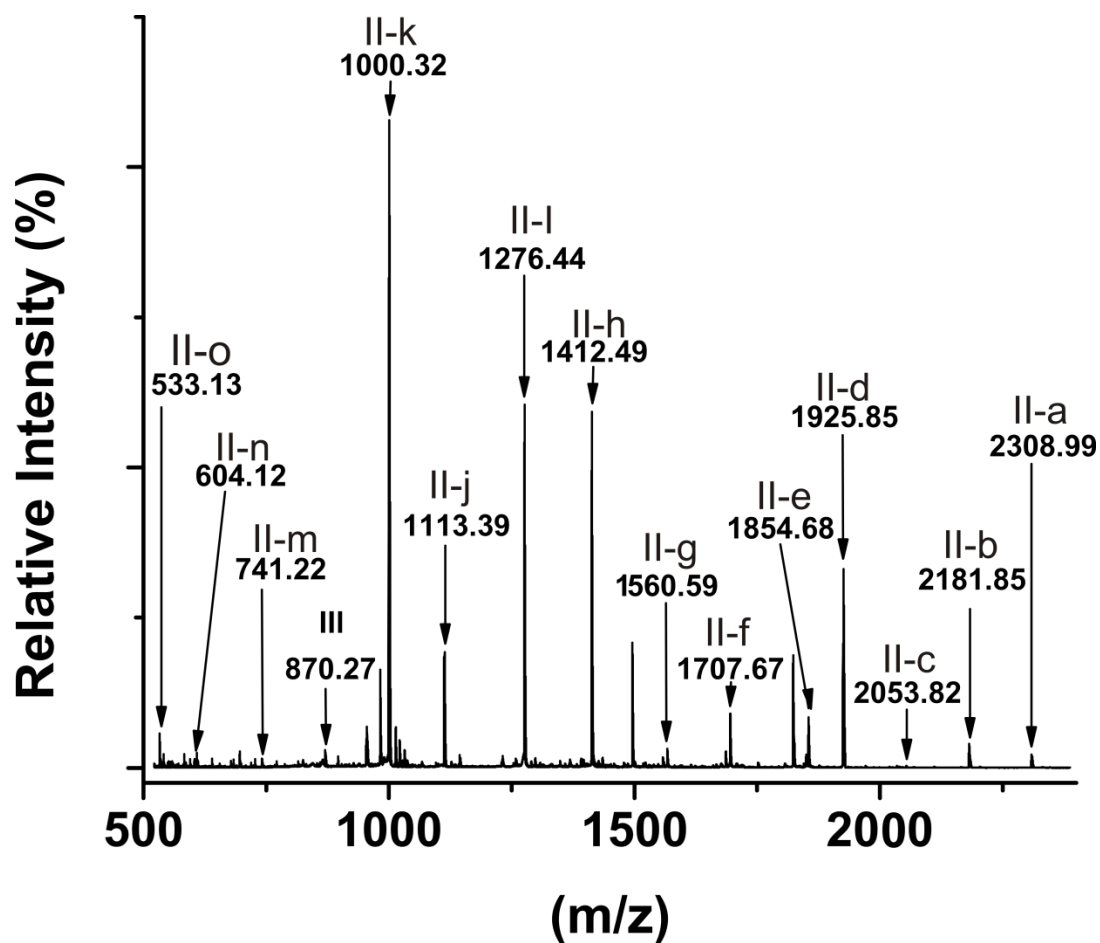
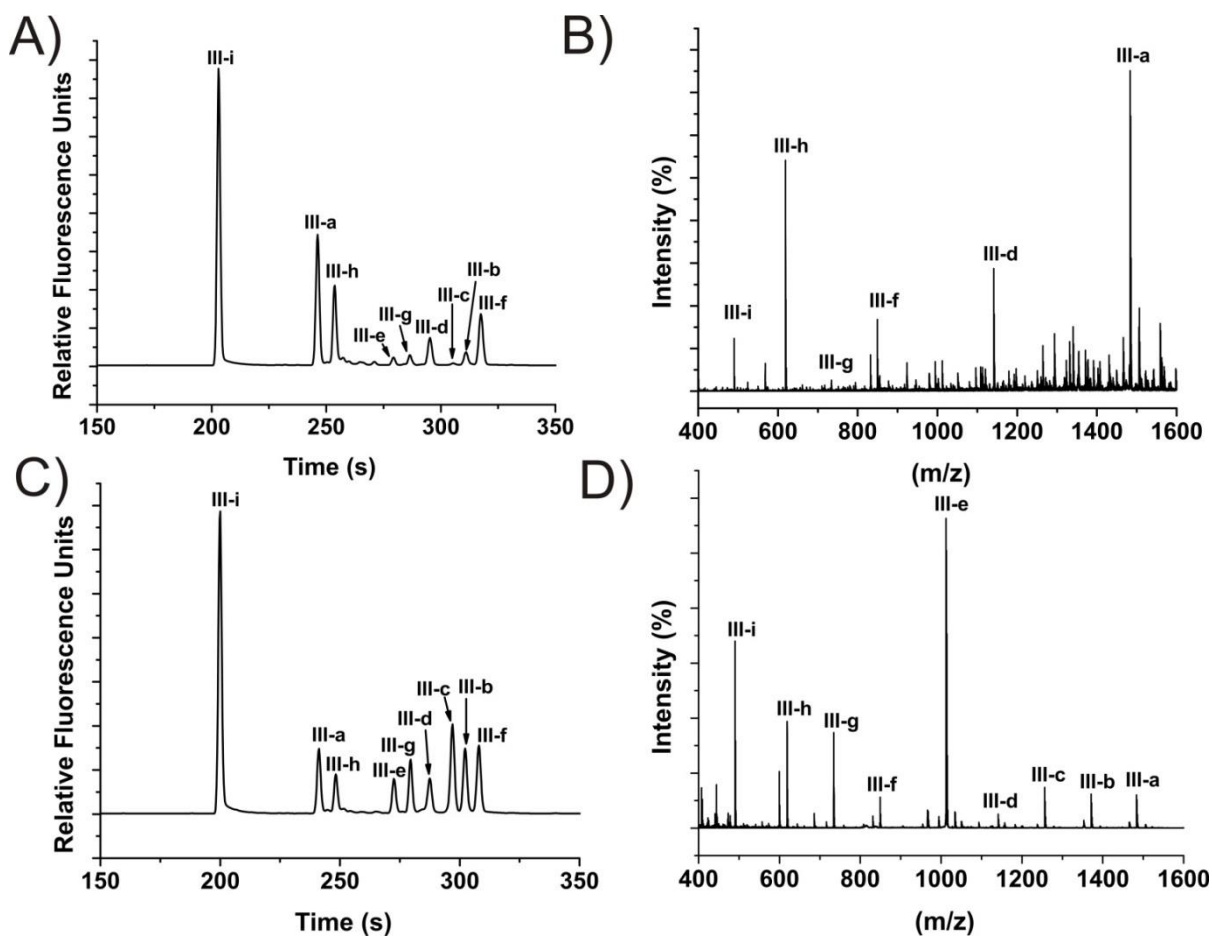**Figure 5.5 Positive-ion MALDI-TOF MS Spectra of Peptide II Fragments Formed by 0.01 μg/mL Pronase E After 15 min.**

Figure 5.6 Digestions of Peptide III. A) Electropherogram of fragments generated with 500 µg/mL Pronase E and separated with CE-LIF. B) MALDI-MS spectra corresponding to digestion of Peptide III with Pronase E alone C) CE-LIF separation of Peptide III fragments generated with 2% formic acid-assisted Pronase E digestion D) MALDI-MS spectra of Peptide III fragments generated with 2% formic acid-assisted Pronase E digestion.
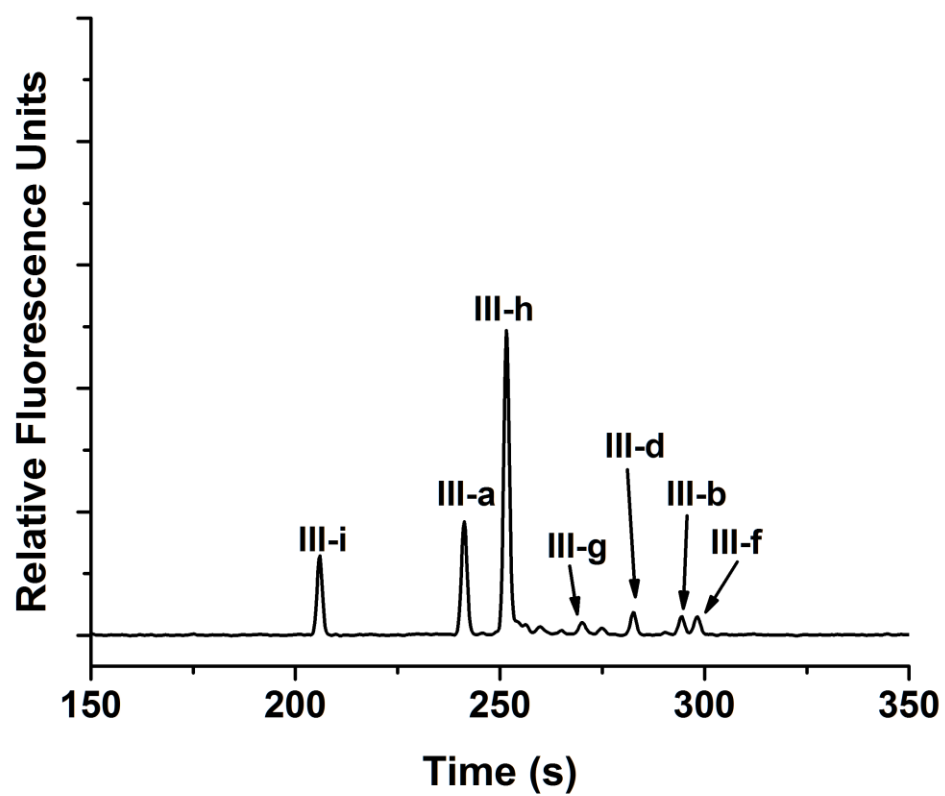
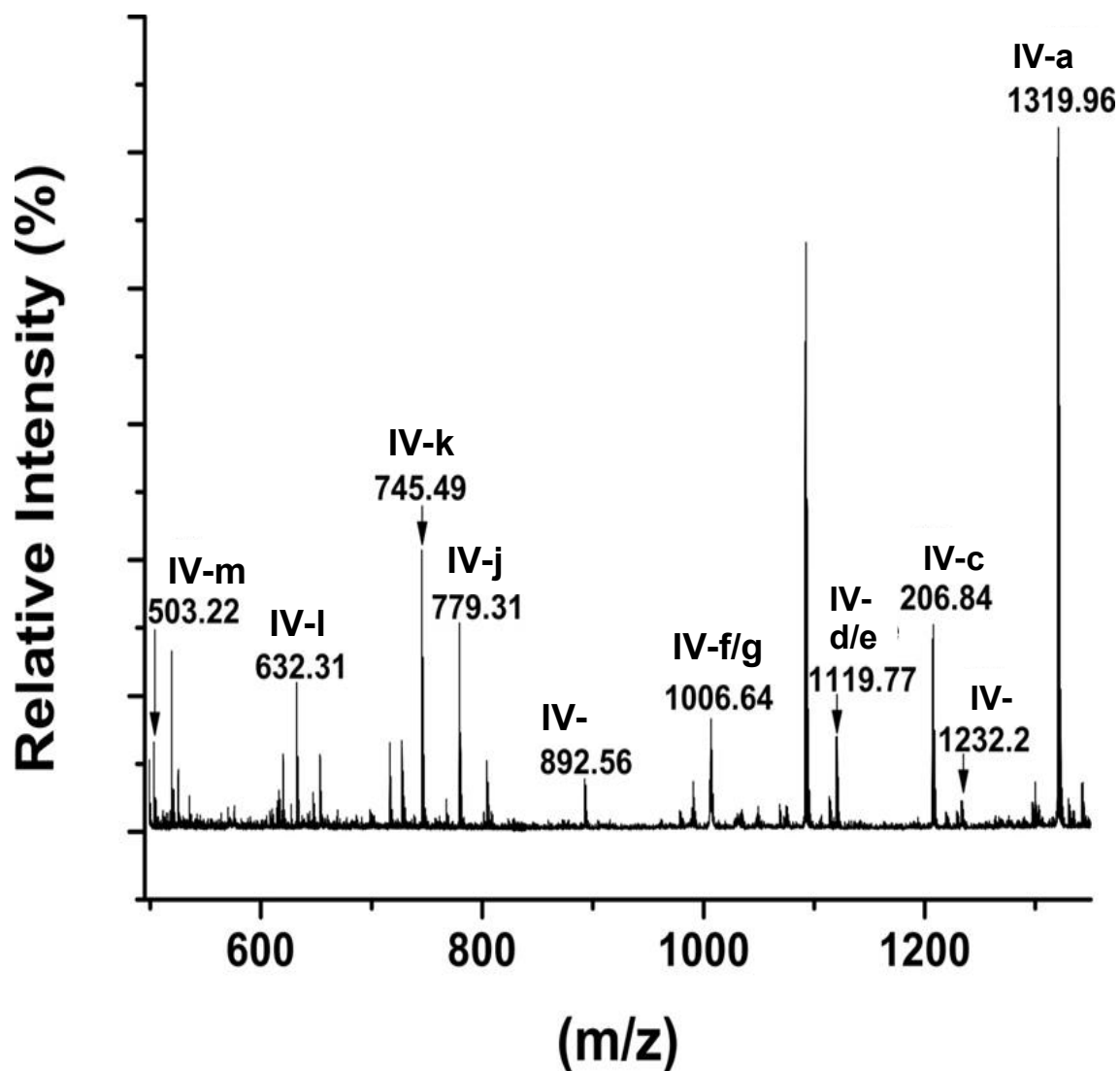**Figure 5.7 Fragmentation of Peptide III After Incubation with 2% Formic Acid for 15 min.**

Figure 5.8 Negative-ion Mode MALDI-MS Spectra of Peptide IV Digested With 5.0 µg/mL Pronase E for 15 min.
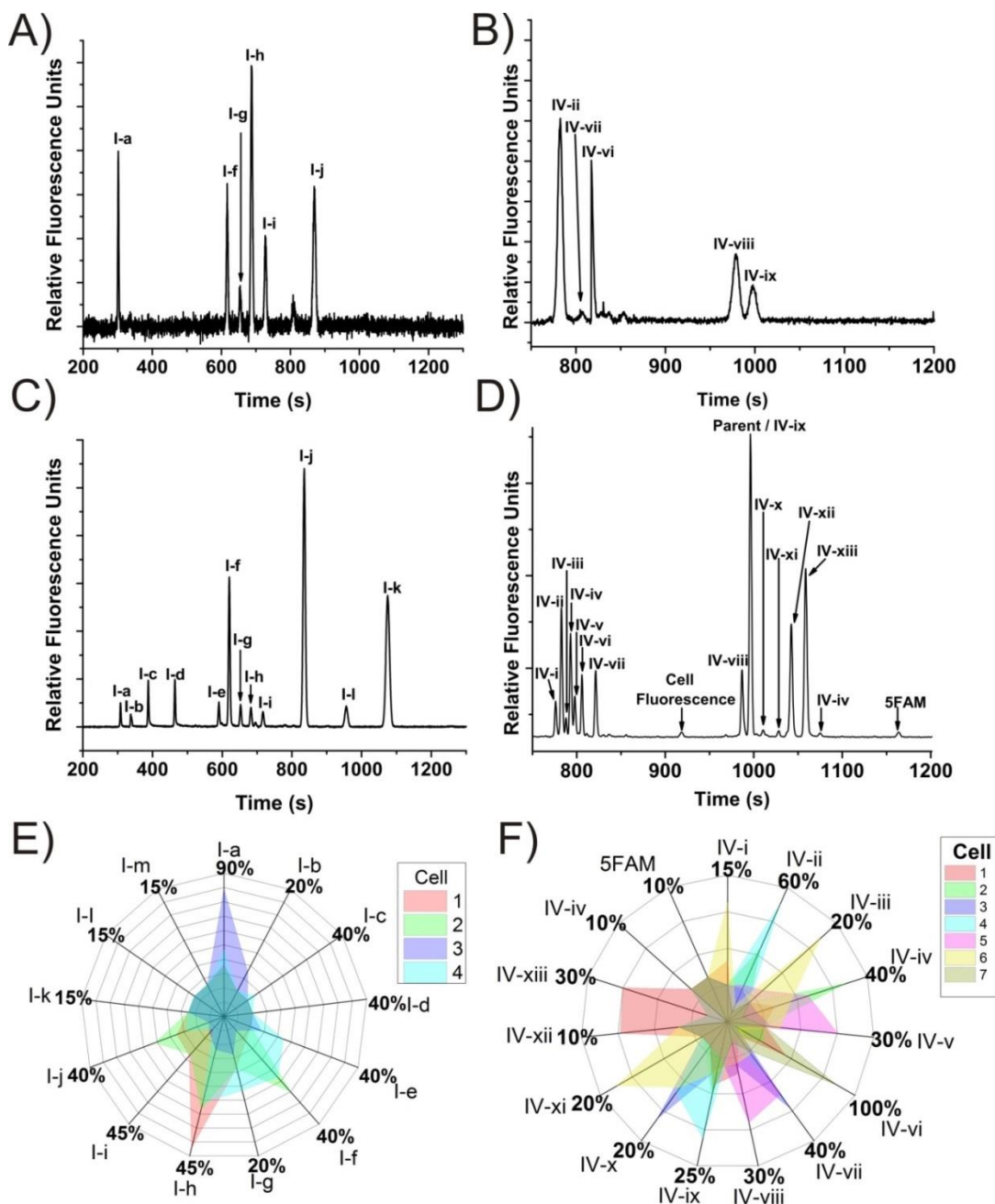
Figure 5.9 Identification of Fragments Formed Due to Peptide Metabolism in Single Cells Based on Pronase E-Generated Standards. PANC-1 cells were microinjected with Peptide I (A,C,E) or Peptide IV (B,D,F). (A,B) Electropherograms of a single PANC-1 cell 2 min after microinjection. The Pronase E generated standards of Peptide I (C) or IV (D) were loaded into the capillary immediately after loading the cell contents. Electrophoresis was then initiated by applying a voltage to the capillary, which resulted in concurrent separation of fragment standards and cellular contents. Radar plots for Peptide I (E) and Peptide IV (F) indicate the fragments formed in individual cells.
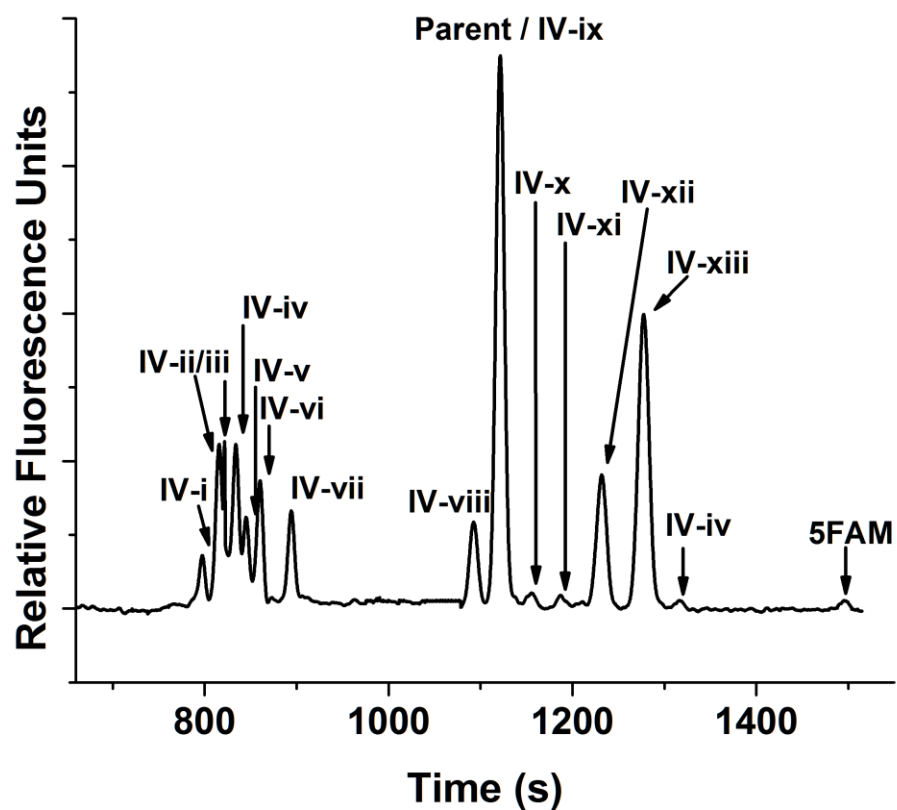
Figure 5.10 CE-LIF Separation of Peptide IV Fragments Generated with Pronase E (5.0 µg/mL) Without the Addition of PANC-1 Cell Contents.
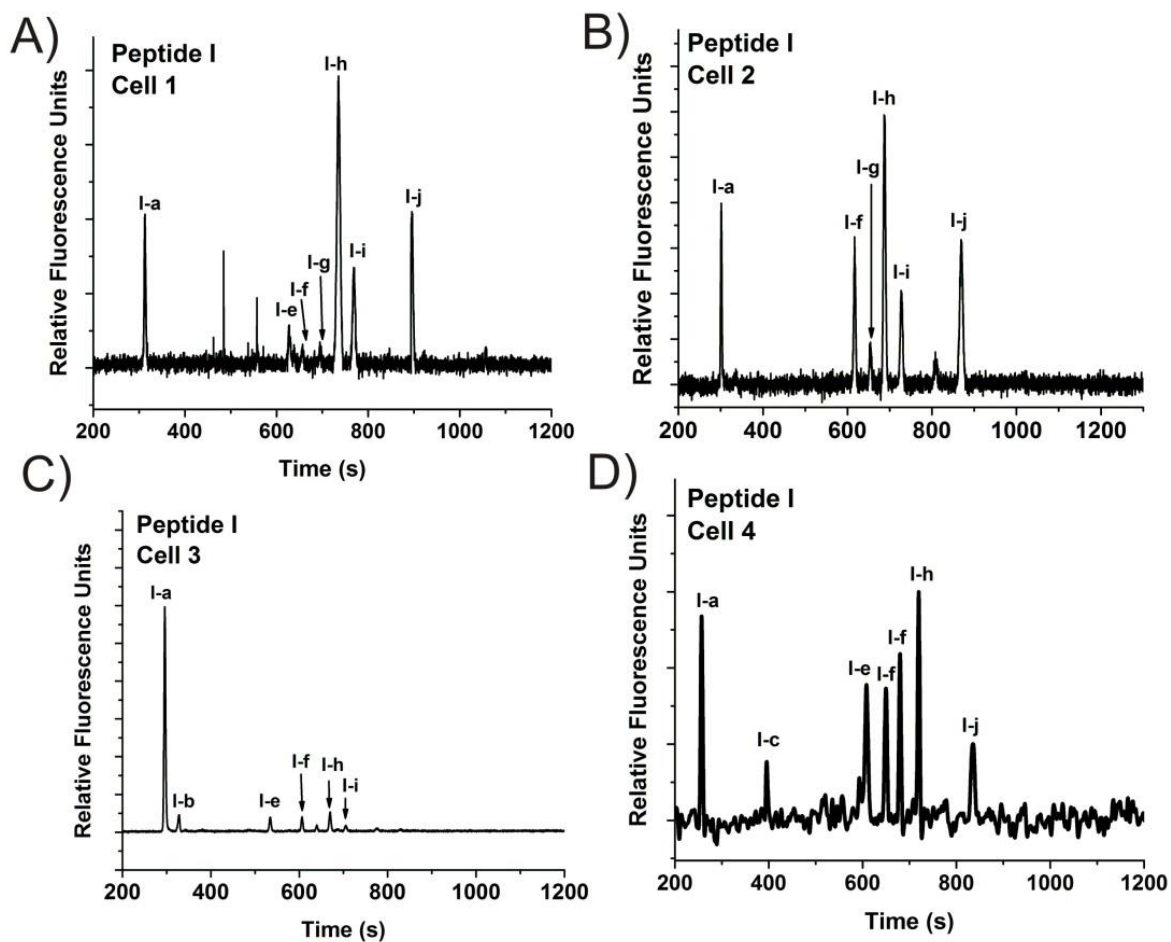
Figure 5.11 CE-LIF Separation of Single PANC-1 Cells Microinjected With Peptide I for 2 min. Electropherograms from Cells 1-4 can be matched with radar plots in Figure 5.8E.
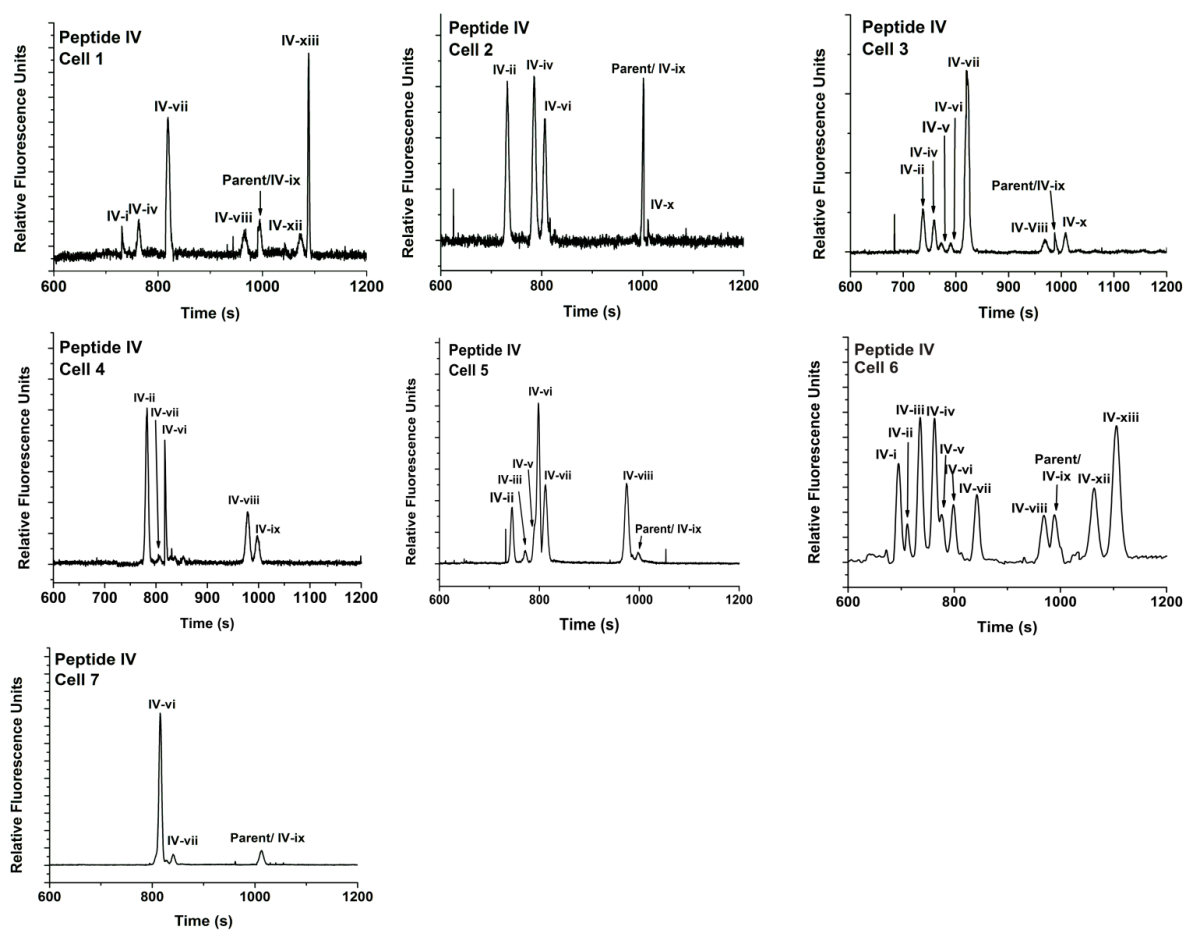
Figure 5.12: CE-LIF Separation of Single PANC-1 Cells Microinjected with Peptide IV for 2 min. Cell identification numbers can be matched to radar plots in Figure 5.8F.
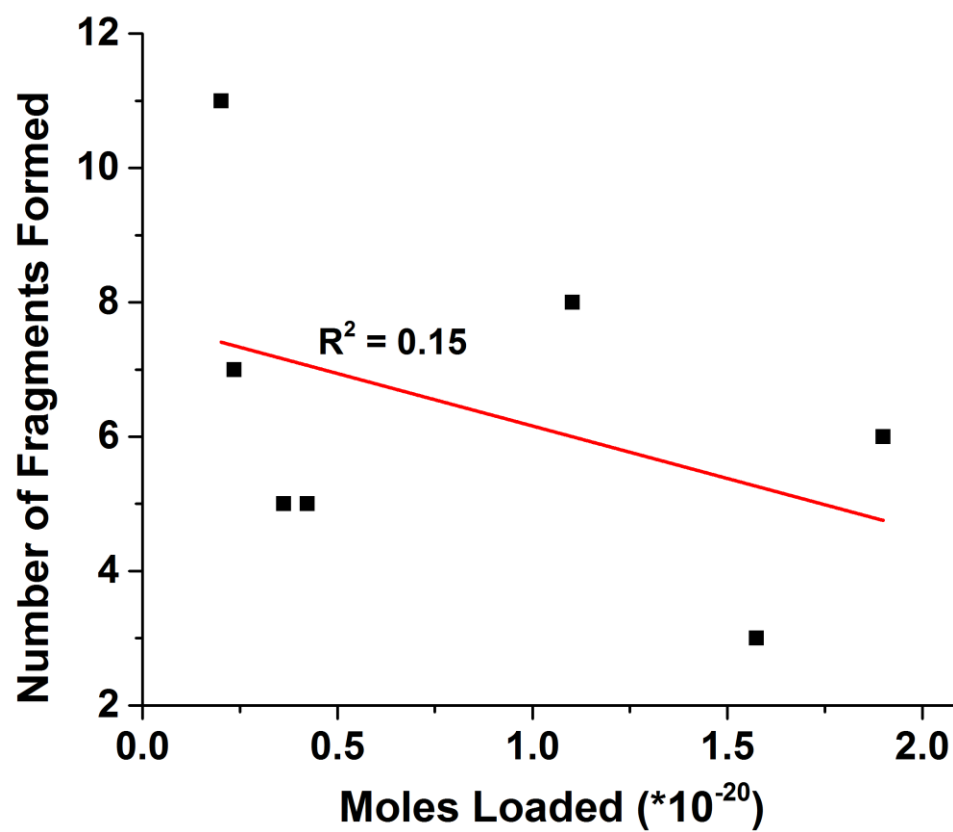
Figure 5.13 Peptide IV Fragmentation as a Function of the Number of Moles of Peptide Loaded into Intact Cells.

Table 5.1: Fragment Nomenclature and Masses for Peptide IV

Name	Sequence	Mass
IV-n	K(5-FAM)-OH	504.15
IV-m	K(5-FAM)L-OH	617.24
IV-l	EK(5-FAM)-OH	634.18
IV-k	EK(5-FAM)L-OH	747.26
IV-j	FEK(5-FAM)-OH	781.25
IV-i	FEK(5-FAM)L-OH	894.33
IV-h	NFEK(5-FAM)-OH	895.29
IV-g	NFEK(5-FAM)L-OH	1008.38
IV-f	INFEK(5-FAM)-OH	1008.38
IV-e	INFEK(5-FAM)L-OH	1121.46
IV-d	IINFEK(5-FAM)-OH	1121.46
IV-c	SIINFEK(5-FAM)-OH	1207.51
IV-b	IINFEK(5-FAM)L-OH	1234.54
IV-a	SIINFEK(5-FAM)L-OH	1320.59

Peptide IVa represents the full-length peptide. In Figure 5.9(B,D), Peptide IV fragments are named by lowercase roman numerals based on migration time.

REFERENCES

1. Ferro, E. S.; Rioli, V.; Castro, L. M.; Fricker, L. D. Intracellular peptides: From discovery to function. *EuPA Open Proteomics* **2014***, 3*, 143-151.

2. Huyer, G.; Kistler, A.; Nouvet, F.; George, C.; Boyle, M.; Michaelis, S. Saccharomyces cerevisiae a-Factor Mutants Reveal Residues Critical for Processing, Activity, and Export. *Eukaryotic Cell* **2006***, 5*, 1560-1570.

3. Cunha, F.; Berti, D.; Ferreira, Z.; Klitzke, C.; Markus, R.; Ferro, E. Intracellular Peptides as Natural Regulators of Cell Signaling. *Journal of Biological Chemistry* **2008***, 283*, 24448-24459.

4. Qvit, N.; Mochly-Rosen, D. Highly specific modulators of protein kinase C localization: applications to heart failure. *Drug Discovery Today: Disease Mechanisms* **2010***, 7*, e93.

5. Ciechanover, A. Proteolysis: from the lysosome to ubiquitin and the proteasome. *Nature Reviews: Molecular Cell Biology* **2005***, 6*, 79.

6. Wiertz, E.; Kikkert, M.; Groothuis, T.; Neefjes, J. In *The Ins and Outs of Intracellular Peptides and Antigen Presentation by MHC Class I Molecules;* Springer Berlin Heidelberg: 2005; pp 127-148.

7. Murphy, R. M. Peptide Aggregation in Neurodegenerative Disease. *Annual Review of Biomedical Engineering* **2002***, 41*, 155-174.

8. McFarland, B.; Sant, A.; Lybrand, T.; Beeson, C. Ovalbumin(323−339) Peptide Binds to the Major Histocompatibility Complex Class II I-A d Protein Using Two Functionally Distinct Registers. *Biochemistry* **1999***, 38*, 16663-16670.

9. Phillips; Dailey; Bair; Samet; Allbritton Ex Vivo Chemical Cytometric Analysis of Protein Tyrosine Phosphatase Activity in Single Human Airway Epithelial Cells. *Analytical Chemistry* **2014***, 86*, 1291-1297.

10. Proctor, A.; Wang, Q.; Lawrence, D. S.; Allbritton, N. L. Metabolism of peptide reporters in cell lysates and single cells. *The Analyst* **2012***, 137*.

11. Yang, S.; Proctor, A.; Cline, E.; Houston, K.; Waters, M.; Allbritton, N. L. β-Turn sequences promote stability of peptide substrates for kinases within the cytosolic environment. *The Analyst* **2013***, 138*.

12. Lowe, S.; Dick, J. A. G.; Cohen, B. E.; Stevens, M. M. Multiplex Sensing of Protease and Kinase Enzyme Activity via Orthogonal Conjugation of Quantum Dot- Peptide Constructs. *ACS Nano ,6*, 851-857.

13. Tung, C. H. Fluorescent peptide probes for in vivo diagnostic imaging. *Biopolymers* **2004**, *76*, 391-403.

14. Bright, R. K. Peptide-Based Cancer Vaccines. *Leukemia* **2002**, *16*, 970-971.

15. Amantonico, A.; Oh, J.; Sobek, J.; Heinemann, M.; Zenobi, R. Mass Spectrometric Method for Analyzing Metabolites in Yeast with Single Cell Sensitivity. *Angewandte Chemie International Edition* **2008**, *47*, 5382-5385.

16. Brown, R. B.; Hewel, J. A.; Emili, A.; Audet, J. Single amino acid resolution of proteolytic fragments generated in individual cells. *Cytometry Part A* **2010**, *77A*, 347–355.

17. Dudek, N. L.; Perlmutter, P.; Aguilar, M. I.; Croft, N. P.; Purcell, A. W. Epitope discovery and their use in peptide based vaccines. *Curr Pharm Des* **2010**, *16*, 3149-3157.

18. White, C.; Yudin, A. Contemporary strategies for peptide macrocyclization. *Nature Chemistry* **2011**, *3*, 509-524.

19. Crimmins, D. L.; Mische, S. M.; Denslow, N. D. Chemical cleavage of proteins in solution. *Current Protocols in Protein Science* **2005**, *11*, 1104-1140.

20. Olsen, J.; Ong, S. E.; Mann, M. Trypsin Cleaves Exclusively C-terminal to Arginine and Lysine Residues. *Molecular & Cellular Proteomics* **2004**, *3*, 608-614.

21. Qasim, M. Specificity of Proteinase K at P_2 to P_3' Sub-sites and its Comparison to other Serine Proteases. *Protein & Peptide Letters* **2013**, *21*, 164-170.

22. Bermejo-Barrera, P.; Fernandez-Nocelo, S.; Moreda-Pineiro, A.; Bermejo-Barrera, A. Usefulness of enzymatic hydrolysis procedures based on the use of pronase E as sample pre-treatment for multi-element determination in biological materials. *J. Anal. At. Spectrom.* **1999**, *14*, 1893-1900.

23. Vosbeck, K. D.; Greenberg, B. D.; Awad, W. M. The proteolytic enzymes of the K-1 strain of Streptomyces griseus obtained from a commercial preparation (Pronase). Specificity and immobilization of aminopeptidase. *The Journal of Biological Chemistry* **1975**, *250*, 3981-3987.

24. Ma, W.; Tang, C.; Lai, L. Specificity of Trypsin and Chymotrypsin: Loop-Motion-Controlled Dynamic Correlation as a Determinant. *Biophysical Journal* **2005**, *89*, 1183-1193.

25. Proctor, A.; Herrera-Loeza, G.; Wang, Q.; Lawrence, D. S.; Yeh, J.; Allbritton, N. L. Measurement of Protein Kinase B Activity in Single Primary Human Pancreatic Cancer Cells. *Analytical Chemistry* **2014**, *86*, 4573-4580.

26. Sims, C. E.; Meredith, G.; Krasieva, T.; Berns, M.; Tromberg, B.; Allbritton, N. L. Laser-Micropipet Combination for Single Cell analysis. *70 , 4570.*

27. Wang, Z.; Raines, L. L.; Hooy, R. M.; Roberson, H.; Leahy, D. J.; Cole, P. A. Tyrosine Phosphorylation of Mig6 Reduces Its Inhibition of the Epidermal Growth Factor Receptor. *ACS Chem. Biol.* **2013***, 8*, 2372-2376.

28. Kumar, R.; Crouthamel, M.; Rominger, D.; Gontarek, R.; Tummino, P.; Levin, R.; King, R. Myelosuppression and kinase selectivity of multikinase angiogenesis inhibitors. *Br. J. Cancer* **2009***, 101*, 1717-1723.

29. Phillips, R.; Bair, P.; Lawrence, D. S.; Sims, C. E.; Allbritton, N. L. Measurement of Protein Tyrosine Phosphatase Activity in Single Cells by Capillary Electrophoresis. *Analytical Chemistry* **2013***, 85*, 6136-6142.

30. Yamaguchi, H.; Kodama, H.; Osada, S.; Kato, F.; Jelokhani-Niaraki, M.; Kondo, M. Effect of alpha,alpha-Dialkyl Amino Acids on the Proteases Resistance of Peptides. *Biosci. Biotechnolo. Biochem.* **2003***, 67*, 2269-2272.

31. Proctor, A.; Wang, Q.; Lawrence, D.; Allbritton, N. Development of a Peptidase-Resistant Substrate for Single-Cell Measurement of Protein Kinase B Activation. **2012***, 84*, 7195.

32. Li, A.; Sowder, R. C.; Henderson, L. E.; Moore, S. P.; Garfinkel, D. J.; Fisher, R. J. Chemical Cleavage at Aspartyl Residues for Protein Identification. *Analytical Chemistry* **2001***, 73*, 5395-5402.

33. Cohen, S. L.; Chait, B. T. Influence of matrix solution conditions on the MALDI-MS analysis of peptides and proteins. *Analytical Chemistry* **1996***, 68*, 31-37.

34. Wilkinson, R.; Woods, K.; D'Rozario, R.; Prue, R.; Vari, F.; Hardy, M.; Dong, Y.; Clements, J. A.; Hart, D. N.; Radford, K. J. Human kallikrein 4 signal peptide induces cytotoxic T cell responses in healthy donors and prostate cancer patients. *Cancer Immunology, Immunotherapy* **2011***, 61*, 169-179.

35. Sun, Y.; Iglesias, E.; Samri, A.; Kamkamidze, G.; Decoville, T.; Carcelain, G.; Autran, B. A systematic comparison of methods to measure HIV-1 specific CD8 T cells. *Journal of Immunological Methods* **2003***, 272*, 23-34.

36. Hulseberg, P. D.; Zozulya, A.; Chu, H. H.; Triccas, J. A.; Fabry, Z.; Sandor, M. The same well-characterized T cell epitope SIINFEKL expressed in the context of a cytoplasmic or secreted protein in BCG induces different CD8+ T cell responses. *Immunology Letters* **2010***, 130*, 36-42.

37. Pan, N.; Rao, W.; Kothapalli, N. R.; Liu, R.; Burgett, A.; Yang, Z. The Single-Probe: A Miniaturized Multifunctional Device for Single Cell Mass Spectrometry Analysis. *Analytical Chemistry* **2014**, *86*, 9376-9380.

38. Rubakhin, S. S.; Sweedler, J. V. Quantitative Measurements of Cell−Cell Signaling Peptides with Single-Cell MALDI MS. *Analytical Chemistry* **2008**, *80*, 7128-7136.

39. Hofstadler, S. A.; Severs, J. C.; Smith, R. D.; Swanek, F. D.; Ewing, A. G. Analysis of Single Cells with Capillary Electrophoresis Electrospray Ionization Fourier Transform Ion Cycloton Resonance Mass Spectrometry. *Rapid Communications in Mass Spectrometry* **1996**, *10*, 919–922.

40. Chang, W.; Hsu, P.; Chen, Y.; Hsein, M.; Lu, P.; Chen, C. Observation of peptide differences between cancer and control in gastic juice. *Proteomics Clinical Applications* **2008**, *2*, 55-62.

41. Kovarik, M. L.; Dickinson, A. J.; Roy, P.; Poonnen, R. A.; Fine, J. P.; Allbritton, N. L. Response of single leukemic cells to peptidase inhibitor therapy across time and dose using a microfluidic device. *Integrative Biology* **2014**, *6*, 164-174.